

UC San Diego

Scripps Institution of Oceanography Technical Report

Title

Oceanographic Considerations for Desalination Plants in Southern California Coastal Waters

Permalink

<https://escholarship.org/uc/item/9br897dx>

Authors

Jenkins, Scott A

Wasyf, Joseph

Publication Date

2005-02-11

Oceanographic Considerations for Desalination Plants in Southern California Coastal Waters

Scripps Institution of Oceanography
Technical Report No. 54



Scott A. Jenkins, Ph. D. and Joseph Wasyl

Marine Physical Laboratory
University of California, San Diego
San Diego, CA 92106

11 February 2005

TABLE OF CONTENTS

Executive Summary	1
1) Introduction	5
A) Physical Setting	6
B) Climate Variation	13
2) Model Description and Capabilities	19
3) Model Initialization	33
A) Seasonal and Climate Effects on Controlling Variables	36
B) Bathymetry	38
C) Wave Climate	39
D) Ocean Water Levels & Tidal Oscillations	49
E) Current Forcing	51
F) Wind Mixing	54
G) Ocean Salinity	56
H) Ocean Temperature	58
I) Scattergood Operating Temperature	59
J) Scattergood Flow Rates and Post-Project Salinity	60
K) Hyperion Operating Temperature	64
L) Hyperion Flow Rates and Post-Project Salinity	67
M) Event Scenarios Derived from Historical Data 1980-2000	69
N) Calibration	73

Table of Contents (continued)

4) Event Analysis of Dilution & Dispersion of Brine 75
 A) Simulations for Scattergood Outfall Option 77
 B) Simulations for Hyperion 1-Mile Outfall Option 85
 C) Simulations for Hyperion 5-Mile Outfall Option 92
5) Conclusions 103
6) Bibliography 109

Appendices

- Appendix-A : TIDE_FEM Code**
- Appendix-B : OCEANRDS Code**
- Appendix-C : SEDXPORT Code**
- Appendix-D : TID_DAYS Code**
- Appendix-E : MULTINODE Code**

Oceanographic Considerations for Desalination Plants in Southern California Coastal Waters

by Scott A. Jenkins, Ph. D. and Joseph Wasyl

Executive Summary

California experiences multi-decadal climate variability in rainfall leading to alternating periods of dry and wet climate, each lasting 20-30 years. A dry period extended from about 1945-1977, followed by an episodically wet period from 1978-1998, that included the occurrence of six strong El Niño events. Because of the previous durations of these climate cycles, we have likely transitioned from a multi-decadal wet cycle that ended in 1998, and are now returning to a period of dry climate similar to what prevailed in California from 1945-1977. Such a transition in climate will put increasing pressures on already limited supplies of fresh water, making the development of alternative sources in California a necessity.

The Los Angeles Department of Water and Power (LADWP) plans to construct and operate a reverse osmosis (R.O.) desalination plant to be located on the site of the Scattergood Generating Station, 12700 Vista Del Mar, Los Angeles CA. Potentially, up to 50 million gallons per day (mgd) of product drinking water produced by this plant will be blended with other supplies to provide supplemental water to water utilities served by LADWP's service area. The source of water for the desalination plant will be seawater drawn from the Santa Monica Bay, about

1,600 feet, ft, offshore. The source water will be pre-treated and filtered through reverse osmosis membranes to produce high quality drinking water. The plant's product drinking water will be blended with other sources and distributed to consumers. The concentrated seawater produced by the reverse osmosis process (brine) will be mixed with the cooling water and then conveyed through one or more of three existing outfall structures: 1) the 17.5 ft diameter thermal outfall servicing Scattergood Generating Station, located 1,200 ft offshore, 2) the 12 ft diameter Hyperion emergency outfall located 5,384 ft offshore; and 3) the 12 ft diameter Hyperion deep outfall located 27,539 ft offshore. The net physical effect of desalination on the ocean receiving waters is in principle no different than the effects of evaporation; except that it would take 2,100 desalination plants of the size being proposed by LADWP at Scattergood to match the evaporative losses occurring naturally in the waters of the Southern California Bight. (The Southern California Bight is a water body bounded by the coastline between Point Conception and the United States-Mexican border, and extending offshore to the island arc formed by the Channel Islands, Catalina Island, San Clemente Island and the Coronado Islands).

The following study has utilized a hydrodynamic model to evaluate the brine dilution and dispersion for each of the three possible discharge options over the historical range of ocean receiving water conditions and host generating station operations. Product water production by the desalination plant was varied in the model between 12 and 50 mgd to evaluate the "carrying capacity" of each discharge option in the presence of long-term ocean variability and host plant operations. Carrying capacity was judged according to how the modeled brine dilution fields compared with the scientific consensus of the salinity tolerance

limits of the marine biota indigenous to the Southern California Bight. (Generally, the salinity tolerance limit for indefinite exposure is believed to be 38 parts per thousand, ppt, as compared to an average salinity in the receiving water of 33.5 ppt). The hydrodynamic model analysis employed for this purpose was the *SEDXPORT* modeling system that was developed at Scripps Institution of Oceanography for the US Navy's *Coastal Water Clarity System* and *Littoral Remote Sensing Simulator*; that has been peer reviewed multiple times and has been calibrated and validated in the Southern California Bight for 4 previous desalination design projects.

Based on hydrodynamic model results derived from 20 years of ocean monitoring data and Scattergood and Hyperion operating data, four primary conclusions have been formed:

- 1) If the production rate of product water by the desalination plant is limited to 12- 25 mgd, then the Scattergood outfall located 1,200 ft offshore provides adequate brine dilution in the receiving waters under all circumstances;
- 2) If the production rate of product water by the desalination plant is increased to 50 mgd, then brine discharges from the Scattergood outfall still remain below marine biology tolerance limits 82 % of the time. During the remaining 18 % of the time when bottom salinity exceeds the marine biology tolerance threshold, an area of benthic habitat covering 51 acres is impacted by hyper-salinity, some of which is in the surf zone;
- 3) Brine discharges from the Hyperion 1-mile emergency outfall will exceed

marine biology tolerances 98% of the time if product water is produced by the desalination plant at a rate of 12 mgd. If product water production is increased to 50 mgd, then marine biology tolerances are exceeded 100% of the time. The Hyperion 1-mile outfall is not a viable discharge option unless the brine is diluted with supplemental seawater prior to being discharged. A dilution ratio of 3.25 to 1 is required with supplemental sea water to eliminate potential benthic hyper-salinity impacts associated with brine discharge through Hyperion 1-mile outfall ;

4) Brine discharges from the Hyperion 5-mile deep outfall cause no hyper-salinity impacts on marine biology and will reduce the footprint of the Hyperion waste field by as much as 42% depending on seasonal and decadal variability of ocean and meteorological conditions. The Hyperion 5-mile outfall offers the lowest risk alternative for marine benthic impacts while allowing the largest desalination production capacity at the Scattergood Generating Station;

5) Discharges from the Hyperion 5-mile deep outfall present no significant impacts on the source water quality derived from the intake flow of the Scattergood Generating Station. Dilution factors for the Hyperion waste field at the intake to the Scattergood Generating Station are greater than 10^8 to 1 for both the pre- and post-project conditions.

SECTION 1: INTRODUCTION

1) Introduction

A) Physical Setting

This study investigates basic water quality issues related to the proposed Los Angeles Department of Water and Power Desalination Project to be sited at the Scattergood Generating Station, (SGS), located at 12700 Vista Del Mar, Los Angeles, CA (Figure 1.1). The desalination project would be connected to the existing cooling water circulation system of the generating station. Physical specifications for the cooling water infall and outfall are listed in the NPDES permit #CA 0000370 (CRWQCB, 2000). Cooling water is drawn from Santa Monica Bay through a velocity cap atop an infall tower located 1,600 ft (488 m) offshore. According to as-built drawings dated 1 October 1957 (Figure 1.2), the velocity cap is located at a depth of 10.5 ft below mean lower low water (MLLW) or about 13.25 ft below mean sea level (MSL). The cooling water is discharged through a single 12 ft internal diameter conduit connected to a seafloor structure identical in dimension to the infall tower (Figure 1.2) located approximately 1,200 feet (366 meters) offshore of Dockweiler State Beach, El Segundo, at a depth of about 15 feet MLLW, or about 17.75 ft MSL, based on National Ocean Survey digital bathymetry. The route of Scattergood discharge pipeline is indicated in brown in Figure 1.3. The coordinates for the discharge are Latitude: $33^{\circ} 55' 00''$; Longitude: $118^{\circ} 26' 02''$. The discharge tower has throat diameter of 17.5 ft with no velocity cap, and discharges the effluent stream vertically upward toward the sea surface. The certified maximum plant flow rate is 495.6 million gallons per day (mgd). Discharges to the outfall consist almost entirely of condenser cooling

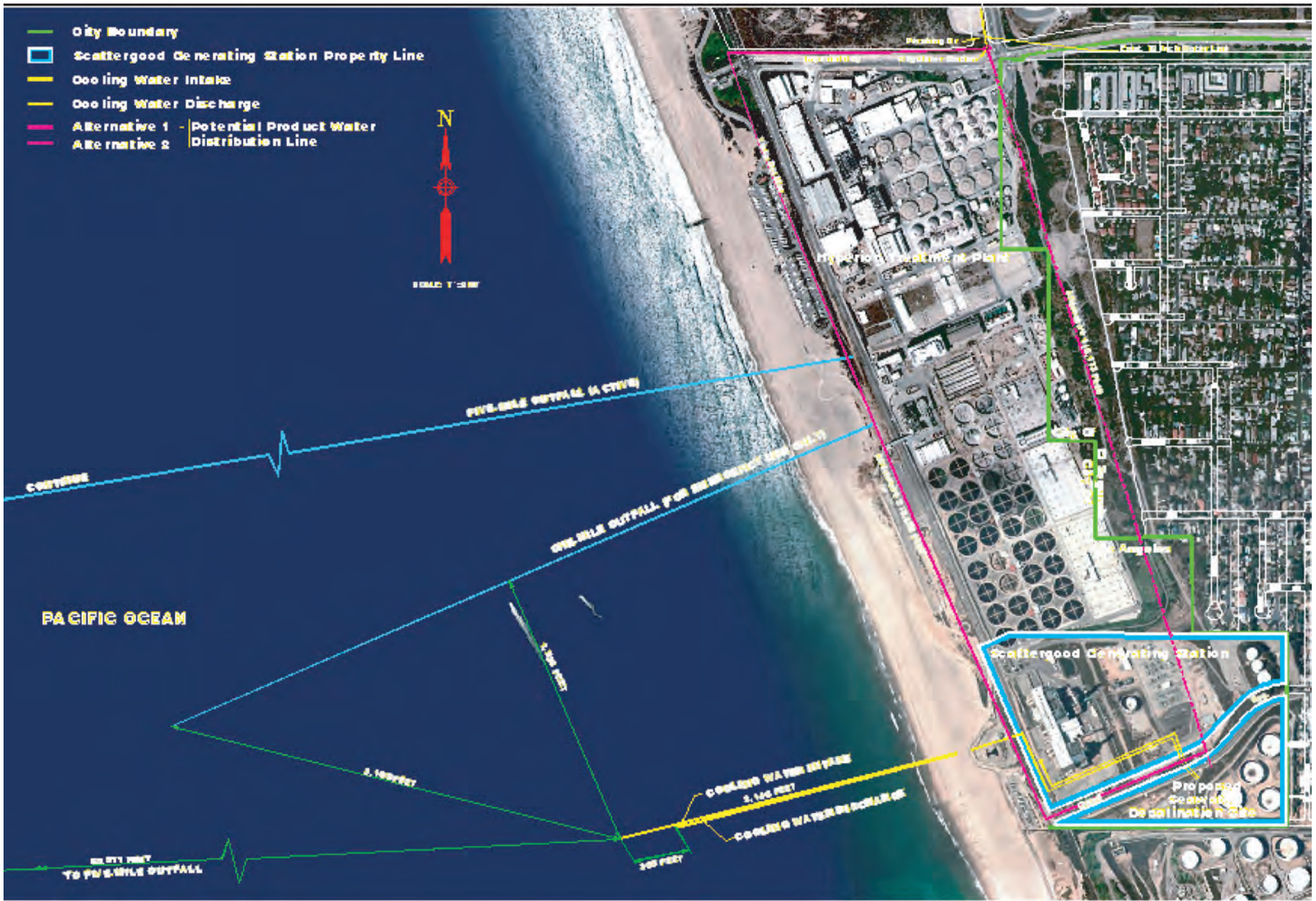
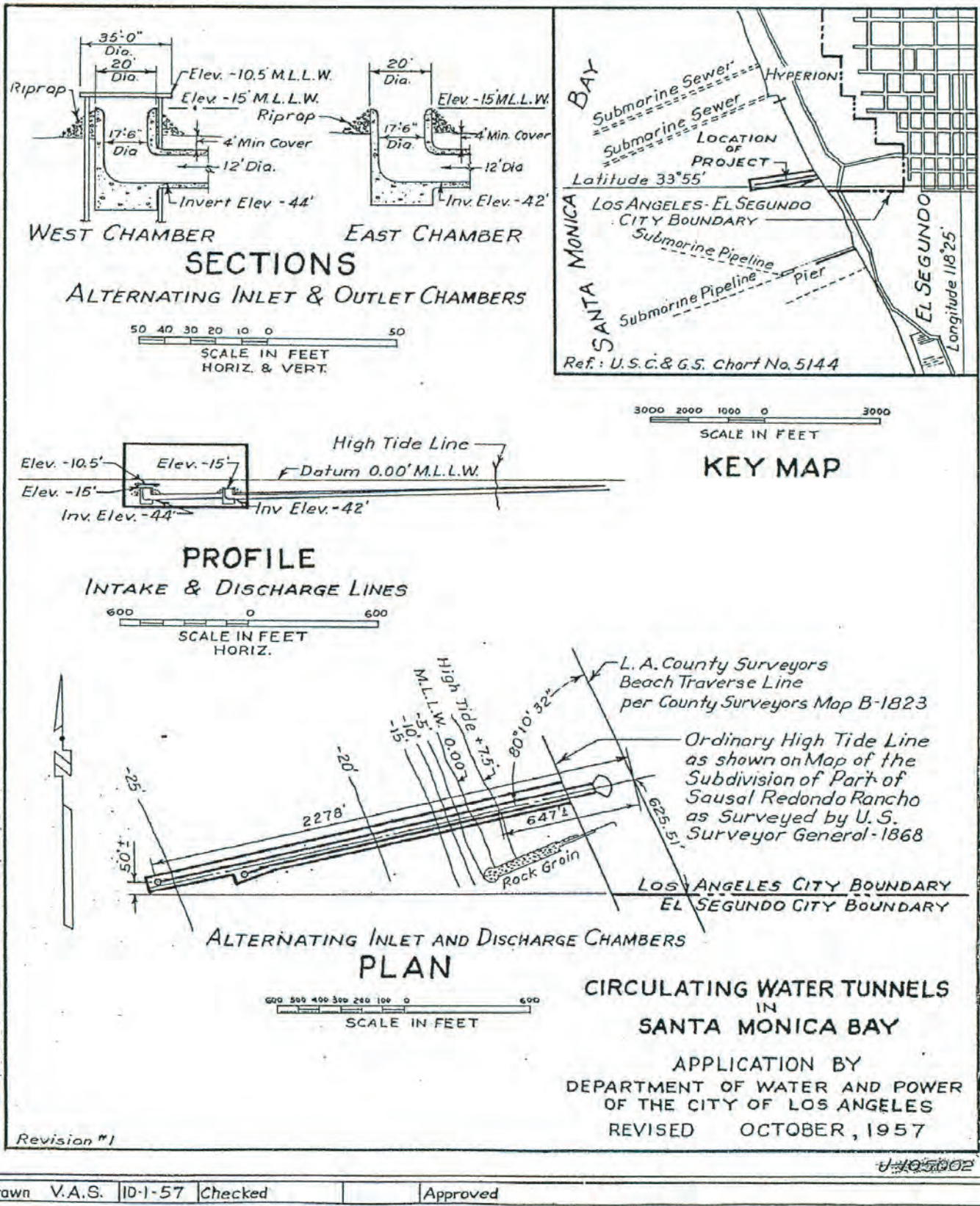


Figure 1.1. Outfall alternatives.



SD-CJ105002

Figure 1.2. As-built drawing of intake (west chamber) and discharge (east chamber) structures, Scattergood Generating Station.

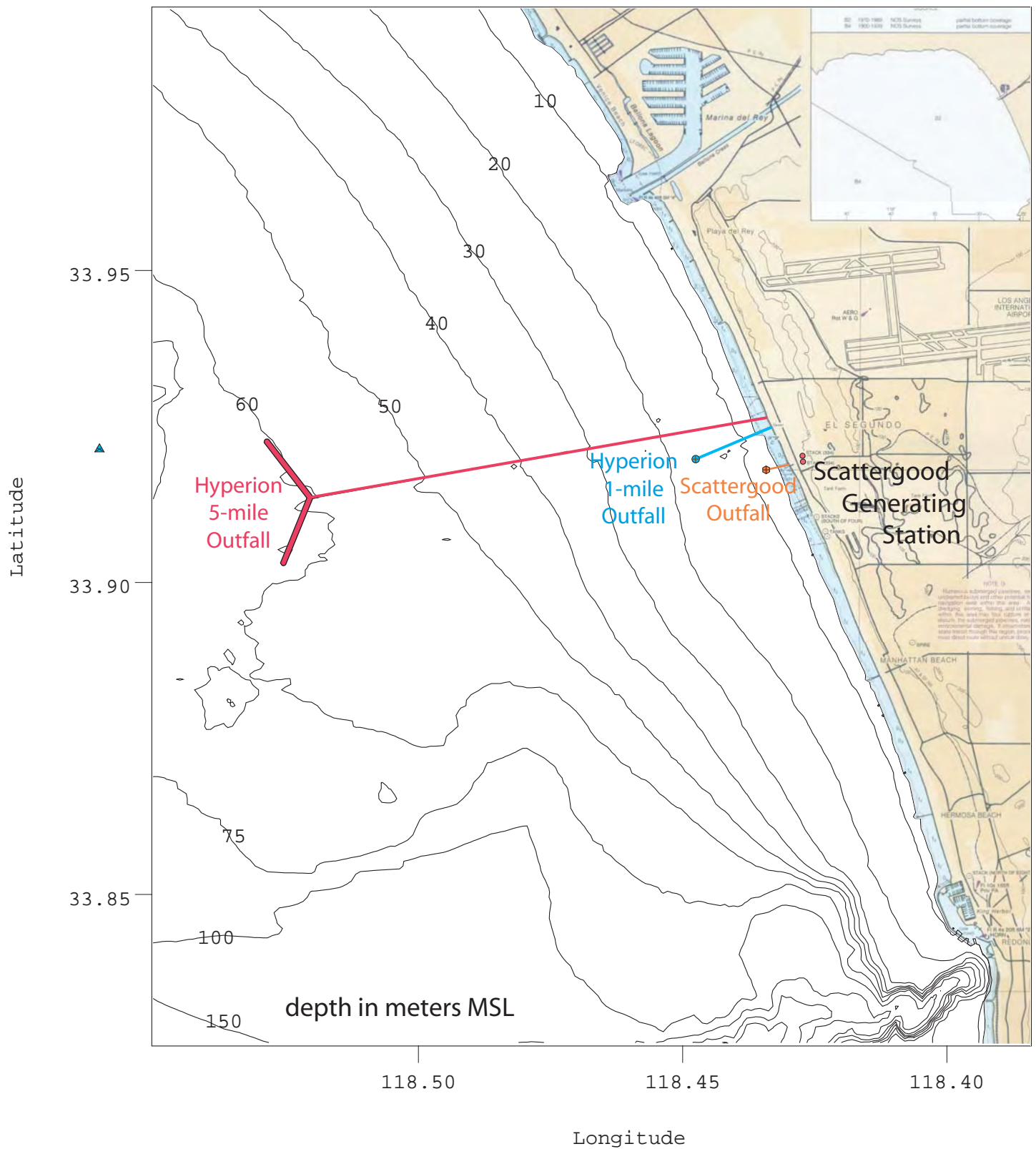


Figure 1.3. Computational grid map for hydrodynamic modeling of the LADWP Scattergood Desalination Project based on NOS digital bathymetry (NIMA, 2004).

water. A small amount of in-plant waste streams are discharged into the condenser cooling water. The Scattergood cooling water discharge is one of three discharge options shown in Figure 1.3 that is being considered herein for disposal of the brine by-product from the proposed desalination plant.

The other two discharge options being considered for the LADWP Desalination Project at Scattergood are the 1-mile and 5-mile Hyperion Treatment Plant outfalls indicated in blue and red, respectively, in Figure 1.3. Physical specifications on these two outfalls are summarized in Table-1. The 1-mile outfall was brought into service in 1951, but is presently used only on an emergency basis during peak wet weather flows with a flow rate capacity of 600 mgd. The 1-mile outfall consists of a 12 ft diameter reinforced concrete pipeline that discharges through a diffuser located at a depth of 50 ft MLLW in Santa Monica Bay, approximately 5,384 offshore of the mean tide line (Stillwell and Kwan, 1996). The coordinates for the seaward end of the 1-mile outfall diffuser are Latitude: $33^{\circ} 55' 10.2''$; Longitude: $118^{\circ} 27' 2.5''$. The diffuser is a linear type that is 300 ft long and 12 ft in diameter with 4 elliptic bulkhead ports and 6 elliptic side ports that each measure 3.25 ft by 1.5 ft, providing an initial dilution ratio of 13 to 1, (CRWQCB, 1994). The 5-mile Hyperion outfall was put into service in 1960 and has a certified flow rate of 765 mgd. It consists of a 12 ft diameter main pipeline section with two diffuser legs extending in a Y-pattern from the end of the pipeline at a distance of 27,539 from the shoreline (Figures 1.3 and 1.4). The diffuser is located at an average discharge depth of 190 ft MLLW, and the coordinates for the two seaward ends of its Y-shaped legs are Latitude: $33^{\circ} 55' 29.1''$; Longitude: $118^{\circ} 32' 3.6''$ and Latitude: $33^{\circ} 54' 20.1''$; Longitude: $118^{\circ} 32' 3.4''$. Each of the diffuser legs measures 4,000 ft in length and is constructed of 8.5

**Hyperion Treatment Plant
Five-Mile Ocean Outfall and Diffuser**

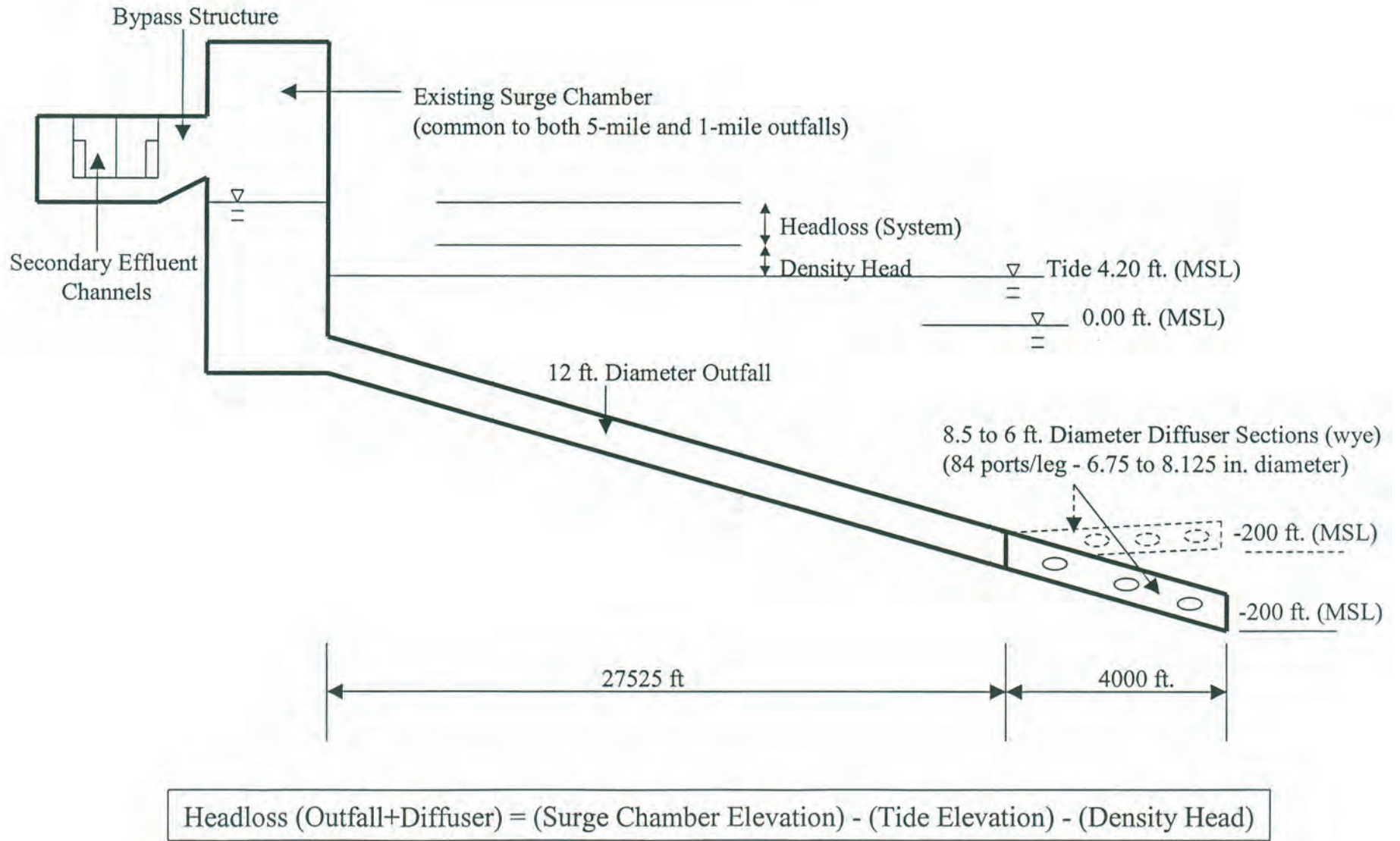


Figure 1.4. Schematic of hydraulics of Hyperion 5-mile outfall.

Table 1. Hyperion Treatment Plant Ocean Outfall Data

[from Stillwell & Kwan, 1996]

Characteristic	5-Mile Outfall	1-Mile Outfall
Outfall diameter	12 feet	12 feet
Outfall pipe material	Precast Concrete	Precast Concrete
Length	27,539 feet	5,384 feet
Discharge depth	190 feet	50 feet
Diffuser diameter	8.5 feet, 6 feet	12 feet
Length of diffuser	2 @ 4000 feet each	1 @ 300 feet
Diffuser ports	83 each	4-bulkhead ports; 6-side ports
Port size	6.75 to 8.13 inches diameter	3.25 by 1.5 feet (elliptical)
Dilution ratio (from NPDES Permit)	84:1	13:1

ft. tapering to 6 ft. diameter reinforced concrete pipe with 84 circular ports varying in diameter from 8.13 inches to 6.75 inches. According to the NPDES permit (CRWQCB, 1994), the initial dilution ratio achieved by the 5-mile outfall diffuser is 84 to 1.

The physical specifications of the three outfall scenarios described above will be used to specify the gridding and boundary conditions of the hydrodynamic model as described in Sections 2 and 3. In Section 4 the hydrodynamic model will be driven by historic wave, current and wind events overlaid on the historic operational history of these outfalls to determine the potential range of variability

in the dilution of brine when the production of desalinated product water is adjusted between 12 mgd and 50 mgd.

B) Climate Variations

The California coast is subject to climate cycles of about 20-30 years duration known as the Pacific/ North American pattern (for atmospheric pressure) or the Pacific Decadal Oscillation (for sea surface temperature). A dry period extended from about 1945-1977, followed by an episodically wet period from 1978-1998 that included the occurrence of 6 strong El Niño events (Inman and Jenkins 1997; and Goddard and Graham 1997). Based on the historic duration of these cycles, 1998 was likely the end of the wet cycle of climate in California with a return to the dry climate that prevailed from 1945-1977 (White and Cayan 1998). To illustrate the historical evidence for these dry and wet climate cycles in Southern California, we evaluate the rain gage records for Santa Ana, Laguna Beach and San Diego (panel-a of Figures 1.5-1.7). These records were selected because they are the longest available in the immediate neighborhood of Scattergood that contain no gaps, and are thereby useful proxies of long term climate for the local service area. The records were analyzed for climate trends using the Hurst (1951, 1957) procedure that was first used for determining decadal climate effects on the storage capacity of reservoirs (Inman and Jenkins, 1999). Climate trends become apparent when the data are expressed in terms of cumulative residuals Q_n taken as the continued cumulative sum of departures of annual values of a time series Q_i from their long term mean value Q_a such that $Q_n = \sum_0^n (Q_i - Q_a)$ where n is the sequential value of the time series.

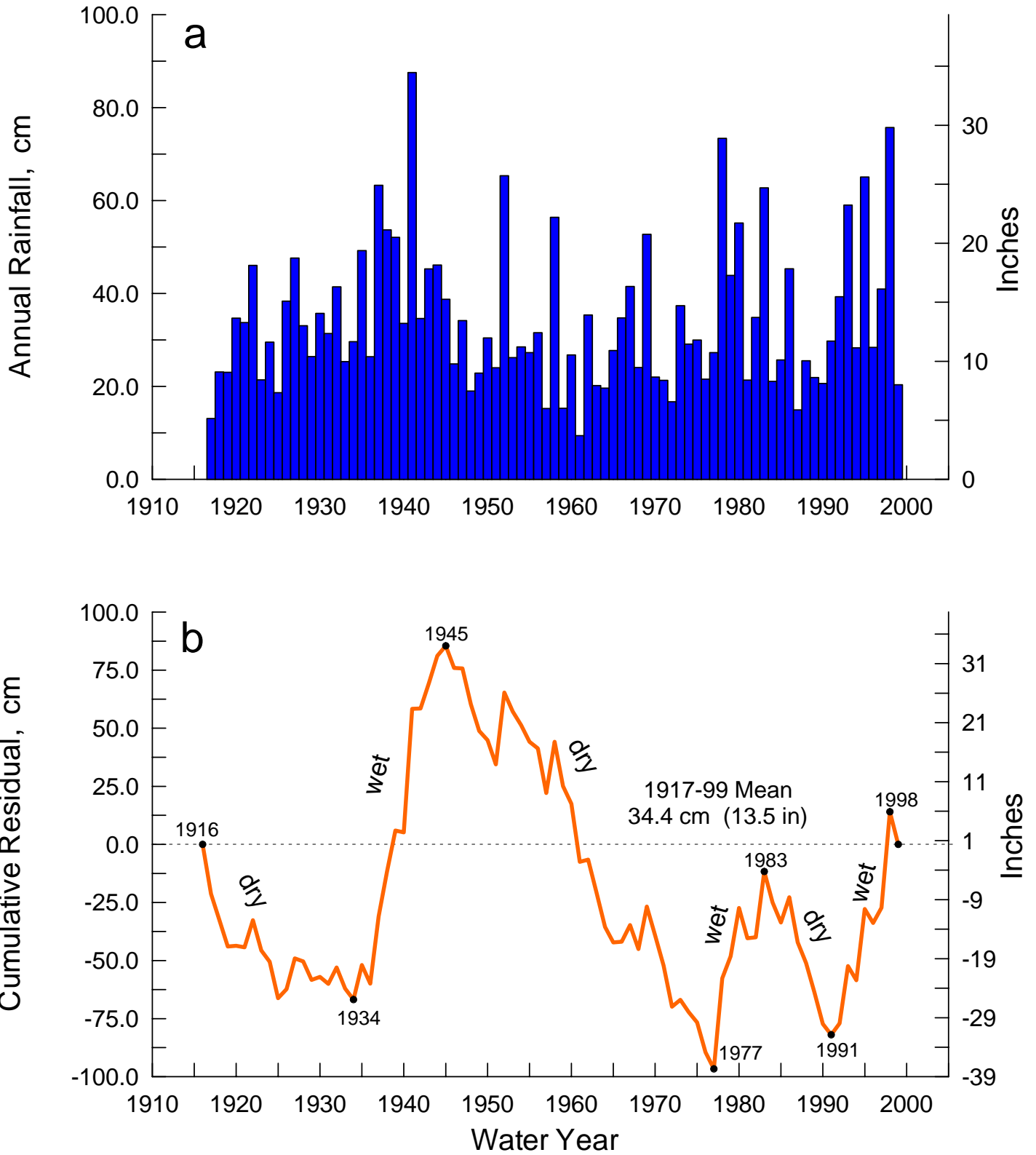


Figure 1.5. a) Total record of annual rainfall, Santa Ana, CA (National Weather Service) and b) Cumulative residual of the annual rainfall for the the period 1917-1999.

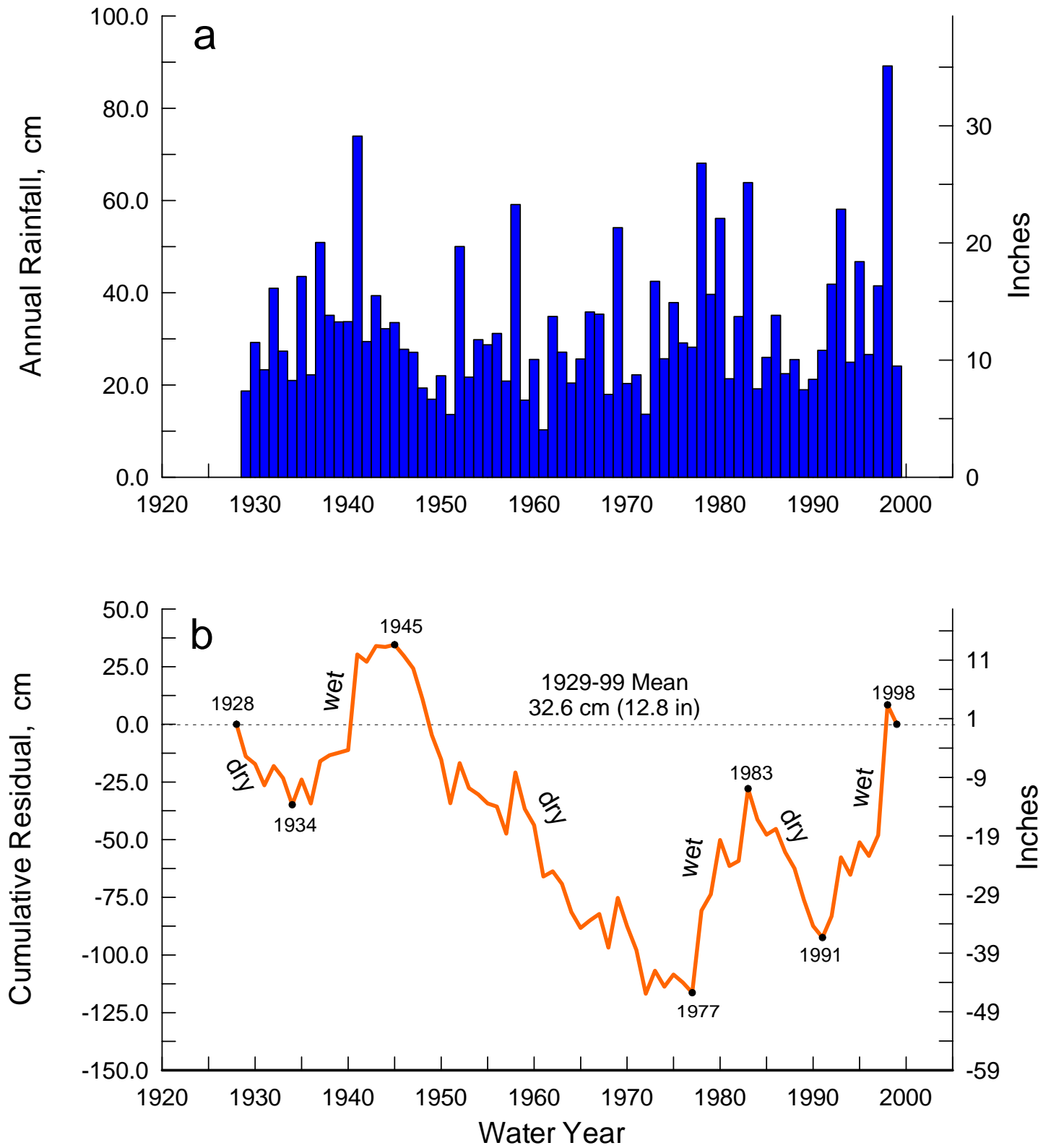


Figure 1.6. a) Total record of annual rainfall, Laguna Beach, CA (National Weather Service) and b) Cumulative residual of the annual rainfall for the the period 1929-1999.

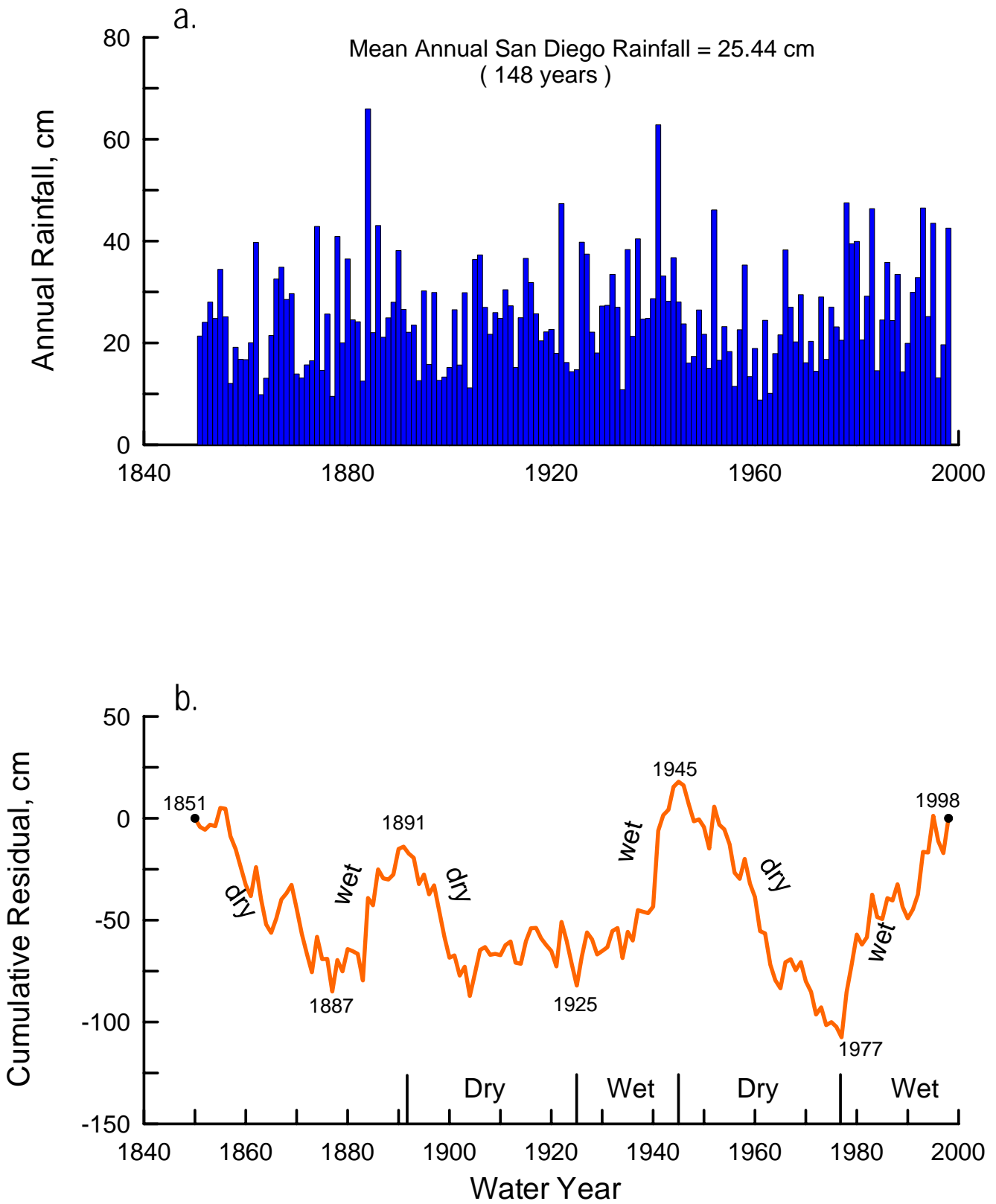


Figure 1.7. Annual rainfall histogram (a) and cumulative residual (b) for the city of San Diego, California.

The records for the total period of rainfall and their cumulative residual graphs are shown in Figures 1.5-1.7. All records show decadal scale climate changes (panel-b of Figures 1.5-1.7). Dry periods are shown by segments of the cumulative residuals having negative (downward) slopes while the wet periods have positive (upward) slopes. A dry period is found in all three records from 1945-1997, (negative slopes) while a wet period (positive slope) is shown from 1978-1998. The wet period of the climate cycle is more irregular caused by 6 strong El Niño events (water years 1978, 80, 83, 93, 95, and 98) and one 4 year period (1987-1990) of low rainfall.

The analysis shows that the average annual rainfall increased by about 38% from the dry to the wet portions of the cycle. Furthermore, both the minimum and maximum ranges in rainfall are higher in the wet period, while the averages of the 6 major rainfall events in 21 year periods before and after the climate change (1977/78) are about 8 to 9 inches greater during the wet period. Therefore, the expected transition back into the dry period for the next 20-30 years is likely to reduce the rates of ground water recharge and in terminal storage levels of Southern California reservoirs. The development of alternative fresh water sources such as the proposed desalination project at LADWP Scattergood is likely to prove extremely timely while addressing a significant societal need.

The physical effect on the ocean environment within the Southern California Bight due to sea water desalination is in principle no different than the effects of evaporation. CalCOFI ocean surveys of the Southern California Bight have measured evaporative losses at 93.4 cm/yr (Roemmich, 1989; Bograd, et. al., 2001). The surface area of coastal waters inside the continental margin of the

Southern California Bight is 160,000 km². Factoring evaporation rate over surface area, it is concluded that the coastal ocean of the Southern California Bight loses 1.49 x 10¹¹ m³ of pure water constituent to evaporation each year. In contrast, a desalination plant producing product water at a rate of 50 mgd will extract 6.9 x 10⁷ m³ of pure water constituent from the coastal ocean in one year's time, (but even then, only if it were operated continuously without any down time for maintenance). Consequently, it would take 2,163 desalination plants the size of the Scattergood project to match the evaporative losses from the ocean that occur naturally in the Southern California Bight each year.

SECTION 2: MODEL DESCRIPTION AND CAPABILITIES

2) Model Description and Capabilities

This study addresses the concerns of desalination plant production levels and brine dilution in the receiving waters by utilizing a coupled set of numerical tidal and wave transport models. The numerical model used to simulate tidal currents in the nearshore and shelf region of Santa Monica Bay near Scattergood is the finite element model **TIDE_FEM** (Appendix-A). Wave-driven currents are computed from the shoaling wave field by a separate model, **OCEANRDS** (Appendix-B). The dispersion and transport of concentrated seawater and storm water discharge by the wave and tidal currents is calculated by the finite element model known as **SEDXPORT** (Appendix-C). The “wiring-diagram” showing the architecture for how these models were coupled together is shown in Figure 2.1.

The finite element research model, **TIDE_FEM**, (Jenkins and Wasyl, 1990; Inman and Jenkins, 1996) was employed to evaluate the tidal currents in a nearshore region surrounding the three outfall options (Figure 1.3). **TIDE_FEM** was built from some well-studied and proven computational methods and numerical architecture that have done well in predicting shallow water tidal propagation in Massachusetts Bay (Connor and Wang, 1974) and along the coast of Rhode Island, (Wang, 1975), and have been reviewed in basic text books (Weiyan, 1992) and symposia on the subject, e.g., Gallagher (1981). The governing equations and a copy of the core portion of the **TIDE_FEM** FORTRAN code are found in Appendix-A. **TIDE_FEM** employs a variant of the vertically integrated equations for shallow water tidal propagation after Connor and Wang (1975). These are based upon the Boussinesq approximations with

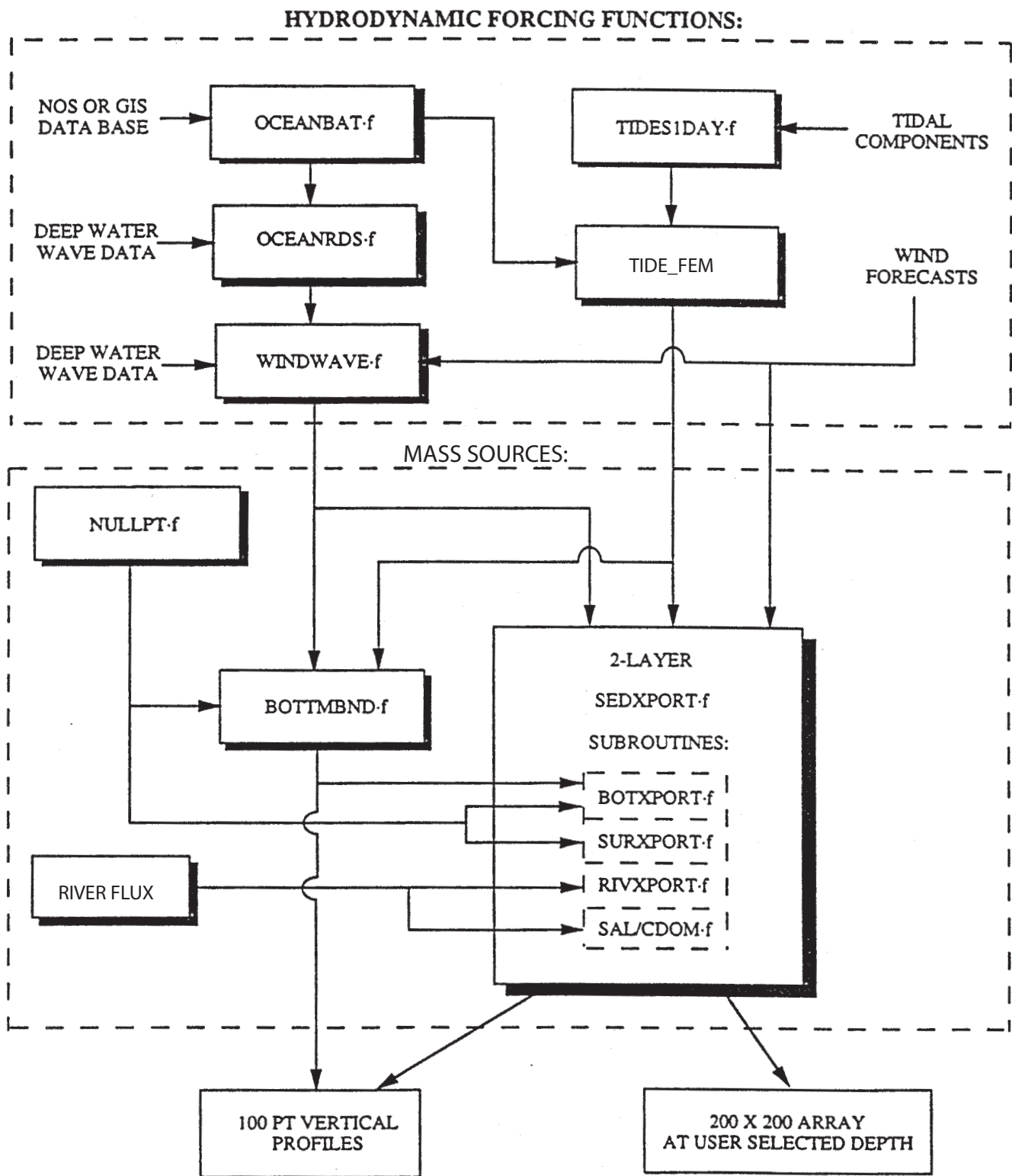


Figure 2.1. SEDXPORT architecture and computational sequence.

Chezy friction and Manning's roughness. The finite element discretization is based upon the commonly used **Galerkin weighted residual method** to specify integral functionals that are minimized in each finite element domain using a variational scheme, see Gallagher (1981). Time integration is based upon the simple **trapezoidal rule** (Gallagher, 1981). The computational architecture of **TIDE_FEM** is adapted from Wang (1975), whereby a transformation from a **global** coordinate system to a **natural** coordinate system based on the unit triangle is used to reduce the weighted residuals to a set of order-one ordinary differential equations with constant coefficients. These coefficients (**influence coefficients**) are posed in terms of a **shape function** derived from the natural coordinates of each nodal point in the computational grid. The resulting systems of equations are assembled and coded as banded matrices and subsequently solved by **Cholesky's method**, see Oden and Oliveira (1973) and Boas (1966). The hydrodynamic forcing used by **TIDE_FEM** is based upon inputs of the tidal constituents derived from Fourier decomposition of tide gage records. Tidal constituents are input into the module **TID_DAYS**, which resides in the hydrodynamic forcing function cluster (see Appendix-D for listing of **TID_DAYS** code). **TID_DAYS** computes the distribution of sea surface elevation variations at Scattergood and adjacent nearshore after compensating for phase shifts associated with travel time between the Los Angeles tide gage station (NOAA #941-0660) and Scattergood. Forcing for **TIDE_FEM** is applied by the distribution in sea surface elevation across the deep water boundary of the computational domain in Figure 1.3. Here the tidal currents reduce to the deep water solutions to Laplace's tidal equations (Lamb, 1932). The x-component (longitudinal) of the deep water tidal current is given by:

$$u_{x,\infty} = \frac{ig}{a} \left[\frac{2\Omega s \cot\theta (\xi - \bar{\xi}) + \varpi \left(\frac{d\xi}{d\theta} - \frac{d\bar{\xi}}{d\theta} \right)}{\varpi^2 - (2\Omega \cos\theta)^2} \right] \quad (1)$$

while the y-component (latitudinal) is:

$$u_{y,\infty} = \frac{g}{a} \left[\frac{s\varpi \csc\theta (\xi - \bar{\xi}) \Omega \cos\theta \left(\frac{d\xi}{d\theta} - \frac{d\bar{\xi}}{d\theta} \right)}{\varpi^2 - (2\Omega \cos\theta)^2} \right] \quad (2)$$

where θ is the co-latitude; $\bar{\xi}$ is the equilibrium tide; g is the acceleration of gravity; Ω is the angular speed of rotation of the earth, a is the mean radius of the earth; s is an integer; ϖ is the radian frequency of the potential tide as determined from the tidal constituents.

Wave driven currents were calculated from wave measurements by the CDIP arrays at Santa Monica Bay, San Pedro, Sunset Beach, Huntington Beach, Beg Rock and San Clemente, CA, see CDIP (2004). These measurements were back refracted out to deep water to correct for island sheltering effects between the monitoring sites and Scattergood. The waves were then forward refracted onshore to give the variation in wave heights, wave lengths and directions throughout the nearshore around Scattergood. The numerical refraction-diffraction code used for both the back refraction from these widely spaced monitoring sites out to deep water, and the forward refraction to the Scattergood site is **OCEANRDS** and may be found in Appendix -B. This code calculates the simultaneous refraction and

diffraction patterns of the swell and wind wave components propagating over bathymetry replicated by the **OCEANBAT-f** code, (Figure 1.3). **OCEANBAT-f** generates the associated depth fields for the computational grid networks of both **TID_FEM** and **OCEANRDS** using packed bathymetry data files derived from the National Ocean Survey (NOS) depth soundings. The structured depth files written by **OCEANBAT-f** are then throughput to the module **OCEANRDS-f**, which performs a refraction-diffraction analysis from deep water wave statistics. **OCEANRDS-f** computes local wave heights, wave numbers, and directions for the swell component of a two-component, rectangular spectrum. These values are then throughput to **WINDWAVE-f**, which completes the refraction-diffraction analysis of the two-component spectrum including wind wave effects up to Nyquist frequencies.

The wave data computed throughout the domain of Figure 1.3 are throughput to a wave current algorithm in **SEDXPORT** which calculates the wave-driven longshore currents, $v(r)$. These currents were linearly superimposed on the tidal current. The wave-driven longshore velocity, $v(r)$, is determined from the longshore current theories of Longuet-Higgins (1970), according to:

$$\begin{aligned}\bar{v}(r) &= v_o \left(\frac{10}{49} \frac{r}{X_b} - \frac{5}{7} \ln \frac{r}{X_b} \right) \text{ if } 0 \leq r \leq X_b \\ &= v_o \frac{10}{49} \left(\frac{r}{X_b} \right)^{5/2} \text{ if } r > X_b\end{aligned}\tag{3}$$

$$v_o = \frac{5\pi}{8} \frac{0.41}{C_D} (gh_b)^{1/2} \beta \sin \alpha_b$$

where r is the shoreline-normal coordinate, X_b is the width of the surf zone, taken as $X_b \equiv 5/4 H_b \tan\beta$, H_b is the breaker height from the refraction solution, $\tan\beta$ is the beach slope, α_b is the breaker angle, h_b is the breaker depth, taken as $h_b = 5/4 H_b$. C_D is the drag coefficient, and g is the acceleration of gravity. Inspection of (3) reveals that the longshore transport is strongest in the neighborhood of the breakpoint, $r = X_b$, where the longshore currents approach a maximum value of $v(r) = v_o$.

Once the tidal and wave driven currents are resolved by **TIDE_FEM**, **OCEANRDS** and **WINDWAVE**, the dilution and dispersion of concentrated seawater discharge in the receiving water is computed by the stratified transport model **SEDXPORT** (Figure 2.1). The **SEDXPORT** code is a time stepped finite element model which solves the advection-diffusion equations over a fully configurable 3-dimensional grid. The vertical dimension is treated as a two-layer ocean, with a surface mixed layer and a bottom layer separated by a pycnocline interface. The code accepts any arbitrary density and velocity contrast between the mixed layer and bottom layer that satisfies the Richardson number stability criteria and composite Froude number condition of hydraulic state.

The source loading and initial dilution mechanics of the three outfalls are handled by a companion code called **MULTINODE** that couples the computational nodes of **TIDE_FEM** and **OCEANRDS** with **SEDXPORT**. The codes do not time split advection and diffusion calculations, and will compute additional advective field effects arising from spatial gradients in eddy diffusivity, i.e., the so-called “gradient eddy diffusivity velocities” after Armi (1979). Eddy mass diffusivities are calculated from momentum diffusivities by means of a series of Peclet number corrections based upon TSS and TDS mass and upon the mixing

source. Peclet number corrections for the surface and bottom boundary layers are derived from the work of Stommel (1949) with modifications after Nielsen (1979), Jensen and Carlson (1976), and Jenkins and Wasyl (1990). Peclet number correction for the wind-induced mixed layer diffusivities are calculated from algorithms developed by Martin and Meiburg (1994), while Peclet number corrections to the interfacial shear at the pycnocline are derived from Lazara and Lasheras (1992a;1992b). The momentum diffusivities to which these Peclet number corrections are applied are due to Thorade (1914), Schmidt (1917), Durst (1924), and Newman (1952) for the wind-induced mixed layer turbulence and to Stommel (1949) and List, et al. (1990) for the current-induced turbulence. The primitive equations for the **SEDXPORT** code may be found in Appendix-C and in Appendix-E for **MULTINODE**.

In its most recent version, **SEDXPORT** has been integrated into the Navy's Coastal Water Clarity Model and the Littoral Remote Sensing Simulator (LRSS) (see Hammond, et al., 1995). The **SEDXPORT** code has been validated in mid-to-inner shelf waters (see Hammond, et al., 1995; Schoonmaker, et al., 1994). Validation of the **SEDXPORT** code was shown by three independent methods: 1) direct measurement of suspended particle transport and particle size distributions by means of a laser particle sizers; 2) measurements of water column optical properties; and, 3) comparison of computed stratified plume dispersion patterns with LANDSAT imagery. An example of the resolution of plumes by the **SEDXPORT** model is shown in Figure 2.2 for the Santa Margarita River. In this figure the isocontours of suspended sediment concentrations computed by **SEDXPORT** (red lines) are overlaid on the LANDSAT image. The colored

Comparison

Suspended Particulate--LANDSAT RGB Image

Modeled Concentration Contours (Log10)

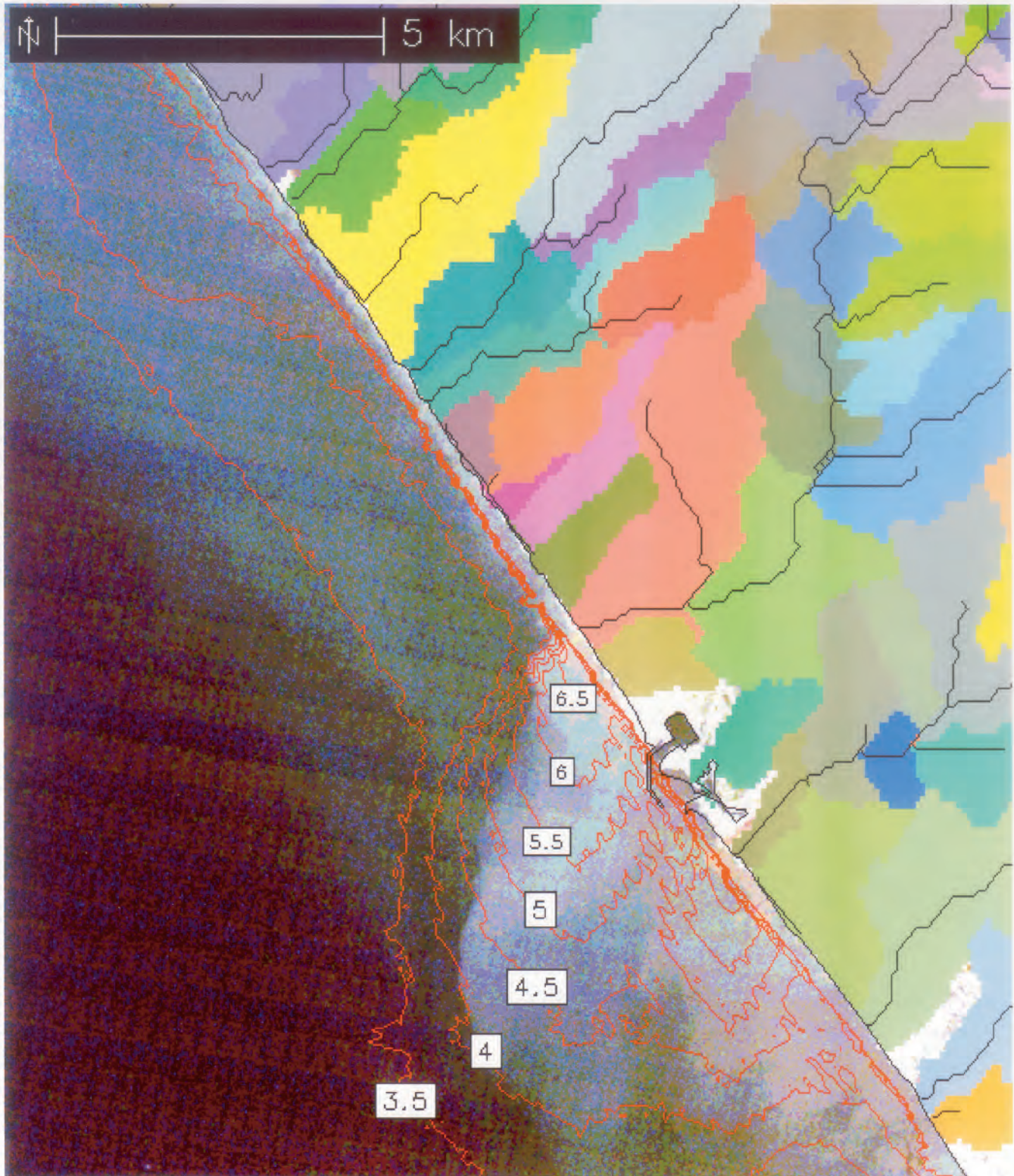


Figure 2.2. Comparisons of the SEDXPORT plume model with a LANDSAT image of the Santa Margarita River discharge on January 23, 1993. Modeled sediment concentration contours are expressed in base-10 log scale of particle number per ml. The color patchwork on the land denotes drainage basins of local streams.

patchwork on the land delineate the primary and secondary drainage basins of streams discharging into the nearshore following the storm of 23 January 1993.

Besides being validated in coastal waters of Southern California, the **SEDXPORT** modeling system has been extensively peer reviewed. Although some of the early peer review was confidential and occurred inside the Office of Naval Research and the Naval Research Laboratory, the following is a listing of 5 independent peer review episodes of SEDXPORT that were conducted by 8 independent experts and can be found in the public records of the State Water Resources Control Board, the California Coastal Commission and the City of Huntington Beach.

1997- Reviewing Agency: State Water Resources Control Board

Project: NPDES 316 a/b Permit renewal, Encina Power Plant,
Carlsbad, CA

Reviewer: Dr. Andrew Lissner, SAIC, La Jolla, CA

1998- Reviewing Agency: California Coastal Commission

Project: Coastal Development Permit, San Dieguito Lagoon
Restoration

Reviewers: Prof. Ashish Mehta, University of Florida, Gainesville
Prof. Paul Komar, Oregon State University, Corvallis
Prof. Peter Goodwin, University of Idaho, Moscow

2000- Reviewing Agency: California Coastal Commission

Project: Coastal Development Permit, Crystal Cove Development

Reviewers: Prof. Robert Wiegel, University of California, Berkeley

Dr. Ron Noble, Noble Engineers, Irvine, CA

2002- Reviewing Agency: California Coastal Commission

Project: Coastal Development Permit, Dana Point Headland Reserve

Reviewers: Prof. Robert Wiegel, University of California, Berkeley

Dr. Richard Seymour, University of California, San Diego

2003- Reviewing Agency: City of Huntington Beach

Project: EIR Certification, Poseidon Desalination Project

Reviewer: Prof. Stanley Grant, University of California, Irvine

SEDXPORT has been built in a modular computational architecture (Figure 2.1). The modules are divided into two major clusters: 1) those which prescribe hydrodynamic forcing functions; and, 2) those which prescribe the mass sources acted upon by the hydrodynamic forcing to produce dispersion and transport. The cluster of modules for hydrodynamic forcing ultimately prescribes the velocities and diffusivities induced by wind, waves, and tidal flow for each depth increment at each node in the grid network.

The lower set of modules in Figure 2.1 compute the mixing and transport induced by the forcing functions acting on mass sources, including the concentrated seawater discharged from the RO process. The subroutine **BOTXPORT-f** in **SEDXPORT-f** solves for the mixing and advection of the

negatively buoyant concentrated seawater in response to the wave and tidal flow using an rms vorticity-based time splitting scheme. The subroutine **RIVXPORT-f**, performs a similar computation on the positively buoyant storm water and treated effluent from Hyperion. Both **BOTXPORT** and **RIVXPORT** solve the eddy gradient form of the advection diffusion equation for the water column density field:

$$\frac{\partial \rho}{\partial t} = (\mathbf{u} - \nabla \epsilon) \cdot \nabla \rho - \epsilon \nabla^2 \rho \quad (4)$$

where \mathbf{u} is the vector velocity from a linear combination of the wave and tidal currents, ϵ is the mass diffusivity and ρ is the water mass density. The water mass density is a function of temperature, T , and salinity, S , according to the equation of state expressed in terms of the specific volume, $\alpha = 1/\rho$, or:

$$\frac{d\alpha}{\alpha} = \frac{1}{\alpha} \frac{\partial \alpha}{\partial T} dT + \frac{1}{\alpha} \frac{\partial \alpha}{\partial S} dS \quad (5)$$

The factor $\partial\alpha/\partial T$, which multiplies the differential temperature changes, is known as the coefficient of thermal expansion and is typically 2×10^{-4} per °C for seawater; the factor $\partial\alpha/\partial S$ multiplying the differential salinity changes, is the coefficient of saline contraction and is typically 8×10^{-4} per part per thousand (ppt) where 1.0 ppt = 1.0 g/L of total dissolved solids (TDS). For a standard seawater, the specific volume has a value $\alpha = 0.97264$. If the percent change in specific volume by equation (5) is less than zero, then the new water mass is heavier than standard seawater, and lighter if the percent change is greater than zero. Solutions to the

density field calculated from equation (1) by **SEDXPORT** are used to calculate the field salinity, $S_{(x,y,z)}$, from equation (5) for an assumed T for the ambient ocean and river water and ΔT for plant thermal effluent. The salinity field in turn can be used to solve for the spacial varying dilution factor, $D_{(x,y,z)}$ according to:

* Hyperion Storm Water and Treated Effluent Dilution:

$$D_{(x,y,z)} = \frac{S_o}{S_o - S_{(x,y,z)}} \quad (6)$$

** Concentrated Seawater (Brine) Dilution:

$$D_{(x,y,z)} = \frac{S_b - S_o}{S_{(x,y,z)} - S_o} \quad (7)$$

where S_o is the ambient seawater salinity in ppt, S_b is the end-of-the-pipe salinity of concentrated seawater and $S_{(x,y,z)}$ is the local salinity from the model solution in ppt. Model solutions will find a significant variation in the salinity with water depth, z . Therefore we introduced a depth averaged dilution factor,

$$\bar{D}_{(x,y,z)} = \frac{1}{H_{(x,y)}} \int_0^H D_{(x,y,z)} dZ \quad (8)$$

where $H = H_{(x,y)} = h + \eta$ is the local water depth, h is the local water depth below mean sea level and η is the tidal amplitude.

The diffusivity, ϵ , in equation (4) controls the strength of mixing and dilution of the concentrated seawater and flood water constituents, and varies with position in the water column relative to the pycnocline interface. Vertical mixing includes two mixing mechanisms at depths above and below the pycnocline: 1) fossil turbulence from the bottom boundary layer, and 2) wind mixing in the surface mixed layer. The pycnocline depth is treated as a zone of hindered mixing and varies in response to the wind speed and duration. Below the pycnocline, only turbulence from the bottom wave/current boundary layer contributes to the local diffusivity. Nearshore, breaking wave activity also contributes to mixing. The surf zone is treated as a line source of turbulent kinetic energy by the subroutine **SURXPORF**. This subroutine calculates seaward mixing from fossil surf zone turbulence, and seaward advection from rip currents embedded in the line source. Both the eddy diffusivity of the line source and the strength and position of the embedded rip currents are computed from the shoaling wave parameters evaluated at the breakpoint, as throughput of **OCEANRDS-f**.

SECTION 3: MODEL INITIALIZATION

3) Model Initialization

Altogether there are eight primary variables that enter into a solution for the simultaneous dispersion and dilution of the waste heat from the generating station and concentrated seawater from the desalination plant. These eight variables may be organized into *forcing functions* and *boundary conditions*. The forcing function variables affect the strength of ocean mixing, ventilation and available dilution volume in shallow water. These include:

- * Waves
- * Ocean Water Levels (tides and sea level anomalies)
- * Currents
- * Winds.

The boundary condition variables control the source strength (concentrated sea salts) and background conditions. Some of these change daily (primary boundary conditions) while others vary slowly in time (stationary boundary conditions). The primary boundary conditions are:

- * Power Plant Flow Rates
- * Ocean Salinity
- * Power Plant Discharge Temperature
- * Ocean Temperature

Storm water flows represent boundary conditions that also vary daily, but their effect on the receiving water is captured by the daily ocean salinity data. The stationary boundary conditions are the local bathymetry, that typically has seasonal variation inshore of closure depth (about 15 m depth). In the following sub-

sections, overlapping 20 year long records for each of the eight controlling variables are reconstructed. These long-term records contain 7,276 to 7,523 consecutive days of daily mean values between 1980 and 2000, depending on the number of unfilled data gaps.

Long-term monitoring of ocean properties in the coastal waters surrounding Scattergood has been on going for about 30 years as required for compliance with NPDES permits for the three ocean outfalls (CRWQCB, 199, 2000). These data were accessed from the NPDES monitoring reports that are periodically released and filed with the Regional Water Quality Control Board. In attempting to reconstruct 20-year long, continuous, unbroken records of all eight controlling variables for the dilution and dispersion modeling problem, certain gaps were found in some of the data bases. These gaps were filled by using ocean data measured at CDIP monitoring sites in Santa Monica Bay, San Pedro, Sunset Beach, Huntington Beach, Beg Rock and San Clemente, CA, see CDIP (2004). Any remaining gaps that could not be filled by these most immediate neighbors were filled by monitoring data from the Scripps Pier in La Jolla, about 90 miles to the southeast of Scattergood . The Scripps Pier site has many physical features in common with the nearshore area around Scattergood. Both sites have a submarine canyon nearby. Consequently internal waves are an active mechanism at both sites in causing daily (diurnal) variations in salinity, temperature, and other ocean properties. The longer period variations at seasonal and multiple year time scales are the same at both sites due to their proximity. Consequently the Scripps Pier Shore Station data (SIO, 2001) and the Coastal Data Information Program monitoring at Santa Monica Bay, San Pedro, Sunset Beach and Huntington Beach, (CDIP, 2004) are reasonable surrogates to fill gaps in the NPDES data for the

Scattergood and Hyperion outfalls. These properties will be shown to exhibit considerable natural variability over the period of record from 1980 to mid 2000 due to daily and seasonal changes, but most especially due to climate changes of global scale.

A) Seasonal and Climate Effects on Controlling Variables

The seasonal variations in the exposure of the hemispheres to the sun produce inter-annual changes in the duration of daylight and the angle of the sun's irradiance. These effects modulate solar heating, resulting in the inter-annual variation of the earth's atmospheric pressure field which in turn introduces seasonal climatic effects. Inter-annual variations are enhanced by the higher convective effects of land and the greater concentration of land mass relative to water in the temperate latitudes of the northern hemisphere.

Upon occasion the typical seasonal weather cycles are abruptly and severely modified on a global scale. These intense global modifications are signaled by anomalies in the pressure fields between the tropical eastern Pacific and Malaysia known as the *El Niño/Southern Oscillation* (ENSO) (e.g., Diaz & Markgraf, eds., 1992). The intensity of the oscillation is often measured in terms of the *Southern Oscillation Index* (SOI), defined as the monthly mean sea level pressure anomaly in mb normalized by the standard deviation of the monthly means for the period 1951-1980 at Tahiti, minus that at Darwin, Australia. A negative SOI (lower pressure at Tahiti, higher pressure at Darwin) is known as an *El Niño* or warm ENSO event, because of the arrival of unusually warm surface water off the coast of Peru at the time of Christmas; hence, the term El Niño. Warm water also occurs along the coast of California and both regions experience unusually heavy rainfall.

A positive SOI is known as *La Niña* and it signals the occurrence of colder than normal surface water in the eastern Pacific, but stronger southwest monsoons in the Indian Ocean with heavy rainfall in India and in the Ethiopian plateau.

ENSO events occur about every 3 to 7 years with dominant spectral peaks at about 3 and 6 plus years. However these ENSO events may induce climate changes that occur on decadal time scales of one quarter to one half century. These changes are often discussed in terms of two atmospheric patterns (PNA, NAO) and a sea surface temperature pattern (PDO). Both PNA and PDO are long period (i.e., inter-decadal) analogs of the seasonal (inter-annual) variations of global pressure and temperature, while NAO is an intensification and relaxation of the January phase of the inter-annual variation. They are aliased by the inter-annual changes because they have the same structure and appear as extreme cases of the inter-annual patterns. This aliasing has delayed the general understanding and acceptance of these concepts.

The Pacific/North American (PNA) pattern is associated with an atmospheric dipole in pressure anomaly over the Pacific Ocean/North America region whose polarity reversals lead to wet and dry climate along the Pacific coast of North America (Wallace & Gutzler, 1981). High pressure anomaly over the North Pacific Ocean and low pressure anomaly over the North American Continent result in dry (*La Niña*) climate along the coast of central and southern California; while the opposite polarity in these longitudinal (zonal) dipole patterns leads to wet (*El Niño*) climate. Inman & Jenkins (1999) show that the coastal rivers of central and southern California have streamflow and sediment fluxes during the wet phase of PNA (1969-1995) that exceed those during the preceding dry phase (1944-1968) by factors of 3 and 5 respectively.

The Pacific (inter) Decadal Oscillation (PDO) is a sea surface temperature pattern associated with the La Niña/El Niño phases of ENSO cycles, with the leading pattern of PDO situated in the tropical Pacific Ocean (Goddard & Graham, 1997; Mantua et al., 1997). The El Niño phase of the PDO cycle is characterized by a weakening of the trade winds that results in an eastward movement (slosh) of the warm pool of equatorial water normally contained in the western Pacific by the trades during La Niña conditions. The stronger trade wind systems during the La Niña phase of PDO are part of a general spin-up of the atmospheric circulation which causes the North and South Pacific Gyres to rotate faster. Both effects (wind and current) induce upwelling that maintains cold water masses along the west coast of the Americas, which sustains the typically cool dry coastal climate of these regions during the La Niña dominated periods of the PDO and PNA.

B) Bathymetry

Bathymetry provides a controlling influence on all of the coastal processes that affect dispersion and dilution. The bathymetry consists of two parts: 1) a stationary component in the offshore where depths are roughly invariant over time, and 2) a non-stationary component in the nearshore where depth variations do occur over time. The stationary bathymetry generally prevails at depths that exceed closure depth which is the depth at which net on/offshore transport vanishes. Closure depth is typically -12 m to -15 m MSL in the Santa Monica Littoral Cell, see Figure 3.1, [Inman et al. 1993]. The stationary bathymetry was derived from the National Ocean Survey (NOS) digital database. Gridding is by latitude and longitude with a 3 x 3 arc second grid cell resolution yielding a

computational domain of 30.9 km x 18.5 km. Grid cell dimensions along the x-axis (longitude) are 77.2 meters and 92.6 meters along the y-axis (latitude).

For the non-stationary bathymetry data inshore of closure depth (less than - 15 m MSL) nearshore and beach surveys were conducted by the US Army Corps of Engineers in 1985, 1990, 1996 and have been compiled in Everts, 1997. These nearshore and beach survey data were used to update the NOS database for contemporary nearshore and shoreline changes that have occurred following the most recent NOS surveys. Maps of the bathymetry in the near and farfield of the three outfalls are found in Figures 1.3 and 3.1, respectively.

To perform both the required wave shoaling and transport computations in the farfield of the infall and outfall, a relatively coarse-scale resolution of the bottom bathymetry is required which gives at least two grid points per wavelength of the highest frequency wave to be shoaled. The farfield grid computes the effects of island sheltering and regional scale refraction and circulation due to the shallow banks of the continental margin (Figure 3.1). A nearfield grid is nested inside the farfield grid and is used to calculate the brine dispersion inside Santa Monica Bay (Figure 1.3).

C) Wave Climate

Waves are the principle driving mechanism of mixing and current ventilation in the very nearshore region off Scattergood. This wave dominated region consists primarily of the surfzone but extends seaward into the wave shoaling zone a few surf zone widths beyond the point of wave breaking. Waves are also the most difficult of the 8 controlling variables to get long unbroken

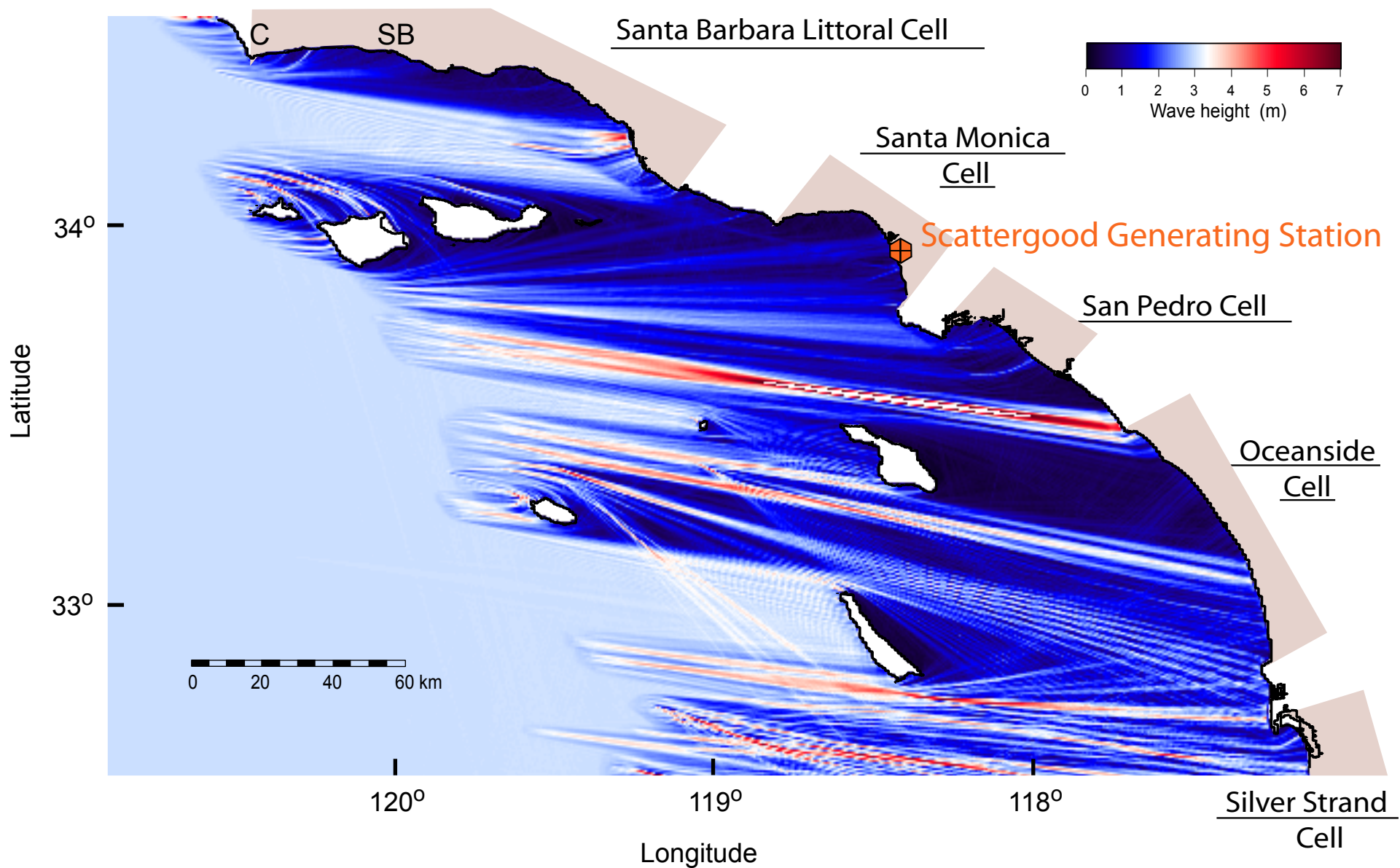


Figure 3.1. Farfield refraction / diffraction computational grid map for hydrodynamic modeling of the LADWP Scattergood Desalination Project based on NOS digital bathymetry (NIMA, 2004); storm of 13 January 1993 with 3 m high 15 sec waves, approaching Southern California Bight from 285°.

records. The availability of wave data in the lower Southern California Bight is what limited the period of record for this long term model analysis to 1980-2000. Waves have been routinely monitored at several locations in the lower Southern California Bight since 1980 by the Coastal Data Information Program, (CDIP, 2004).

In considering the wave climate of the Santa Monica Bay and the Scattergood area, the sheltering effects of the Channel Island System must be taken into account. Figure 3.1 shows that only certain gaps or “wave windows” between the islands and intervening land masses will allow the high energy, long period swells of distant storms to reach Scattergood area. Because these island sheltering effects are directionally dependent, it is not sufficient to use wave monitoring data that does not include wave direction. Wave energy and direction have been routinely monitored at several locations in the lower Southern California Bight since 1980 by the Coastal Data Information Program, (CDIP, 2004). The nearest CDIP directional wave monitoring sites are:

a) Huntington Beach Array

- Station ID: 072
- Location:
 - 33 37.9'North, 117 58.7'West
 - Approximately 1 mile west of lifeguard headquarters at Huntington Beach, CA
- Water Depth (m): 10
- Instrument Description:
 - Underwater Directional Array
- Measured Parameters:

- Wave Energy
- Wave Period
- Wave Direction

b) San Clemente

- Station ID: 052
- Location:
 - 33 25.2'North, 117 37.8'West
 - 1000 ft NW of San Clemente Pier
- Water Depth (MLLW): 10 m
- Instrument Description:
 - Underwater Directional Array
- Measured Parameters:
 - Wave Energy
 - Wave Direction

c) San Pedro

- Station ID: 092
- Location:
 - 33 37.07 N 118 19.02 W
- Water Depth (MLLW): 457 m
- Instrument Description:
 - Datawell directional buoy
- Measured Parameters:
 - Wave Energy
 - Wave Direction

d) Santa Monica Bay

- Station ID: 028
- Location:
 - 33 51.27 N 118 37.98 W
- Water Depth (MLLW): 365 m
- Instrument Description:
 - Datawell directional buoy
- Measured Parameters:
 - Wave Energy
 - Wave Direction

e) Sunset Beach

- Station ID: 027
- Location:
 - 33 42.30 N 118 4.20 W
- Water Depth (MLLW): 8 m
- Instrument Description:
 - directional array
- Measured Parameters:
 - Wave Energy
 - Wave Direction

e) Begg Rock

- Station ID: 138
- Location:
 - 33 22.80 N 119 39.80 W

- Water Depth (MLLW): 110 m
- Instrument Description:
 - buoy
- Measured Parameters:
 - Wave Energy
 - Wave Direction

These data sets possessed gaps at various times due to system failure and a variety of start ups and shut downs due to program funding and maintenance. The undivided data sets were pieced together into a continuous record from 1980-2000 and entered into a structured preliminary data file. The data in the preliminary file represent partially shoaled wave data specific to the local bathymetry around each monitoring site. To correct these data to the nearshore of Scattergood, they are entered into a refraction/diffraction numerical code, back-refracted out into deep water to correct for local refraction and island sheltering, and subsequently forward refracted into the immediate neighborhood of Scattergood. Hence, wave data off each monitoring site was used to hindcast the waves at Scattergood.

The backward and forward refractions of CDIP data to correct it to Scattergood was done using the numerical refraction-diffraction computer code, OCEANRDS. The primitive equations for this code are lengthy, so a listing of the FORTRAN codes of OCEANRDS appear in Appendix-B. These codes calculate the simultaneous refraction and diffraction patterns propagating over a Cartesian depth grid. A large outer grid (Figure 3.1) was used in the back refraction calculations to correct for island sheltering effects, while a high resolution inner grid (Figure 1.3) was used for the forward refraction over the local bay bathymetry

around the Scattergood and the Hyperion outfalls. OCEANRDS uses the parabolic equation method (PEM), Radder (1979), applied to the mild-slope equation, Berkhoff (1972). To account for very wide-angle refraction and diffraction relative to the principle wave direction, OCEANRDS also incorporates the high order PEM Pade approximate corrections modified from those developed by Kirby (1986a-c). Unlike the recently developed REF/DIF model due to Dalrymple, et al. (1984), the Pade approximates in “OCEANRDS” are written in tesseral harmonics, per Jenkins and Inman (1985); in some instances improving resolution of diffraction patterns associated with steep, highly variable bathymetry such as found near the Redondo Submarine Canyon. These refinements allow calculation of the evolution and propagation of directional modes from a single incident wave direction; which is a distinct advantage over the more conventional directionally integrated ray methods which are prone to caustics (crossing wave rays) and other singularities in the solution domain where bathymetry varies rapidly over several wavelengths.

An example of a reconstruction of the wave field throughout the Bight is shown in Figure 3.1 using the back refraction calculation of the CDIP data from the San Clemente array. Wave heights are contoured in meters according to the color bar scale and represent 6 hour averages, not an instantaneous snapshot of the sea surface elevation. Note how the sheltering effects of Catalina and San Clemente Islands have induced longshore variations in wave height throughout the Southern California Bight. Figure 3.2a shows the significant wave heights inside Santa Monica Bay, with corresponding periods and directions, resulting from the series of back-refraction calculations for the complete CDIP data set at $\Delta t = 6$ hour intervals over the 1980-2004 period of record. The data in Figure 3.2a are

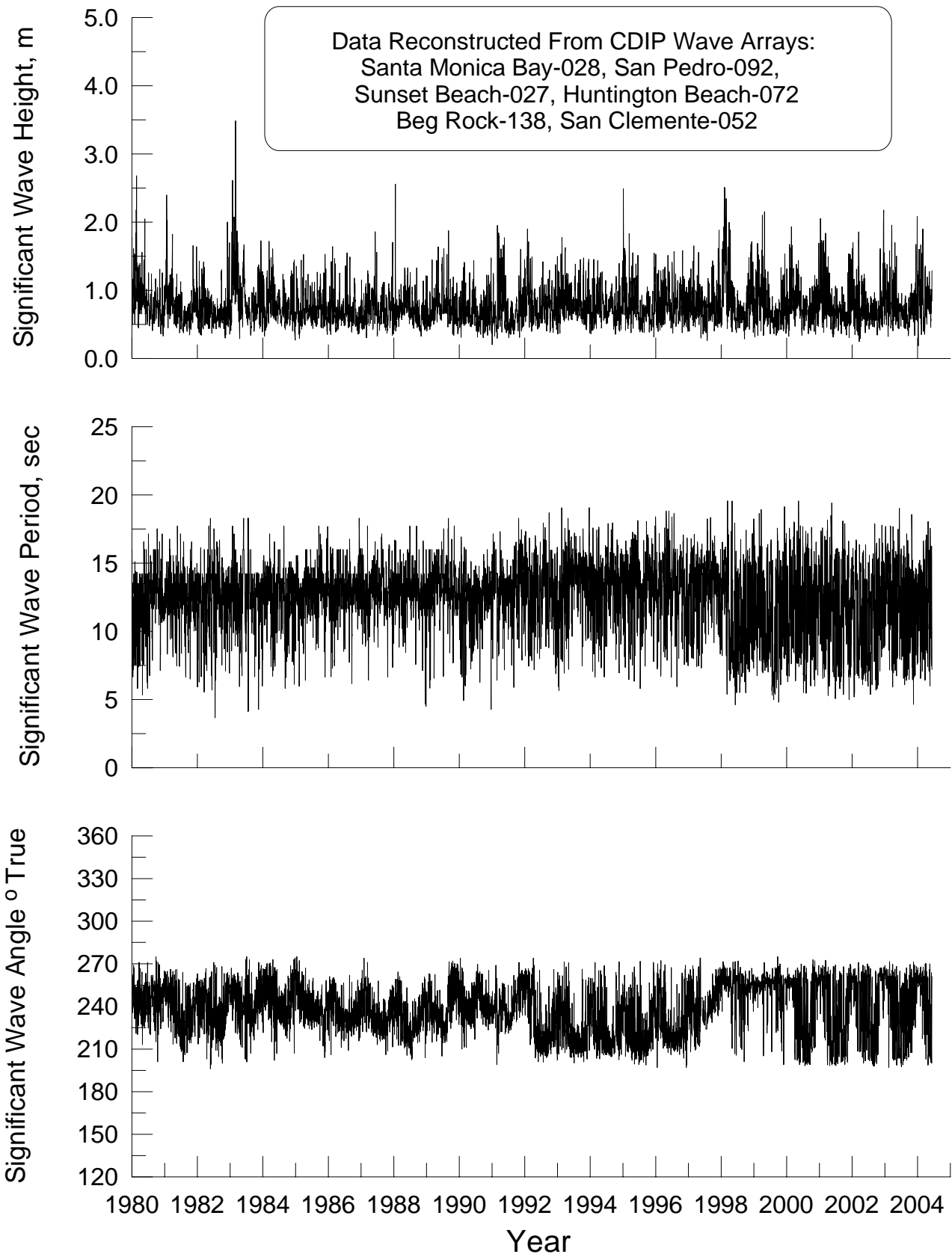


Figure 3.2a. Wave data reconstructed from farfield refraction/diffraction analysis of CDIP measurements. This data used as deep water boundary conditions on nearfield for dispersion and dilution analysis at Scattergood, CA, as shown in Figure 3.2b.

values used as the deep water boundary conditions on the nearfield grid (Figure 1.3) for the forward refraction computations into the Scattergood region. The deep water wave angles are plotted with respect to the direction (relative to true north) from which the waves are propagating at the deep water boundary of the nearfield grid (Figure 1.3). Inspection of Figure 3.2a reveals that a number of large swells lined up with the wave windows open to Scattergood during the El Niño's of 1980-83, 1986-88, 1992-95, and 1997-98. The largest of these swell events was the 1 March 1983 storm, producing 3.5 m deep water swells off Scattergood .

Figure 3.2b gives an example of the forward refraction calculation over the nearfield grid of the Scattergood region for the El Niño storm of 13 January 1993. Although the swells in deep water from this storm were 2.25 m high, we find in Figure 3.2b that the refraction effects over local bay bathymetry create areas to the south of the outfalls where wave heights increase to 4 m. In these areas, the bay bathymetry has focused the incident wave energy and these regions of intensified wave energy are referred to as "bright spots." In this case the bright spot is caused by the narrowing of the shelf in the vicinity of the Redondo Submarine Canyon. The increased wave heights in these bright spots increase the mixing and turbulence generated over the seabed boundary layer and by oscillatory wakes of the infall tower structure. This increases the mixing and dilution rates of the heavy brine that disperses along the seabed into the bright spots. Conversely, the dark areas in Figure 3.2b where wave heights have been diminished are termed "shadows," and represent areas of reduced mixing and retarded dilution rates. For the 13 January 1993 storm, the areas around the 3 outfalls are indeed shadow zones. However, one mitigating aspect of the diminished mixing in such areas is

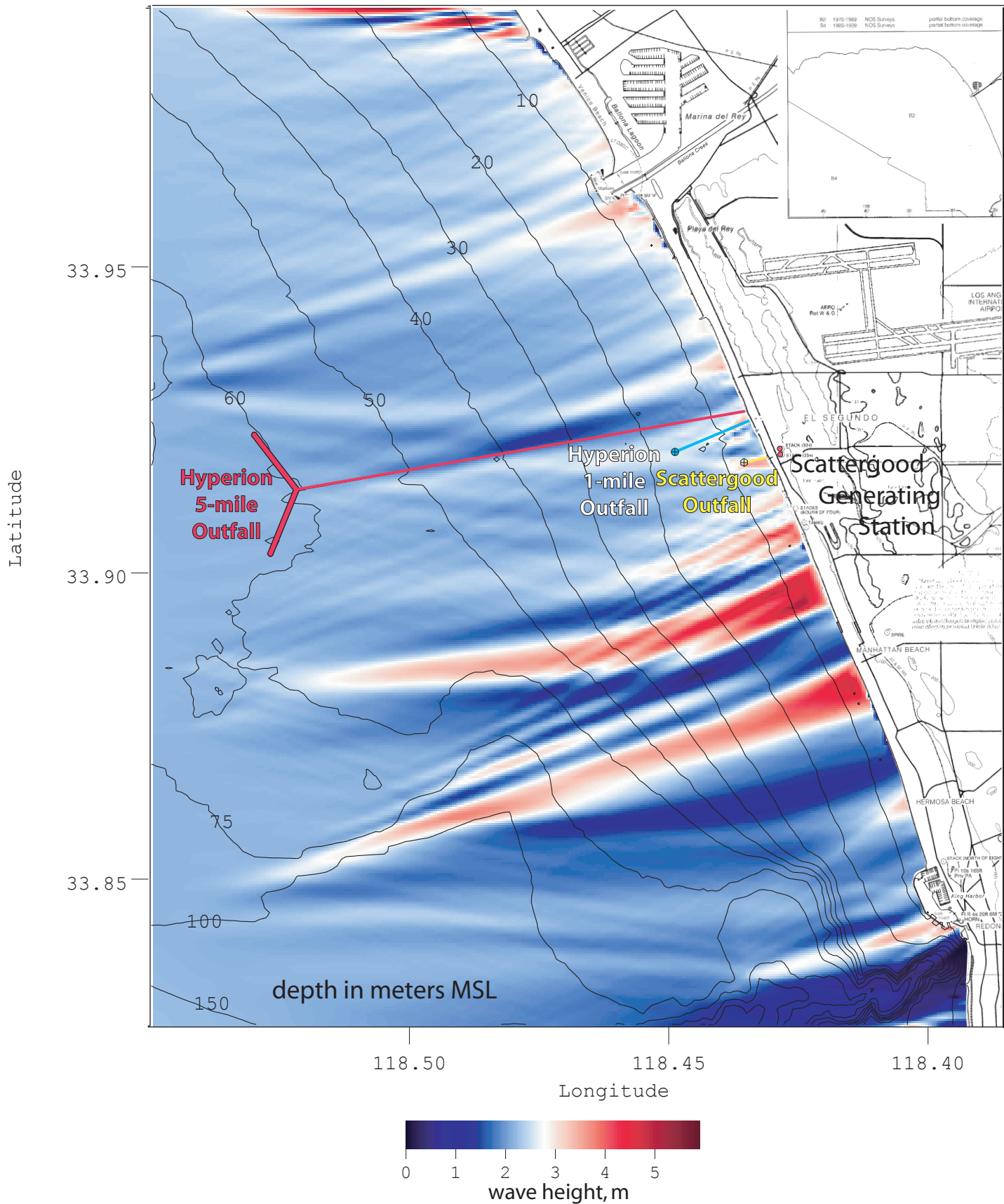


Figure 3.2b. Nearfield refraction / diffraction computation for hydrodynamic modeling of the LADWP Scattergood Desalination Project based on NOS digital bathymetry (NIMA, 2004); storm of 13 January 1993 with 2.25 m high 15 sec waves, approaching Santa Monica Bay from 265° .

the phenomena of wave-driven currents (sometimes referred to as mass transport). Refraction patterns of the type shown in Figure 3.2b were generated for 7,523 wave events between 1980 and the end of 2000, and the resulting arrays of local wave heights, periods and directions were throughput to SEDXPORT for continuous dilution modeling. Average deep water wave heights off Scattergood for this period were 2.5 ft (0.77 m).

D) Ocean Water Levels & Tidal Oscillations

The local water column depth over the outfall of the Scattergood Generating Station is nominally 17.75 feet relative to mean sea level. Spring tidal ranges can reach as high as 8.9 feet or 50 % of the water column above the outfall. Hence tides can significantly vary the local water volume around the outfall that is available for dilution. The nearest ocean tide gage station that has measured ocean water levels continuously over the long term is at Los Angeles (NOAA #941-0660). This tide gage was last leveled using the 1960-78 tidal epoch, but tide tables based on the 1960-78 tidal epoch frequently misrepresent high and low tide elevations. This is due to several factors including: 1) the long-term upward creep in eustatic sea level during the last part of the modern sea level high stand 2) seasonal warming and cooling of the ocean and 3) climate effects. Flick & Cayan (1984) have shown that seasonal warming and cooling accounts for an interannual variation in mean sea level of about 0.5 ft. El Niño or ENSO events can result in sea level anomalies of 1.0 ft. or more due to the thermal expansion effects of the coastal warm water anomalies of El Niño and by the inverse barometer effects on sea level associated with the ENSO induced North Pacific low pressure anomaly. Therefore, we base

our analysis on direct water level measurements rather than on tide table estimates.

Water levels measured by the Los Angeles Tide Gage (NOAA #941-0660) have been archived by NOAA (2000) for the preceding 20.5 year period, 1980 through mid 2000. Time series of the daily high and low ocean water levels were reconstructed from these archival measurements for each year in this period of record. Here, tide measurements are recorded in one hour intervals. This sampling interval is too coarse to use these records directly as forcing functions for the tidal hydraulics computations. If the tidal flow becomes critical in any shallow water region of the model, by achieving the phase speed of a shallow water tidal wave, $c = \sqrt{gh}$, then the 2-dimensional Courant-Friedricks-Lewy (CFL) criterion (Gallagher, et al. 1981) is used as a generalized constraint to ensure stability of the finite element calculations. Some nodes must be closely spaced with $\Delta x = 30$ m in order to resolve the geometry around the infall and outfall towers (Figure 1.2). The CFL criterion requires a minimum time step length:

$$\Delta t \leq \frac{\Delta x}{2c} \quad (10)$$

For a spring tide condition, maximum water depths could vary from 3 m to 7 m at certain sections of the infall and outfall towers. Therefore, the tidal forcing function must be resolved into time step intervals of less than 3.2 sec. if the tidal currents over the infall velocity cap approached critical speeds.

The tides were reconstructed at 2 sec time intervals from the Los Angeles tidal measurements using the amplitudes and phases of 21 non-zero tidal constituents derived from the long-term records of the tide gage. This tidal reconstruction was performed by the program, TID_DAYS, which is found in Appendix-D. TID_DAYS uses a version of LONG'S CODE from U. S. Dept. of Commerce SP #98_1988. The tidal constituents for Los Angeles that were input to TID_DAYS are based upon the NOAA datums derived from the 1960-78 tidal epoch. Because of sea level anomalies due to El Niño warming of the coastal ocean, and inverse barometer effects due to storm passage, the reconstructed tides were assigned a sea level anomaly in a leap-frog scheme to minimize the variance between the measured water elevations and the reconstructed tides at 2 second intervals. Reconstructed tides were generated for 7,523 tidal days 1980-2000, and the water elevation time series were throughput to SEDXPORT for continuous dilution modeling. Average daily high water levels off Scattergood for this period were 2.97 ft MSL, while average daily lows were -2.33 ft MSL.

E) Current Forcing

While waves dominate the initial dilution and dispersion of heat and concentrated seawater discharge in the inshore domain, the tidal currents control dilution and dispersion in the offshore domain, particularly in the immediate neighborhood of the Scattergood and Hyperion outfalls. Tidal currents were calculated using the tidal constituents from the tide gage station at Los Angeles (NOAA #941-0660). Current forcing is predominantly tidal in the offshore domain of Santa Monica Bay in Figure 1.3, and is a combination of tidal and wave-induced currents in the nearshore domain.

Tidal currents are mixed semi-diurnal with both progressive and standing components in the mid to inner shelf. Tidal currents flow parallel to the shore in a northwestward direction on flood tide and southeastward on an ebb tide (Figure 3.3). The tidal current speed diminishes towards shore due to friction in the shallow coastal boundary layer, and the phase of the tidal motion varies in the cross-shore direction such that during tidal reversals from ebb to flood, the phase of the inshore motion is lagging the offshore motion (see shore zone in Figure 3.3). The maximum currents in the offshore domain are typically 40 to 70 cm/sec. Along the Santa Monica/ Manhattan Beach coast, the tidal currents are ebb dominated such that over one tidal day (24 hr 50 min) the net current flows downcoast to the southeast as shown in Figure 3.3. The progressive vector plot in Figures 3.3 is composed of self-scaling vectors in units of cm/sec proportional to the vector length in the lower left hand corner, which represents the largest current vector found anywhere on the plot.

Wave induced currents predominate in the nearshore where wave shoaling effects are maximum. Wave induced currents increase with increasing wave height and remain significant over a nearshore domain extending 4 to 5 surf zone widths seaward of the shoreline. They flow longshore generally in the direction of longshore wave energy flux (down-drift). These longshore currents increase with increasing wave height and obliquity and flow away from bright spots and converge on shadows. This convergence results in a compensating seaward flowing current within the shadow known as a “rip current.” Even though the dilution of brine by mixing may be less in a shadow, dilution by rip current advection (ventilated dilution) will be increased. As a net result, shadows can sometimes be areas of enhanced overall dilution.

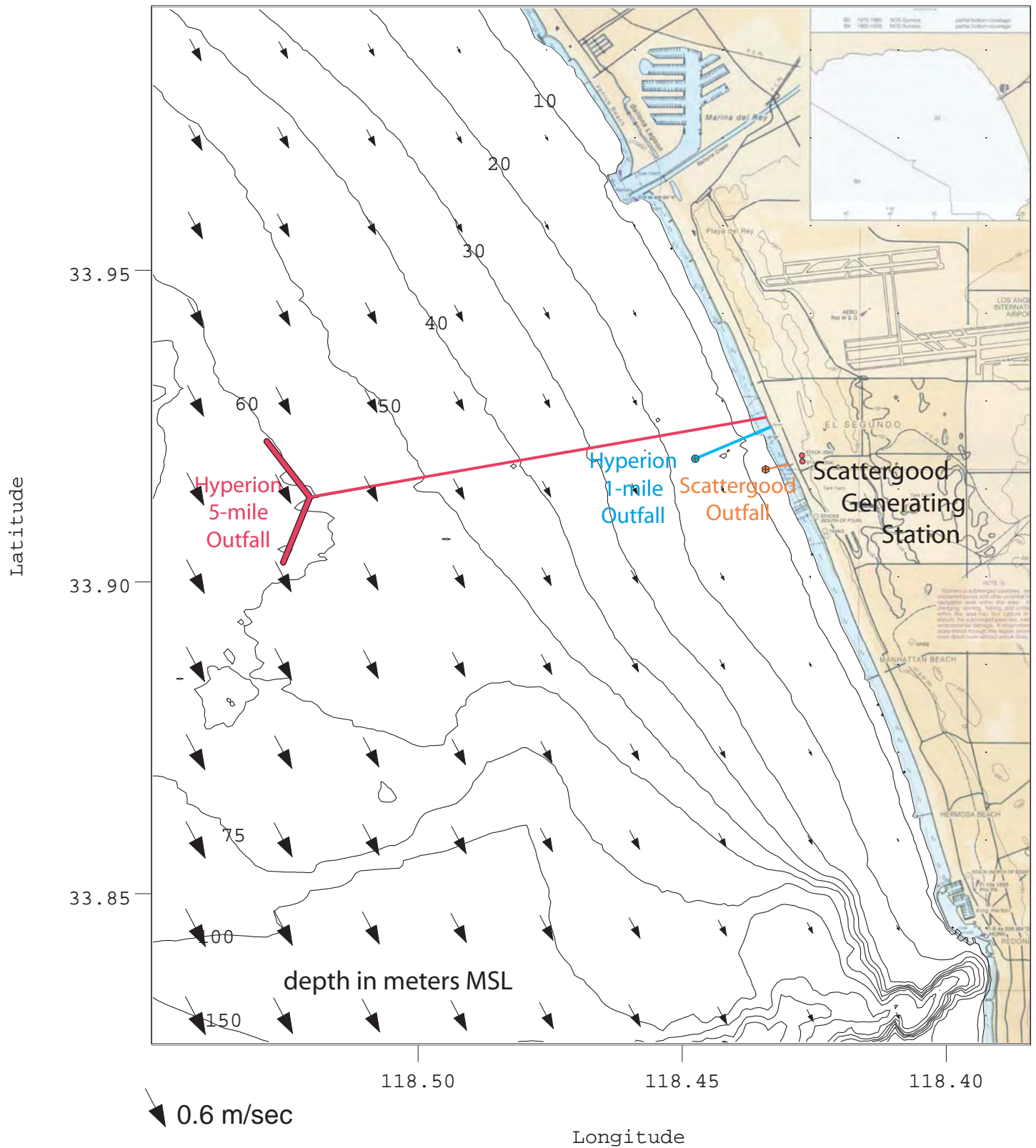


Figure 3.3. Progressive vector map for net tidal drift during mean tidal range, used in hydrodynamic modeling of the LADWP Scattergood Desalination Project. Vectors scaled to largest arrow = 0.6 m/sec.

Progressive vector arrays of the type shown in Figure 3.3 were generated for 7,523 tidal days 1980-2000, and the resulting current vectors were throughput to SEDXPORT for continuous dilution modeling. Figure 3.4c gives a continuous time series 1980-2000 of the daily maximum tidal currents at the Scattergood outfall that were derived from the ocean water level variation shown in Figure 3.4b. Average daily maximum tidal currents over the Scattergood outfall during this period were 45.1 cm/sec (0.9 kts).

F) Wind Mixing

Winds provide mixing in the surface layer above the thermocline that typically extends down to depths of 10-20 m. Winds also provide wind drift which although weak can bridge the gap between the off shore tidally dominated regime and the inshore wave-dominated regime. The collection of historical wind data are compiled in US Surface Airways Data available from the National Climate Data Center document library (NCDC , 2004). The closest NCDC Surface Airways monitoring location relative to Scattergood is Los Angeles International Airport. Here, human observations of surface winds were collected and archived by NCDC beginning 1 January 1964 until 28 February 1997, after which wind observations were taken by means of the Automated Surface Observing System (ASOS). Combining these 2 data bases, a continuous surface wind record was assembled for the period 1980-2000 as shown in Panel-d of Figure 3.4. These wind data were throughput to SEDXPORT for continuous dilution modeling. Because the lower Southern California Bight is a “wind drought” region due to orographic

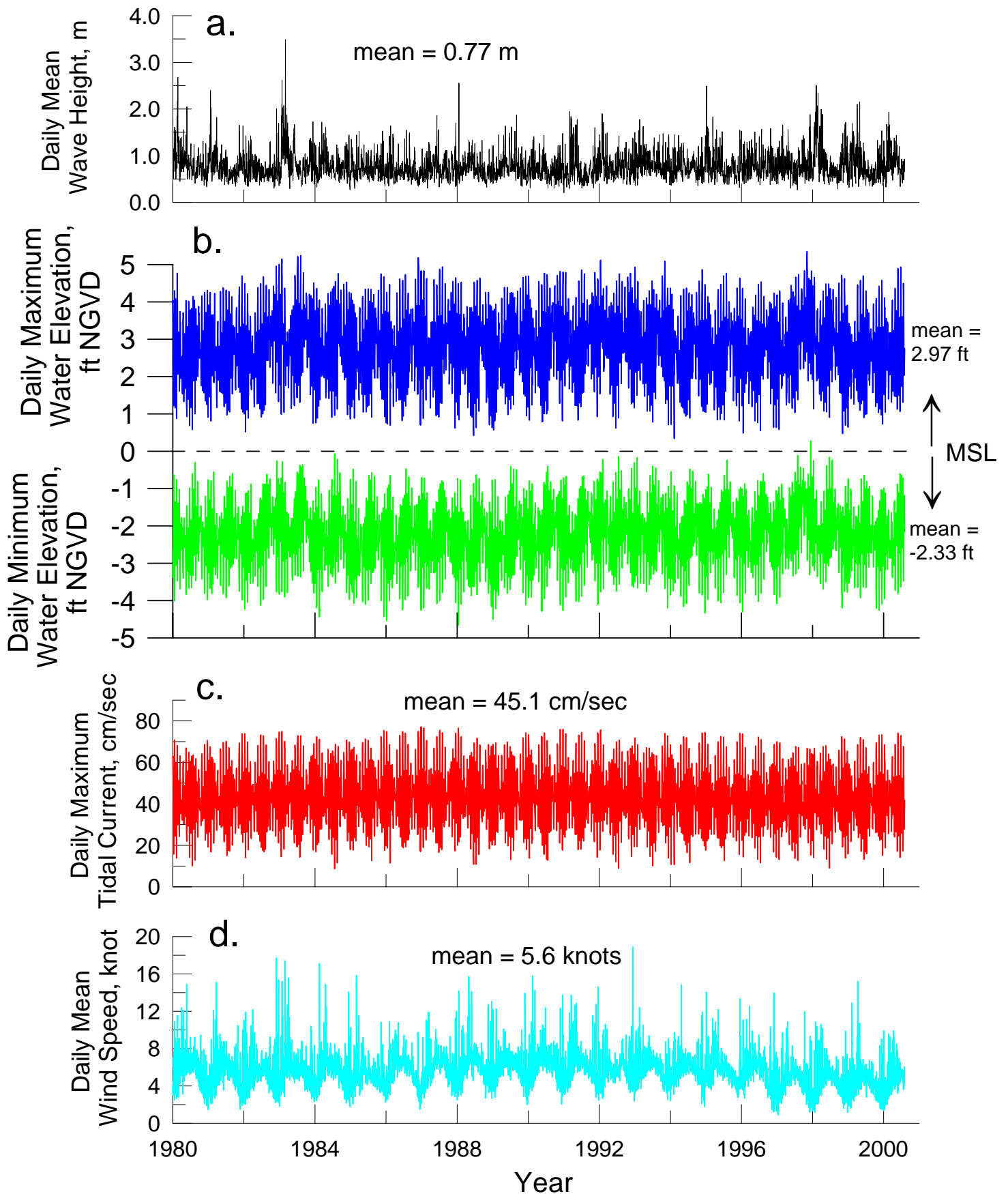


Figure 3.4. Controlling environmental variables for brine dilution, forcing functions at Scattergood: a) daily mean wave height, b) daily high and low water elevation, c) daily maximum tidal current velocity, and d) daily mean wind speed. [data from CDIP, 2004, NOAA, 2004, UCAR, 2004]

blocking by the Penninsular Range, the 20.5 year mean wind speed is only 5.6 knots. However, El Niño storms and North Pacific cold fronts episodically increase wind speeds to a maximum 24 hour mean of 19.6 knots, as occurred during the 1997 El Niño storms. The minimum daily mean wind speed is 0 knots. The long term record in Figure 3.4d shows a well defined inter annual (seasonal) modulation of daily mean winds, with a 3-7 year intensification associated with El Niño.

G) Ocean Salinity

Ocean salinity variation exerts a modulating effect on the concentration of sea salts discharged from the desalination plant. The proposed desalination plant will divert approximately 100 mgd of heated HBGS condenser seawater through a reverse osmosis system (R.O.) before in-plant waste streams are added to the cooling water discharge. The R.O. system will produce 50 mgd of product from the 100 mgd of cooling water diverted from the condenser cooling stream. The R.O. system will discharge 50 mgd of concentrated seawater by-product at twice ambient ocean salinity, which is subsequently diluted in the remaining cooling water discharge stream. Therefore, the concentration of sea salts in the discharge varies directly with ocean salinity at the intake to the generating station.

Figure 3.5b shows the variation in daily mean salinity in the coastal waters off Scattergood derived from 20.5 years of NPDES monitoring data of the Scattergood and Hyperion outfalls for the period from 1980 until mid-2000. Gaps in these daily records were filled salinity monitoring data from the CDIP Santa Monica Station (#028) with residue gaps filled by the Scripps Pier Shore Station, (SIO, 2001). These wind data were throughput to SEDXPORT for continuous dilution modeling. Inspection of Figure 3.5b indicates that the ocean salinity

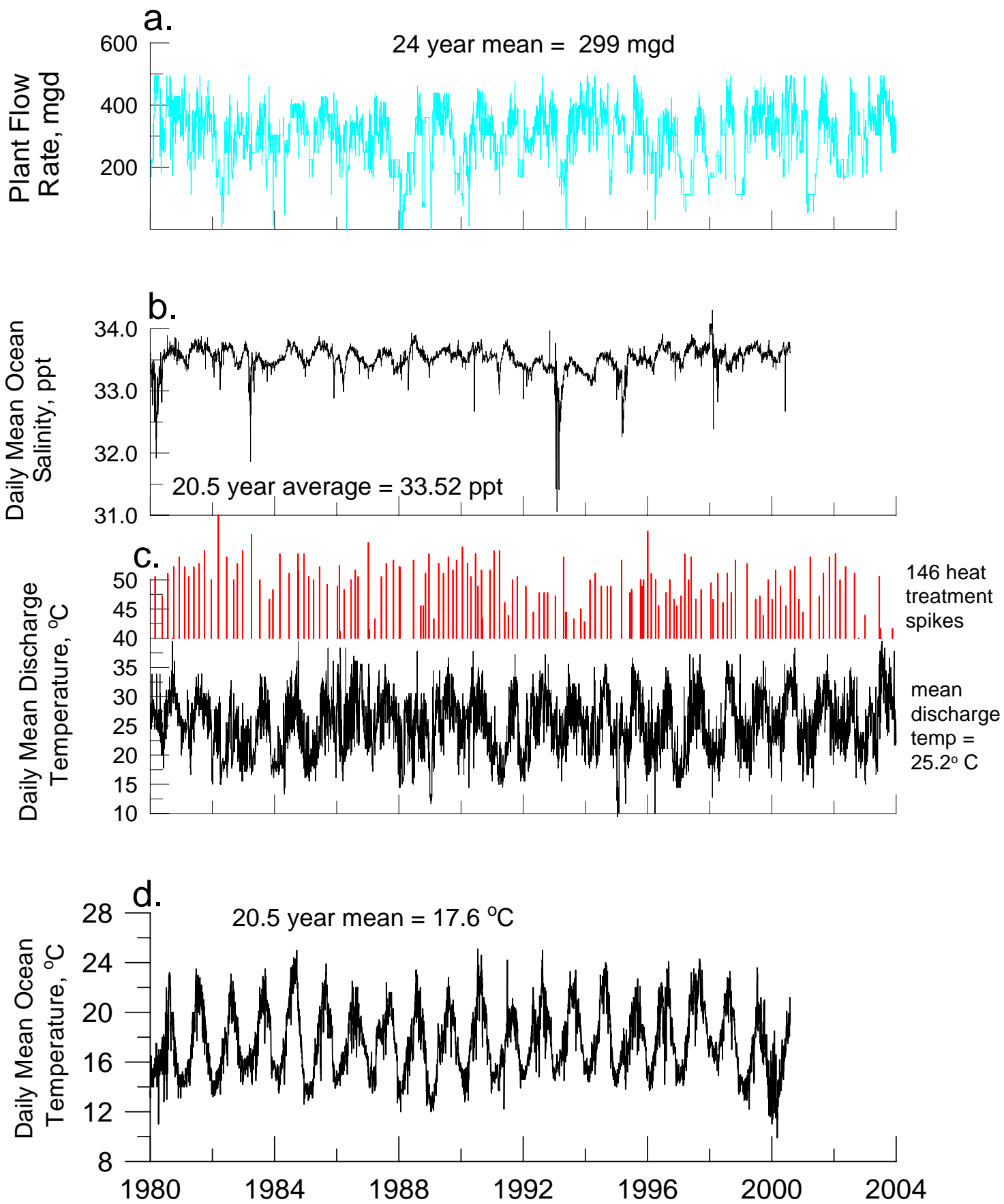


Figure 3.5. Controlling environmental variables for brine dilution, boundary conditions at Scattergood Outfall: a) plant flow rate b) daily mean ocean salinity, c) daily mean discharge temperature, and d) daily mean ocean temperature. [data from LADWP, 2004, SIO, 2004]

varies naturally by 10% between summer maximums and winter minimums, with a long term average value of 33.52 parts per thousand (ppt). Maximum salinity was 34.34 ppt during the 1998 summer El Nino when southerly winds transported high salinity water from southern Baja up into the Southern California Bight. Minimum salinity was about 31.02 ppt during the 1993 winter floods. The variation between maximum and minimum salinity is about 3.32 ppt, which is about 10 % of the average value of 33.5 ppt. The ocean salinity exceeded the 33.5 ppt average value during 2,488 days out of 7,523 days during the period of record, and were below average during 1,543 days. Therefore above average salinities are more common than below average salinities. Average salinities were observed a total of 3,492 days of the period of record, or about 46 % of the time. (These data are also confirmed by long term salinity monitoring at Scripps Pier NOAA Station #941-0230, and by 55 CalCOFI cruises in the Southern California Bight between 1984 and 1997, see SIO, 2001; Roemmich, 1989, and Bograd, et al, 2001).

H) Ocean Temperature

Ocean temperature effects the buoyancy of the combined discharge of the generating station and the desalination plant. The ocean temperature further effects the buoyancy of the discharge through the absolute temperature of the plant discharge, which is regulated under the NPDES permit by a ΔT limit relative to ocean temperature. This buoyancy effect is calculated by the specific volume change of the discharge relative to the ambient ocean water according to Equation (5). The buoyancy of the plume exerts a strong effect on the mixing and rate of assimilation of the excess heat and sea salts by the receiving waters.

We use the average of temperature records from NPDES monitoring data with gaps filled by temperature monitoring data from the CDIP Santa Monica Station (#028) and by the Scripps Pier Shore Station, (SIO, 2001). The 20.5 year record of daily mean ocean water temperatures is plotted in Panel-d of Figure 3.5. These temperature data were throughput to SEDXPORT for continuous dilution modeling. A pronounced seasonal variation in these temperatures is quite evident with the maximum recorded daily mean temperature reaching 25.1 °C during the summer of the 1993 El Niño and the minimum falling to 9.9 °C during the winter of the 1999-2000 La Niña. The 20.5 year mean temperature was found to be 17.6 °C. On a percentage basis, the natural variability of the temperature of coastal waters in the vicinity of the Scattergood Generating station is significantly greater than that of salinity (on the order of $\Delta T = 86\%$ vs $\Delta S = 10\%$).

I) Scattergood Operating Temperatures

California's Thermal Plan incorporates provisions of Section 316(a) of the Federal Water Pollution Control Act of 1972 and defines the relevant regulatory requirements for cooling water discharge from the Scattergood Generating Station. Although certified to discharge thermal waste at as much as 30 °F (16.5 °C) above ambient ocean temperatures, ($\Delta T = \Delta T = 30$ °F), the Scattergood plant operators have adopted operating procedures that typically discharge below the maximum certified Delta-T. NPDES monitoring data in Figure 3.5c for the period 1980 to 2004 was 25.2 °C as compared to a daily mean ocean temperature of 17.6 °C. Consequently, Scattergood Generating Station is more typically operated over the long term at a $\Delta T = \Delta T = 16.7$ °F (7.6 °C). Although we use the actual

discharge time series in Figure 3.5c for brine dilution modeling the average Delta-T is a reasonable value for characterizing average discharge temperatures for desalination during normal electrical generation activities. The discharge temperatures occasionally spike to as high as 135 °F(57 °C) during short term heat treatment cycles performed to remove bio-fouling from the cooling water circulation system. There were 146 such heat treatment spikes during the period of record shown in Figure 3.5c. Since the desalination plant will not operate during heat treatments, the heat treatment temperature spikes are neglected in the analysis. Regardless, high discharge temperatures promote rapid mixing and assimilation of the excess sea salts from desalination by reducing the negative density anomaly caused by the heavy brine. Therefore, we include in this study model results for “cold water” discharges (Delta-T of 0 °F) under conditions of a worst-case scenario.

J) Scattergood Flow Rates and Post-Project Salinity

Generating station flow rates determine the volume of water available in-the-pipe to dilute the concentrated seawater discharge from the desalination plant. The operational patterns of the plant will be an important determinant of the variability of the salinity of the combined discharge once the desalination plant is added to the sea water circulation loop of LADWP Scattergood. The Scattergood Generating Station operates three generating units with a combined once-through rated flow rate capacity of 495.36 mgd. The NPDES permit certifies an additional 0.24 mgd of in-plant waste streams, for a combined certified discharge rate of 495.6 mgd. The Los Angeles Department of Water and Power has provided daily discharge flow rate data for the period 1980 to 2004, as plotted in Figure 3.5a. These flow

rate data were throughput to SEDXPORT for continuous dilution modeling. The 24-year mean of daily flow rate is 299 mgd, with maximum daily flow rates reaching cooling system capacity at 495.3 mgd. The minimum daily flow rate is 0 mgd when the plant is shut down for service intervals. The lowest non-zero flow rates in the 24-year period of record are 2 mgd, 19mgd, 45 mgd, 52 mgd, 85 mgd and 101 mgd. These minimal daily flow rates would support desalination over a production range of 1 mgd to 50 mgd of product water.

For every gallon of product water produced, the proposed desalination plant must divert 2 gallons of heated condenser water through a reverse osmosis system (R.O.) before in-plant waste streams are added to the cooling water discharge. After those 2 gallons pass through the R.O. system, 1 gallon of brine at double ambient sea water salinity will be returned to the cooling water stream and blended in the pipe with the residual condenser water and in-plant waste streams to be discharged from the offshore outfall. Consequently the end-of-pipe salinity of the effluent discharged from the offshore outfall is a function of both the available flow rate of the power plant and the production rate of the desalination plant. Figure 3.6 plots this function for six possible levels of product water production by reverse osmosis, ranging from 12 mgd to 50 mgd. The end-of pipe discharge salinity increases with increasing R.O. production regardless of the power plant flow rate. For any given level of R.O. production, end-of pipe discharge salinity decreases with increasing power plant flow rate. Not every point on these curves can be reproduced by the existing combinations of circulation pumps within the Scattergood Generating Station, but all possible flow rate capabilities of the power plant do have a corresponding solution point for one of the six R.O. production

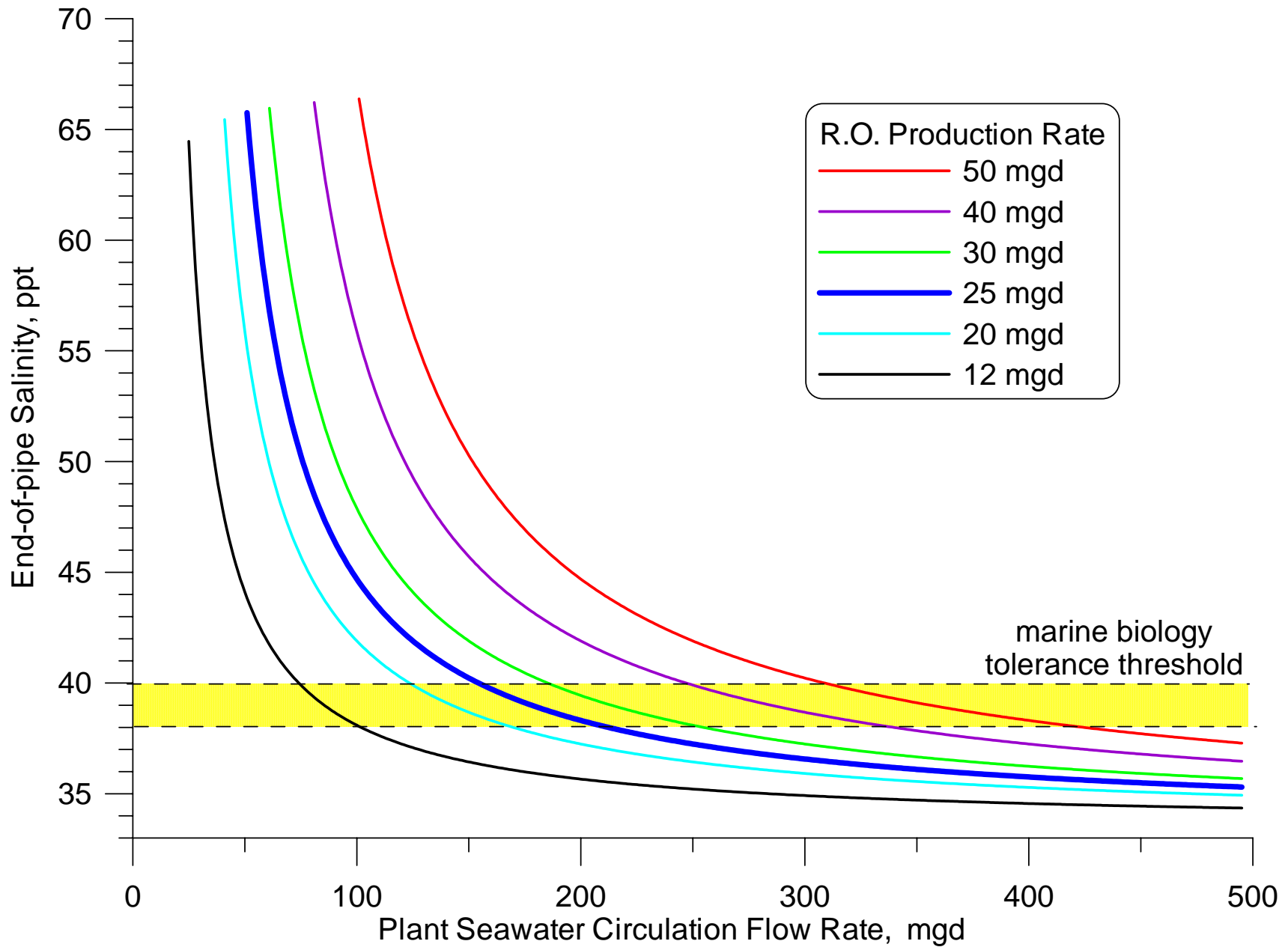


Figure 3.6. Sensitivity analysis of end-of-pipe salinity for LADWP desalination project at Scattergood Generating Station.

levels represented by these curves. For comparison, a yellow band denoting the marine biology salinity tolerance thresholds is overlaid on the end-of-pipe solutions. These tolerance thresholds are derived from bio assays due to Le Page (2004) using keystone species indigenous to the coastal waters of the Southern California Bight. At salinities of around 38 ppt, larvae begin to suffer recruitment impairment, while at 40 ppt salinity levels, some juveniles begin showing failure to thrive symptoms and/or mortality. Inspection of the curves in Figure 3.6 indicates that end-of-pipe salinities for an R.O. production rate of 12 mgd remain below this tolerance threshold if the power plant flow rate is greater than 100 mgd. The average power plant flow rate (299 mgd) would support a 35 mgd R.O. production level without causing end-of-pipe salinities to exceed these tolerances, while 50 mgd of R.O. production would require 425 mgd of cooling water circulation to keep discharge salinity below marine biology tolerance limits. However, these assessments of marine biology tolerance only apply to organisms trying to survive on the discharge tower, and do not account for the further dilution of brine that occurs in the receiving water due to ocean mixing and current advection (ventilation). To account for this, the hydrodynamic model simulations are invoked.

For most of the discharge solutions in Figure 3.6 that lie below the marine biology tolerance limits, the combined thermal and brine discharge remains a fraction of a percent heavier than seawater. Consequently, the discharge water will sink to the seafloor after the initial vertical momentum of the discharge has diffused into the water column. This has several positive implications: 1) it will increase initial dilution of the combined discharge, 2) it will remove the majority of the thermal footprint from the sea surface, and 3) it should diminish the size of the

thermal footprint. Sinking of the discharge plume to the seafloor after the initial vertically upward discharge from the outfall tower will produce trajectories of the effluent that engage the entire water column in the dilution process. These trajectories should increase initial dilution. Subsidence of the discharge plume to the seafloor following this higher initial dilution should isolate both the concentrated seawater and the waste field of the generating station from subsequent ingestion by the in-fall tower (400 ft seaward of the outfall tower). This is a favorable circumstance with respect to re-circulation of the brine and thermal effluent. On the other hand, the heavier than seawater discharge plume will bring the elevated salinities into contact with the seafloor where there could be an effect on benthic biology. The extent of seabed effected in this way is studied in terms of the worst case scenario presented in following sections.

K) Hyperion Operating Temperatures

The Hyperion outfalls are discharging essentially fresh water of terrigenous origin, which has approximately a salinity of 0 ppt and a temperature more representative of the seasonal variation of land temperatures than ocean temperatures. Differences between the ocean and discharge temperatures results in buoyancy effects that alter the dispersion of brine when added to these fresh water discharges. Figure 3.7c gives the temperatures of 171 separate discharge events from the 1-mile Hyperion emergency outfall that have occurred since 1980 (primarily during peak wet weather flows). The temperature maximum of these discharges from the 1-mile outfall was 30.0 °C; the minimum was 18.3 °C, and the average discharge temperature was 25.4 °C. The temperature of 8,766 daily discharges from the Hyperion 5-mile outfall are plotted in Figure 3.8c which

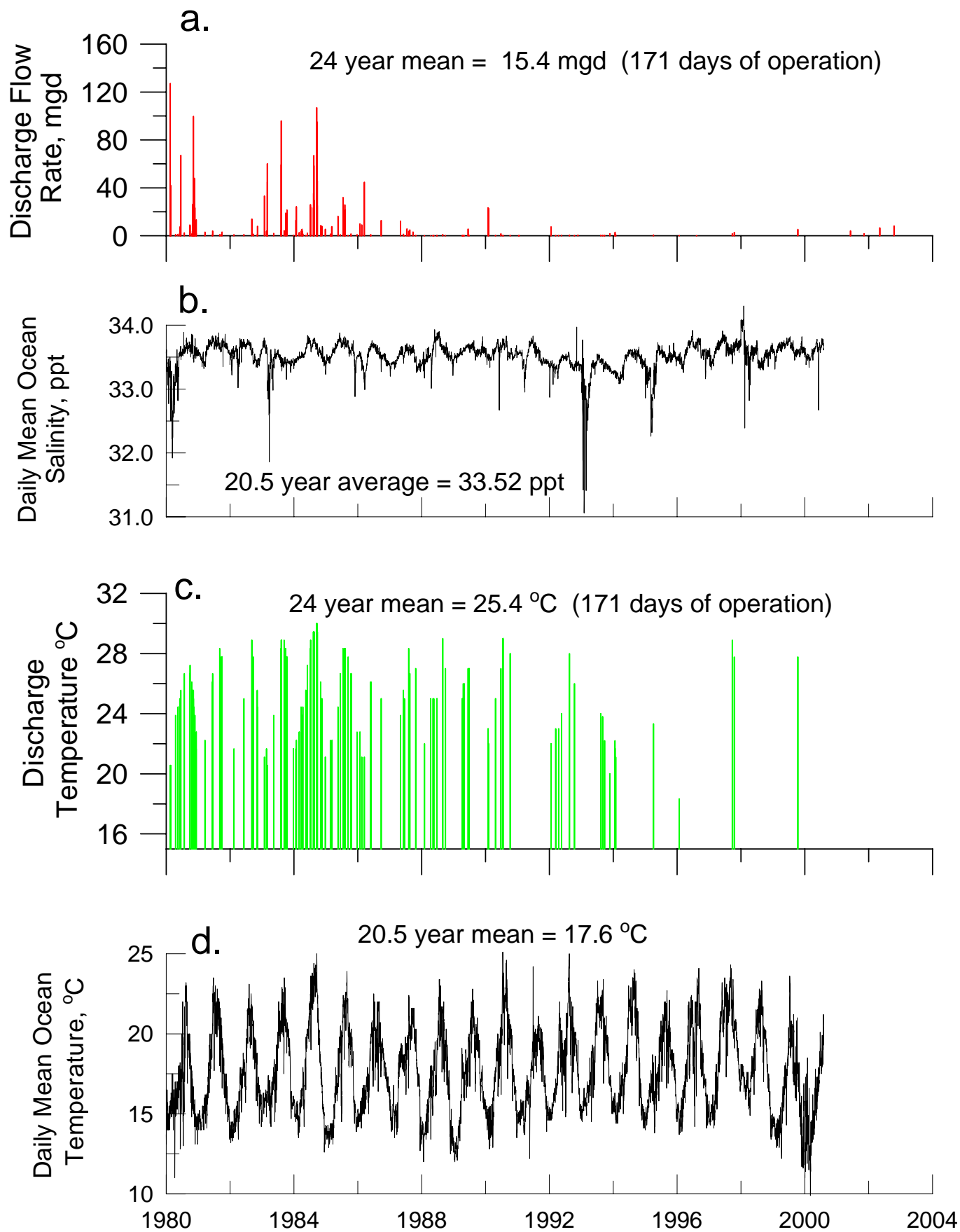


Figure 3.7. Controlling environmental variables for brine dilution, boundary conditions for Hyperion 1 mile: a) discharge flow rate b) daily mean ocean salinity, c) daily mean discharge temperature, and d) daily mean ocean temperature. [data from LADWP, 2004, SIO, 2004]

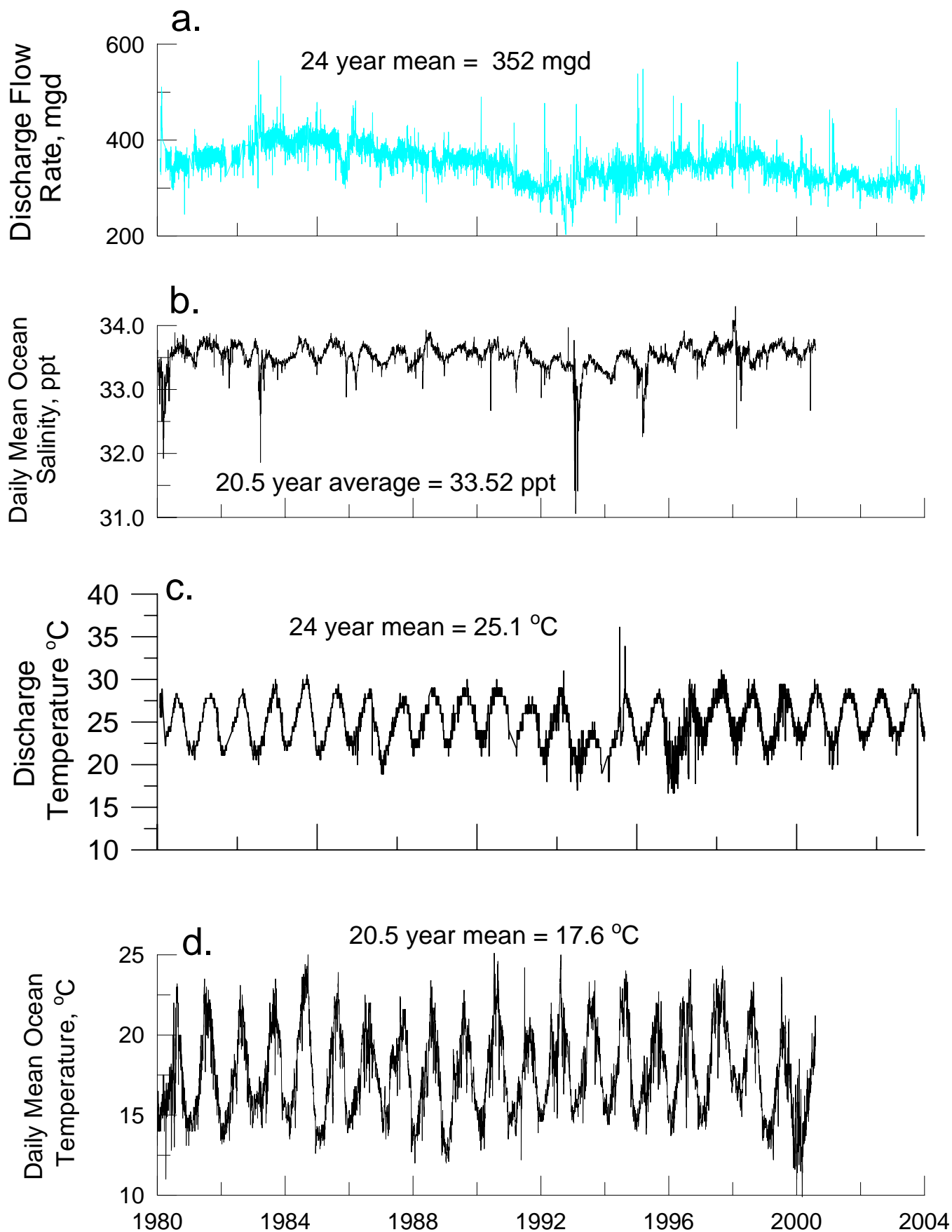


Figure 3.8. Controlling environmental variables for brine dilution, boundary conditions for Hyperion 5 mile: a) discharge flow rate b) daily mean ocean salinity, c) daily mean discharge temperature, and d) daily mean ocean temperature. [data from LADWP, 2004, SIO, 2004]

showed a similar temperature range. Maximum discharge temperatures from the 5-mile outfall were 36.1 °C, the minimum was 11.7 °C, and the average discharge temperature was 25.1 °C. These temperature data were throughput to SEDXPORT for continuous dilution modeling. Hyperion discharge temperatures are generally 5-8 °C warmer than ocean temperatures, further augmenting the positive buoyancy of these fresh water discharges. This positive buoyancy is diminished by the addition of brine, and the effect on the dispersion of the waste field is studied by hydrodynamic model simulation in Section 4.

L) Hyperion Flow Rates and Post-Project Salinity

Figure 3.7a gives the discharge flow rates of the 171 discharge events from the 1-mile Hyperion emergency outfall that occurred 1980-2004. The maximum discharge rate from the 1-mile outfall was 127 mgd and the average discharge rate was 15.4 mgd. Figure 3.8a gives the daily discharge flow rates from the Hyperion 5-mile outfall over the same time period, and indicates an historic maximum discharge rate of 566 mgd; a minimum of 203 mgd, and an average discharge rate of 352 mgd.. These flow rate data were throughput to SEDXPORT for continuous dilution modeling.

The end-of-pipe salinity and the degree to which the brine will effect the positive buoyancy of the Hyperion discharges is a function of both the effluent flow rate and the R.O. production rate. This function is calculated in Figure 3.9 for six possible levels of daily product water production by the proposed desalination plant over a range of 12 mgd to 50 mgd. As with the Scattergood outfall, the end-of pipe discharge salinity increases with increasing R.O. production regardless of the treatment plant discharge rate; and, for any given

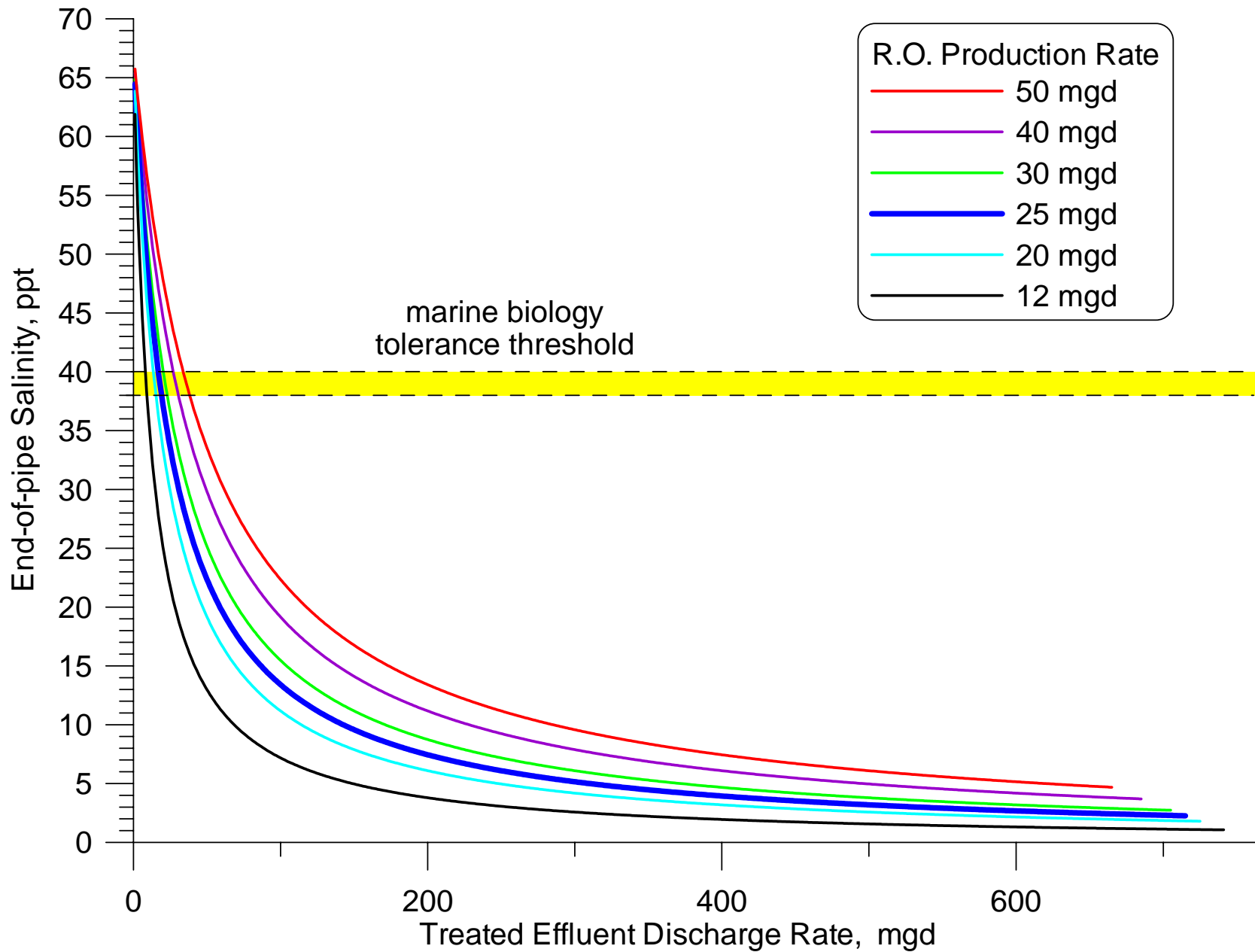


Figure 3.9. Sensitivity analysis of end-of-pipe salinity for LADWP desalination project at Scattergood Generating Station using the Hyperion 1-mile and 5-mile outfalls.

level of R.O. production, end-of pipe discharge salinity decreases with increasing treatment plant discharge rate. However, unlike the Scattergood outfall, the end-of pipe discharge salinity from the Hyperion outfalls become brackish (less than ambient seawater salinity) at relatively low discharge rates due to the fresh water make-up of the treated effluent. For example, even the 24-year minimum discharge from the 5-mile outfall (203 mgd) will produce end-of pipe discharge salinities of less than 15 ppt for any R.O. production rate up to 50 mgd, thereby eliminating any potential hyper salinity effects in the marine environment and reducing the buoyancy of the wastefield by at least 40 %. A similar effect would be expected for peak wet weather discharges from the 1-mile, but these only occur on average 1 week per year. The remainder of the time, brine would be discharged from the 1-mile outfall with no in-the-pipe dilution, resulting in end-of pipe discharge salinities of about 67 ppt (twice ambient seawater). The brine-induced effects of reduced buoyancy on the dispersion of the wastefields from the Hyperion outfalls is simulated by the hydrodynamic model in Section 4.

M) Event Scenarios Derived From Historical Data 1980-2000

Overlapping 20.5 year long records of the 4 primary boundary condition variables are plotted in Figure 3.5 for the Scattergood outfall, and in Figures 3.7 and 3.8 for the Hyperion 1-mile and 5-mile outfalls, respectively. Coincident records for the 4 primary forcing functions are shown in Figure 3.4 for waves, tides, currents and winds. These records contain 7,523 consecutive days between 1980 and 2000. We adopt a commonly used approach in environmental sciences of assessing potential impact in terms of a worst case scenario. We pose this worst case by searching this long period record of 7,523 days for historical events that

match a worst case criteria. The criteria for worst case and worst month was based on the simultaneous occurrence of eight variables having the highest combination of absolute salinity and temperature during periods of low plant flow rates concurrent with low mixing and advection in the local ocean environment. Table-2 summarizes the worst case criteria applied to each controlling variable in the computer search of the historic record.

Table 2: Search Criteria for Worst Case Scenario

Variable	Search Criteria	Ecological Significance
Plant Flow Rate	Minimize	Lower flow rate results in less initial dilution in the pipe of the concentrated sea salts from desalination
Ocean Salinity	Maximize	Higher salinity leads to higher initial concentrations of sea salts in the pipe from desalination
Ocean Temperature	Maximize	Higher temperature leads to greater stress on resident marine biology
Ocean Water Levels	Minimize	Lower water levels result in less dilution volume in the nearshore and consequently slower dilution rates
Waves	Minimize	Smaller waves result in less mixing in surfzone and less inshore dilution
Currents	Minimize	Weaker currents result in less advection and less offshore dilution
Winds	Minimize	Weaker winds result in less surface mixing and less dilution in both the inshore and offshore
Discharge Temperature	Minimize	Colder discharge temperatures maximize the seabed contact of the heavy brine

Minimum ocean mixing levels were obtained from a computer search of 20 year long records of winds, waves and currents. However, the ocean salinity during the event day when minimal mixing conditions prevailed was 33.49 ppt, not the salinity maximum of 34.3 ppt identified in Figure 3.21a. This is due to the fact that salinity maximums are mutually exclusive with mixing minimums. Salinity maximums are caused by vigorous southerly winds that create a well-mixed coastal ocean while pushing high salinity water masses into the Southern California Bight. A series of sensitivity analyses determined the salinity maximum would increase the concentration of brine discharge by 2%, but that the effects of this increase on brine dilution were smaller than the dilution impairment caused by the effects of retarded mixing during low energy conditions . In fact the dilution rates for the conditions are 99% smaller than the dilution rates during the salinity maximum. Therefore, minimal ocean mixing conditions became the dominant set of environmental variables in defining the worst case scenario. Accordingly worst case dilution modeling was based on the following set of parameters:

Table 3: Input Parameters for Worst-Case Simulations

- 1) Scattergood intake flow rate = 45-112 mgd
- 2) Desalination production rate = 12-50 mgd
- 3) Combined discharge = 76.7 mgd
- 4) Ocean salinity = 33.49 ppt
- 5) End-of pipe combined discharge salinity = 43-61 ppt
- 6) Combined discharge temperature anomaly $\Delta T = 0^{\circ} \text{C}$
- 7) Discharge density anomaly $\Delta\rho/\rho = -0.4\%$ to -1.6% (Scattergood)

- 8) Discharge density anomaly $\Delta\rho/\rho = -1.6\%$ to $+1.7\%$ (Hyperion)
- 9) Wave height = 0.16 m
- 10) Wave period = 8 sec
- 11) Wave direction = 255°
- 12) Wind = 0 knots
- 13) Tidal range = Syzygial spring/neap cycle
- 14) Daily maximum tidal current = 8.7 cm/sec

The particular values of plant flow rate, end-of-pipe salinity, and density anomaly specified for worst-case within the range shown in Table-3 are dependent upon the desalination production rates chosen for each modeling problem in Section 4. Regardless, the density anomaly produced by any selection of R.O. production rate produces a combined discharge with the cooling water stream that is heavier than seawater. These worst case settings are selected from histogram analyses, also detailed in Section 4. Ocean conditions represented by the Table-3 parameter assignments did not persist in the long term record of Figure 3.4 for more than a week. However, in the model simulations these conditions were perpetuated for 30 days to verify the stability of the computed results and to insure that all possible cumulative effects had reached steady state. Historically, the recurrence of worst-case environmental extremes is about 1 week every 3 to 7 years, commensurate with the dominant ENSO frequencies. By perpetuating low flow case conditions in the model for 30 continuous days the recurrence interval is actually more rare, about 1 month every 13 to 31 years.

L) Calibration

The coupled sets of models shown in Figure 2.1 were calibrated for end-to-end simulations of the salinity and temperature fields based on salinity and temperature depth profile measurements conducted over a nearshore sampling grid collected as part of an NPDES compliance monitoring program for LADWP Scattergood. Wave and current forcing for the model were reconstructed for this period based on the wave data in Figure 3.2a and tidal current reconstructions like those in Figures 3.4. Free parameters in the subroutines were adjusted iteratively until a best fit was achieved between the measured and simulated salinity fields.

The subroutines of SEDXPORT-f contain seven free parameters which are selected by a calibration data set specific to the coastal type for which the hindcast simulation is run. These parameters are as follows according to subroutine:

BOTXPORT·f

- *ak2 - stretching factor for vertical eddy diffusivity, ϵ
- *ak - adjusts mixing lengths for outfalls

NULLPOINT·f

- *ak7 - adjusts the asymmetry of the bedform distribution curve,
 μ

SURXPORT·f

- *aks - adjusts the surf zone suspended load efficiency, K_s
- ak4 - stretching factor for the horizontal eddy diffusivity, ϵ_x

RIVXPORT·f

- *ak3_1 - adjusts the jetty mixing length and outfall mixing lengths
- *ak3 - stretching factor for the horizontal eddy diffusivity of the river plume, ϵ_H

The set of calibration values for these parameters was used without variation or modification for all model scenarios contained in Sections 4. A similar calibration successfully duplicated the dilution findings of the recently completed California Energy Commission study at the AES Huntington Beach Generating Station (KOMEX,2003: Jones and Major, 2003). Here dye discharged from the HBGS outfall gave measured dilution ratios of 36 to 1 at the shoreline as compared to the 32 to 1 prediction obtain with the SEDXPORT modeling system two years earlier (Jenkins and Wasyl, 2001).

**SECTION 4: EVENT ANALYSIS OF DILUTION AND
DISPERSION OF BRINE**

4) **Event Analysis of Dilution and Dispersion of Brine**

In this section we solve for the worst-case solutions for the dispersion and dilution of the concentrated seawater by-product of the proposed desalination plant at Scattergood. By agreement with LADWP, we evaluate these worst-case simulations for three possible R.O. production rates by the desalination plant: 12mgd, 25 mgd and 50 mgd. The objective here is to determine persistent levels of disturbance to the ambient ocean salinity field. We consider a *worst case* model scenario in which maximum salinity levels are produced in-the-pipe as a consequence of minimum power generation (or standby) and are subsequently discharged into a tranquil, summer-time ocean environment wherein ambient mixing is minimal as prescribed in Section 3. These worst-case scenarios are run continuously in the model for 30 days, and then the solutions are time averaged. The purpose of running these event scenarios for 30 days was to provide a long enough simulation that would reveal any possible cumulative effects, ie to verify that the receiving waters were fully saturated and that a steady state was achieved. This is common practice for impact assessment modeling. Modeling for shorter periods of time tends to result in slightly lower salinities in the receiving waters. Our sensitivity analyses performed during the development of these solutions show that the receiving waters reach steady state within 5 days. Thereafter, there are no significant changes in the event scenario solutions.

A) Simulations for Scattergood Outfall Option

The Scattergood flow rate history in Figure 3.5 was applied to the desalination transform function in Figure 3.6 for R.O. production rates ranging from 12mgd to 50 mgd. Out of 7,523 daily outcomes for the period of record 1980-2000, 7,486 outcomes were adequate to produce desalinated product water at a rate of 12 mgd. Figure 4.1 provides a histogram of the ocean salinities vs the end-of-pipe salinities that would have resulted had the desalination plant been operated according to this historical data base. The green histogram bars in Figure 4.1 represent the % occurrence of ocean salinity levels varying over the range shown in Figure 3.5b. The red histogram bars give the % occurrence of the end-of-pipe salinities that would be produced by adding the brine from a 12 mgd desalination plant to the cooling water stream. Also shown in Figure 4.1 is the cumulative probability of the end-of-pipe salinity outcomes. From the cumulative probability, we find that 99.9% of the 7,486 daily outcomes produced end-of-pipe salinities below the marine biology tolerance threshold of 38 ppt. (Only 6 outcomes exceeded 38 ppt and the largest was 42.6 ppt). Therefore it is concluded that a 12 mgd desalination plant discharging its brine through the Scattergood outfall presents no significant impacts to the marine environment.

Figure 4.2 presents a histogram of 7,483 daily outcomes for end-of-pipe salinity levels that would result from a 25 mgd desalination plant operating from the historic flow rate history of the Scattergood Generating Station 1980-2000. Here we find that 17% of the daily outcomes exceed the marine biology tolerance threshold of 38 ppt, and the highest end-of-pipe salinity reaches 43.8 ppt which is used to initialize the hydrodynamic model for the worst-case simulation. Using

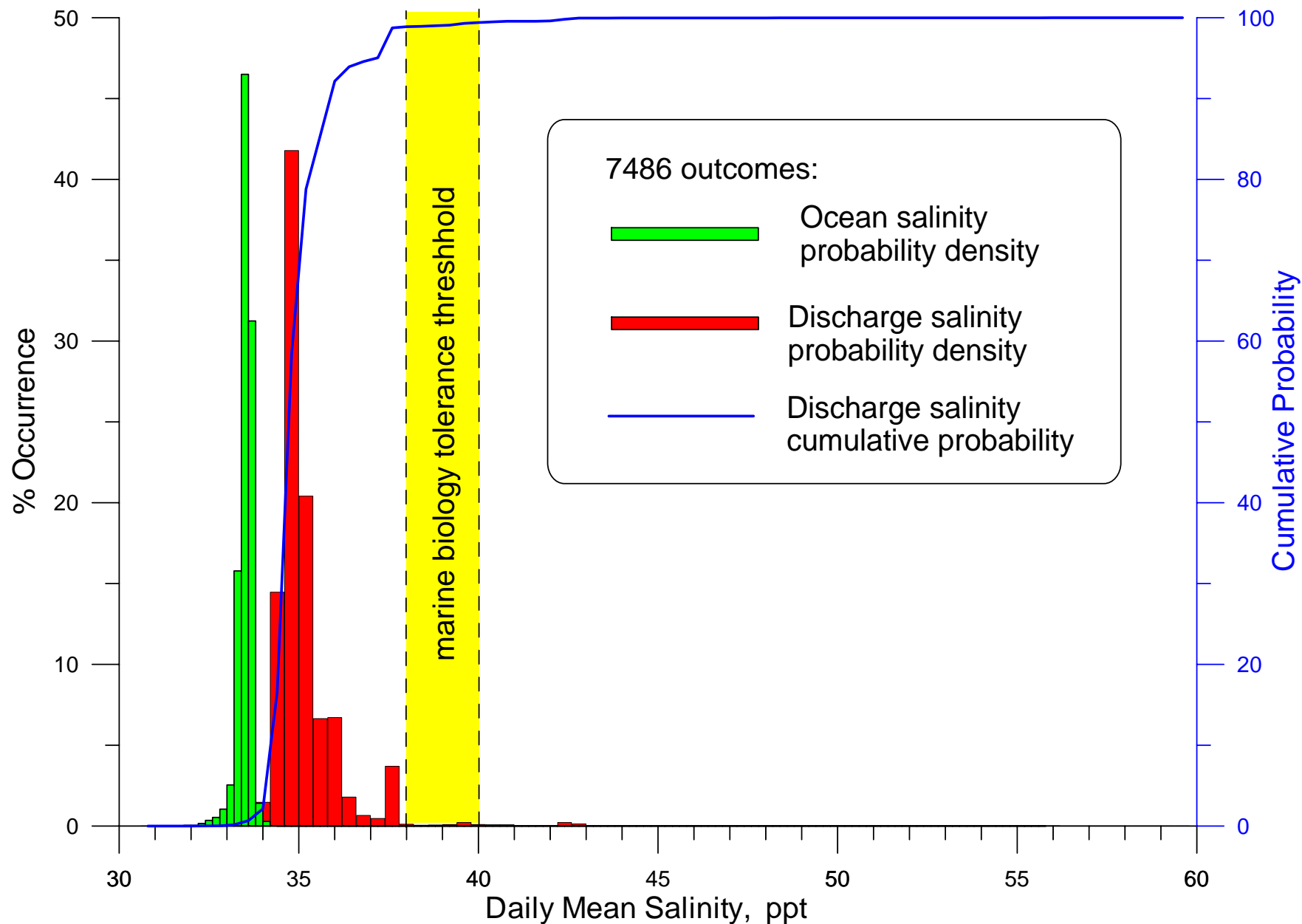


Figure 4.1. Histogram of daily mean ocean and discharge salinity at end-of-pipe of the Scattergood outfall for desalination production rate of 12 mgd. Percent occurrence based on historic observations of ocean mixing, water mass properties, and Scattergood Generating Station daily plant flow rates, 1980-2000.

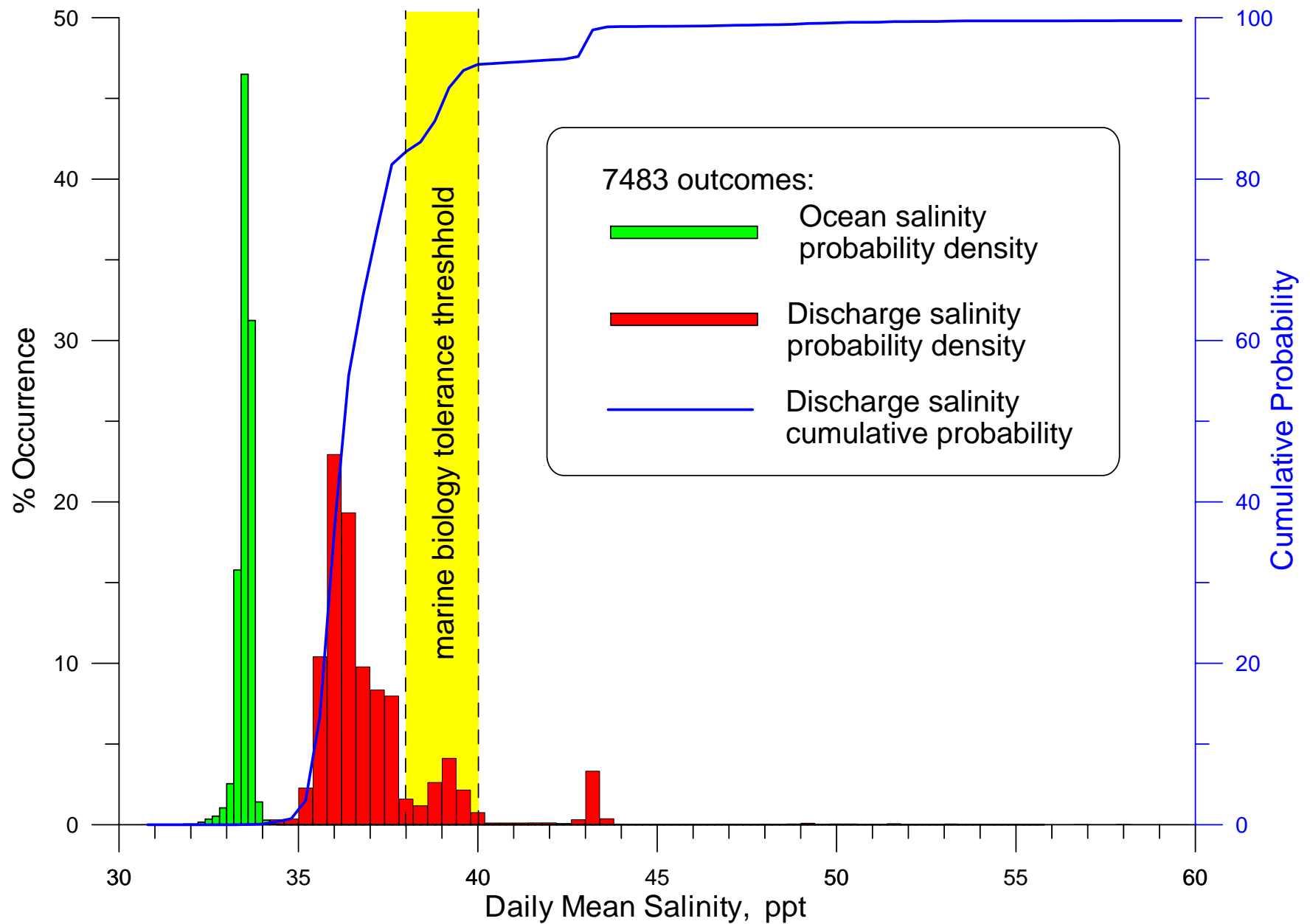


Figure 4.2. Histogram of daily mean ocean and discharge salinity at end-of-pipe of the Scattergood outfall for desalination production rate of 25 mgd. Percent occurrence based on historic observations of ocean mixing, water mass properties, and Scattergood Generating Station daily plant flow rates, 1980-2000.

this value in combination with the other worst case variables in Table 3, we obtain the bottom salinity dispersion map shown in Figure 4.3 from a 30 day simulation. We find that the brine rapidly dilutes to 37 ppt in the immediate neighborhood of the discharge tower, thereby presenting no significant impact to the benthic habitat in this area. This rapid dilution occurs because the discharge plume consists of two primary features: 1) a high-salinity core that forms a narrow column around the outfall tower, and 2) a broad-scale salt wedge spreading outward from the core in which the salinities are weakly hyper-saline. The core is formed by the initial discharge jet emanating from the top of the outfall tower. The core has two distinct dynamical zones: an inner core comprised of an axi-symmetric turbulent jet whose momentum is directed vertically upward, and an outer core comprised of a collapsing inversion zone around the jet. The maximum salinity in the center of jet is 43.0 ppt immediately above the outfall tower, but the turbulence of the jet quickly dilutes salinities in the inner core to about 40 ppt, with sufficient residual momentum to broach the sea surface, creating a "surface boil" of hyper-saline water. In the outer core surrounding the jet, entrainment of water leads to formation of a vertical column of convective cells in which the salinity dilutes from 40 ppt to 37 ppt. The radius of the inner core varies between 40 and 50 meters (measured from the center of the outfall). The outer core is asymmetric, extending outward to a maximum distance of 150 meters from the outfall in the cross shore direction and 300 meters in the longshore direction toward the southeast (down-drift bias). The upward momentum of the initial jet discharge supports the weight of the core above the bottom which otherwise is "top heavy" relative to the surrounding water mass. Thus, along the outer edges of the core

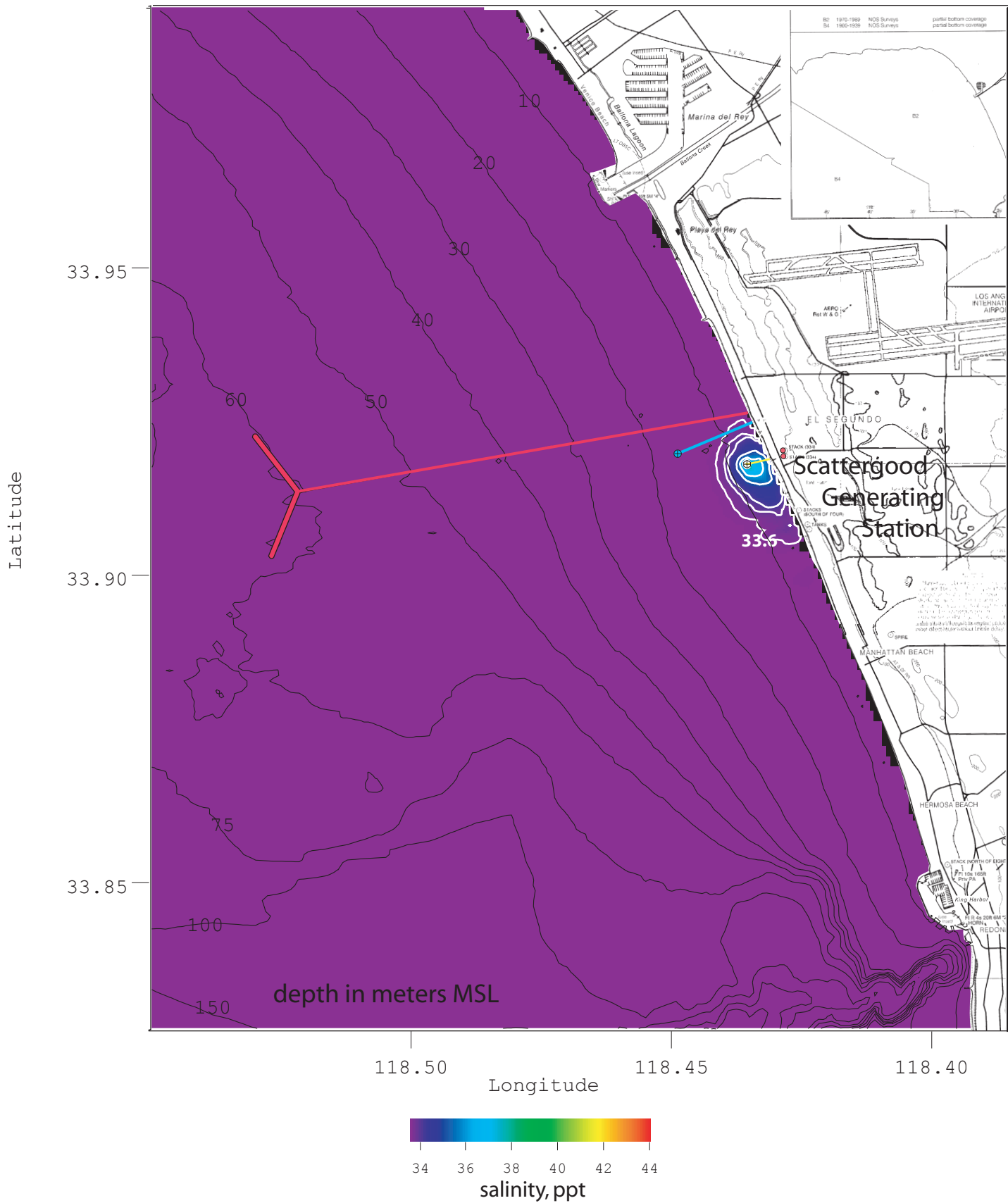


Figure 4.3. Bottom salinity field for worst case outcome of a 25 mgd desalination plant discharging through the Scattergood outfall. Worst case based on ocean and plant operating parameters, 1980-2000.

where there is insufficient upward jet momentum to support the weight core water in a vertical column structure, the core collapses and subsides into the ambient water mass, forming a salt wedge that spreads outward as a slowly creeping density flow. The salt wedge spreads predominantly downslope (offshore) in the cross shore direction (Figure 4.3) under the influence of gravity, and downdrift in the alongshore direction as it is advected towards the southeast by the net tidal transport (Figure 3.3). To a lesser degree, there is also some dispersion of the discharge plume shoreward and upcoast (towards the northwest) due to mixing of the salt wedge under the influence of shoaling waves. Salinities in the salt wedge nominally range from about 1.5 ppt above ambient (4 % salinity anomaly) to only 0.01 ppt above ambient (0.1 % salinity anomaly), well within the envelope of natural variability. The salt wedge is highly asymmetric, with a large offshore and downdrift bias toward the southeast. The salt wedge extends 800 meters offshore of the outfall and 1800 meters downdrift toward El Segundo.

Figure 4.4 presents a histogram of 7,402 daily outcomes for end-of-pipe salinity levels that would result from a 50 mgd desalination plant operating from the historic flow rate history of the Scattergood Generating Station 1980-2000. Now we find that 90% of the daily outcomes exceed the marine biology tolerance threshold of 38 ppt, and the highest end-of-pipe salinity is 60.7 ppt. Using this value to initialize the hydrodynamic model for the worst-case simulation, we obtain the bottom salinity dispersion map shown in Figure 4.5 from a 30 day simulation of a 50 mgd desalination plant. The hyper-saline discharge plume has the same basic structure of inner and outer core with salt wedge as described above, only now the dilution is not adequate to avoid benthic impacts. Bottom

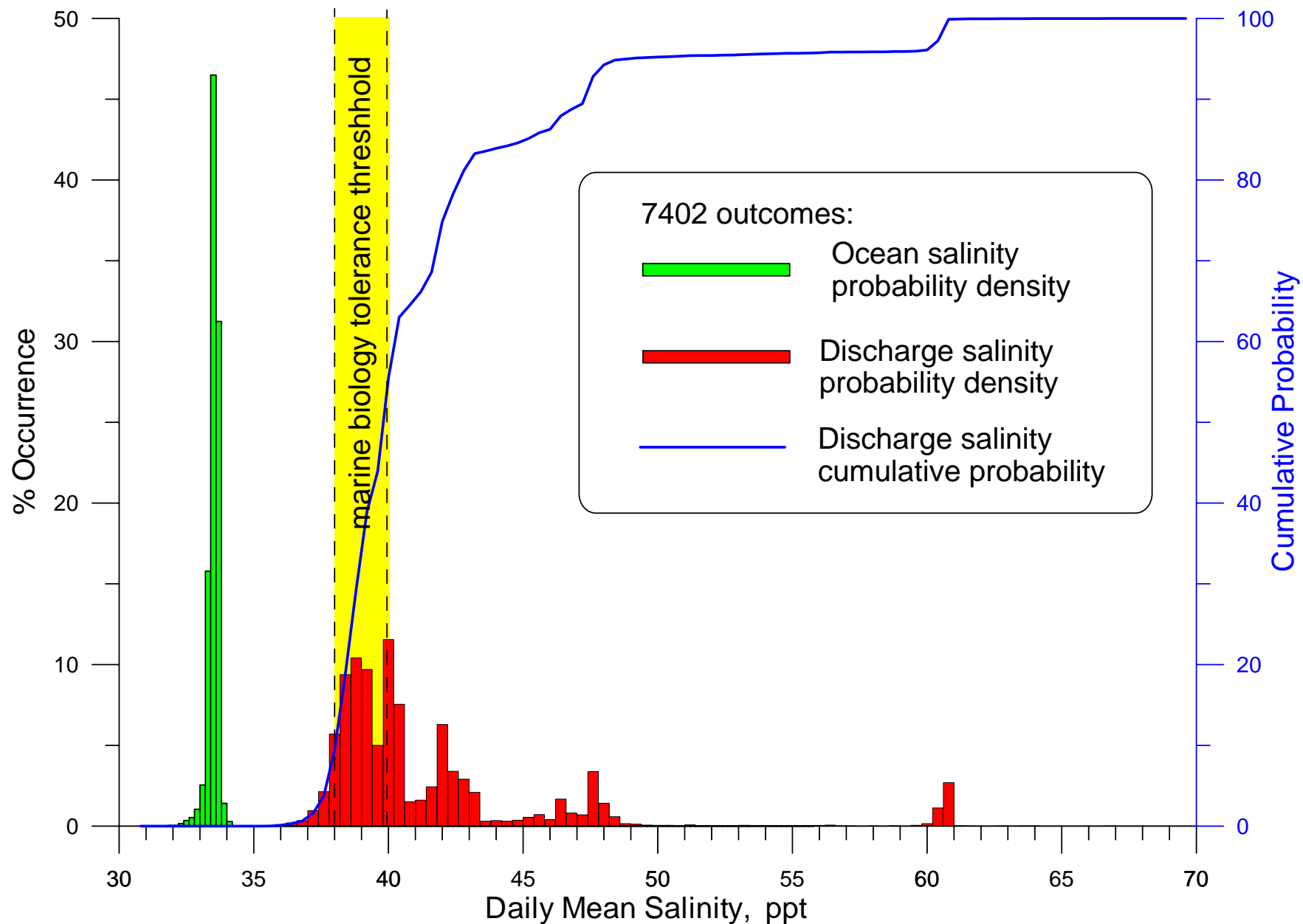


Figure 4.4. Histogram of daily mean ocean and discharge salinity at end-of-pipe of the Scattergood outfall for desalination production rate of 50 mgd. Percent occurrence based on historic observations of ocean mixing, water mass properties, and Scattergood Generating Station daily plant flow rates, 1980-2000.

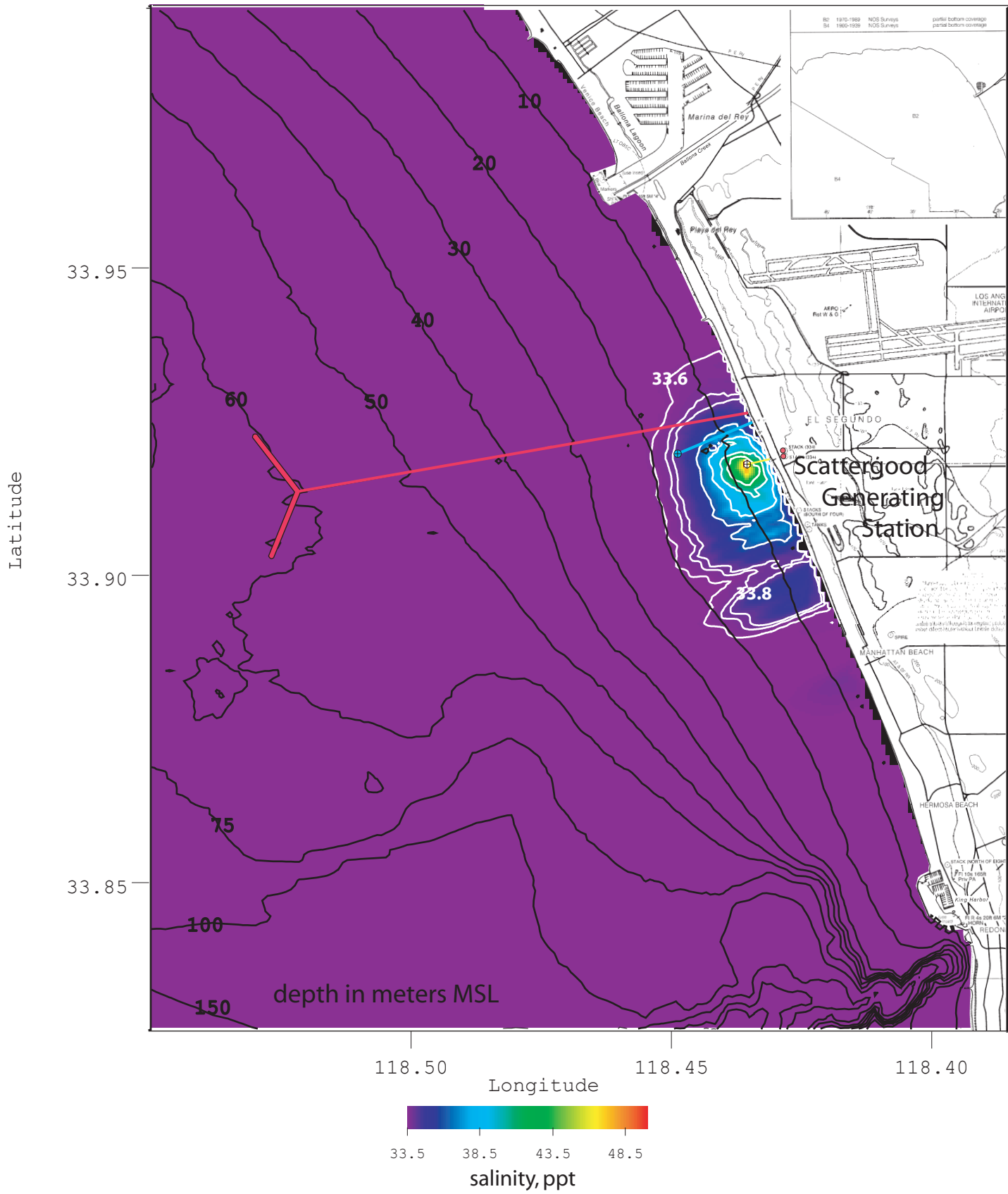


Figure 4.5. Bottom salinity field for worst case outcome of a 50 mgd desalination plant discharging through the Scattergood outfall. Worst case based on ocean and plant operating parameters, 1980-2000.

salinity in the nearfield of the Scattergood outfall is raised to 46 ppt over an area of 8.2 acres of benthic habitat. Bottom salinity remains in excess of the marine biology tolerance threshold of 38 ppt across an area of benthic habitat covering 51 acres, some of which is in the surf zone. The area of impact extends down-coast toward El Segundo and Manhattan Beach due to the mass exchange that occurs between rip cells in the presence of the southerly littoral drift, as shown schematically in Figure 4.6. While this down-coast area of impact is a large, it results from worst case conditions (both ocean and operations) which have a joint probability of occurrence of less than 1 %. The modeling of the worst case for the 25 mgd plant has shown from Figures 4.2 and 4.3 that the benthic impacts vanish when the end-of-pipe salinity drops to 43.8 ppt. Figure 4.4 shows that cumulative probability is 82 % that end-of-pipe salinities will be 43.8 ppt or less for the 50 mgd desalination plant. Therefore, it can be concluded that brine discharge from a 50 mgd desalination plant will only exceed marine biology salinity tolerance limits 18 % of the time.

B) Simulations for Hyperion 1-Mile Outfall Option

The discharge history of the Hyperion 1-mile outfall in Figure 3.7 was applied to the desalination transform function in Figure 3.9 for R.O. production rates ranging from 12mgd to 50 mgd. This produced the histogram in Figure 4.7 for end-of-pipe salinity due to a 12 mgd desalination plant at Scattergood diverting its brine discharge to the Hyperion 1-mile outfall. Histogram figure formats are the same as used for the Scattergood outfall results in Figures 4.1,4.2 and 4.4. We find the histogram outcomes for end-of-pipe salinity fall into two separate groups, a brackish group accounting for the 171 discharge events that occurred 1980-2000,

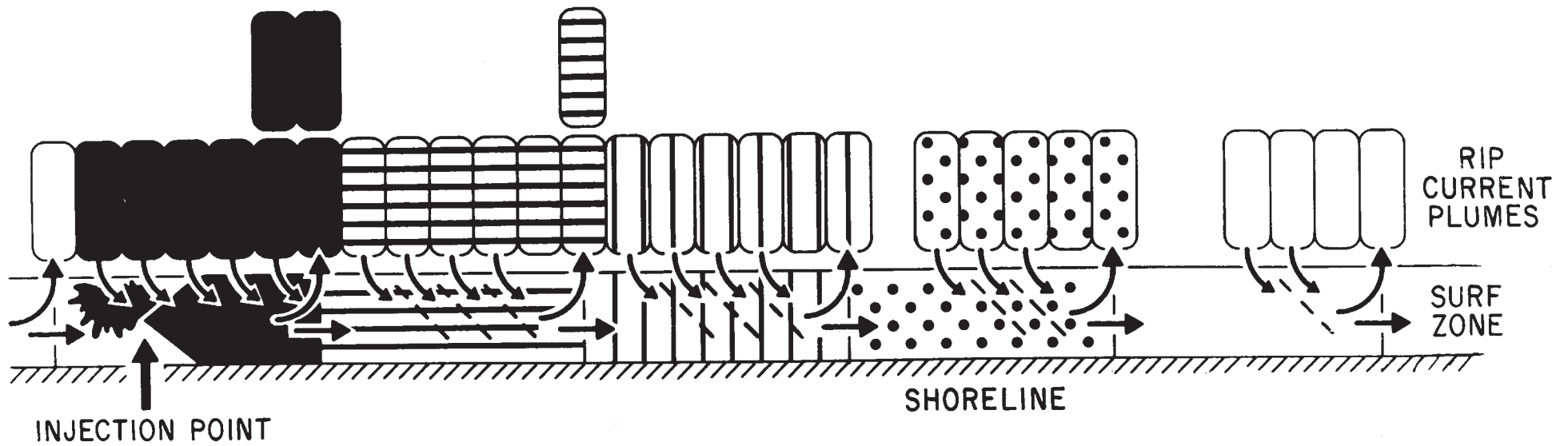
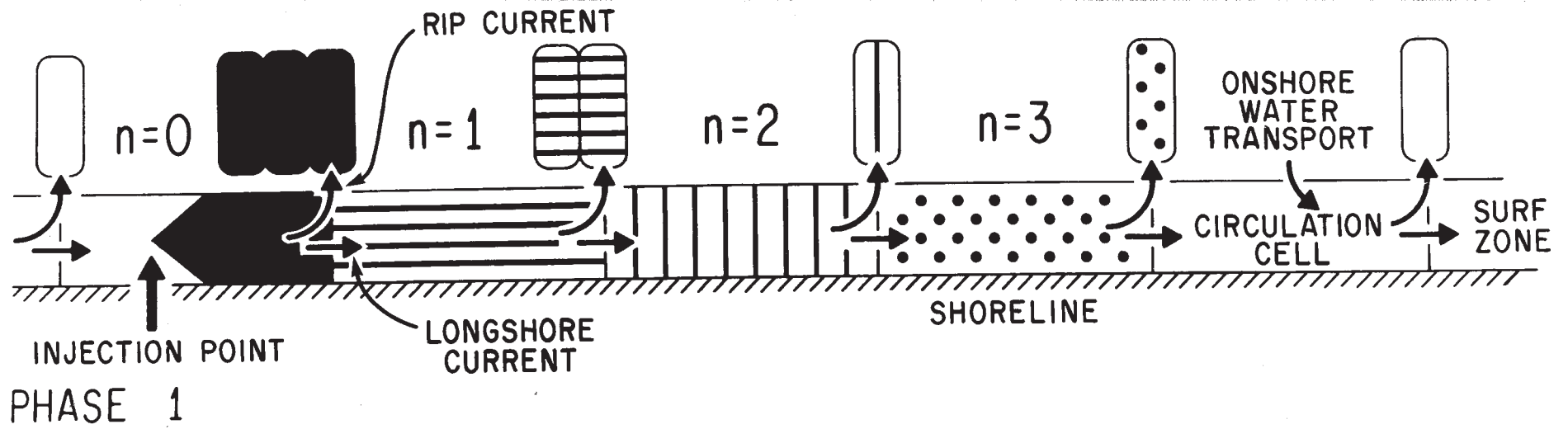


Figure 4.6. Schematic of dilution by rip cell mass transport of pollutants entering the surf zone from a shoreline source [after Inman et al., 1971].

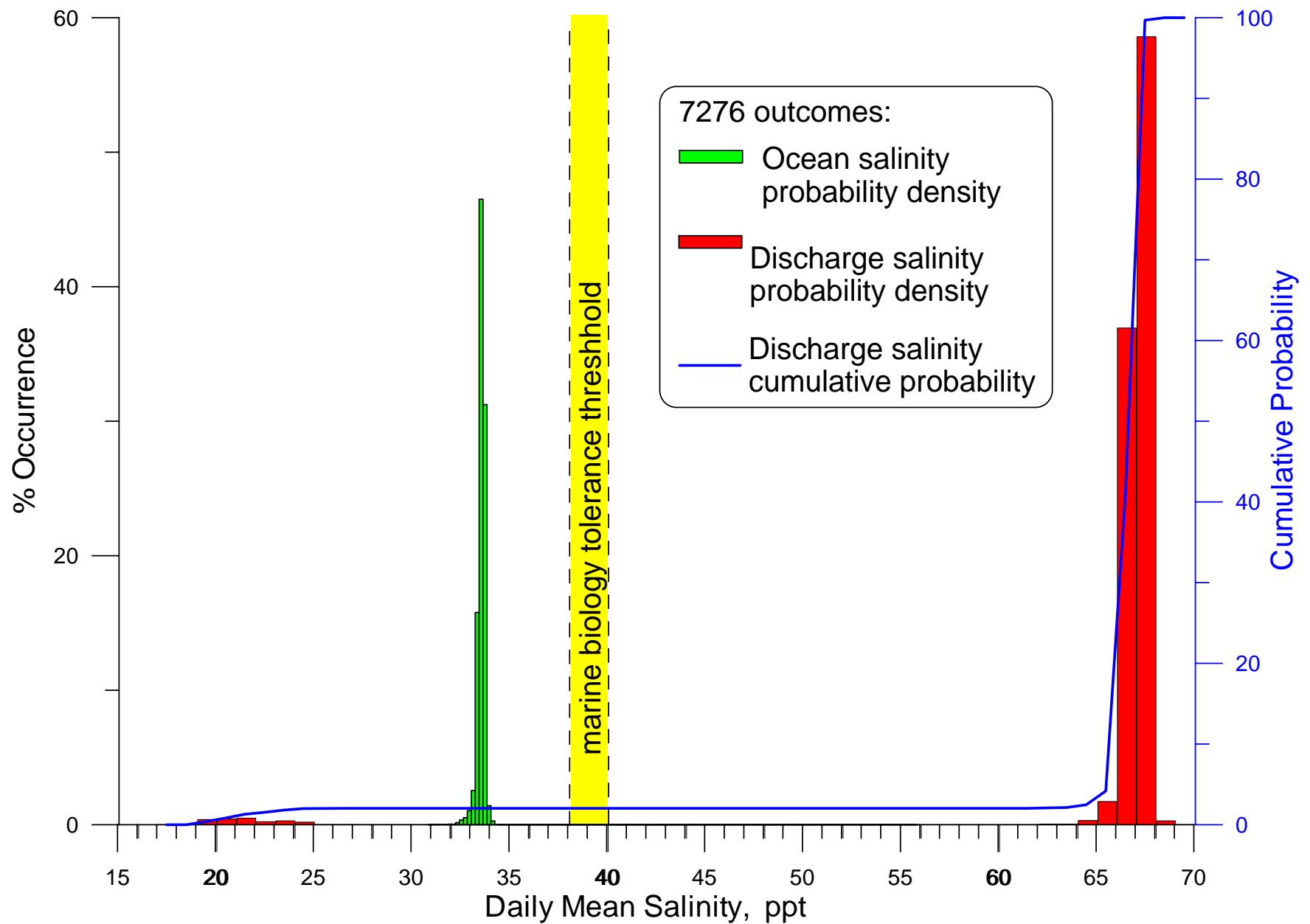


Figure 4.7. Histogram of daily mean ocean and discharge salinity at end-of-pipe of the Hyperion 1-mile outfall for desalination production rate of 12 mgd. Percent occurrence based on historic observations of ocean mixing, water mass properties, and daily effluent discharge rates of the Hyperion Treatment Plant, 1980-2000.

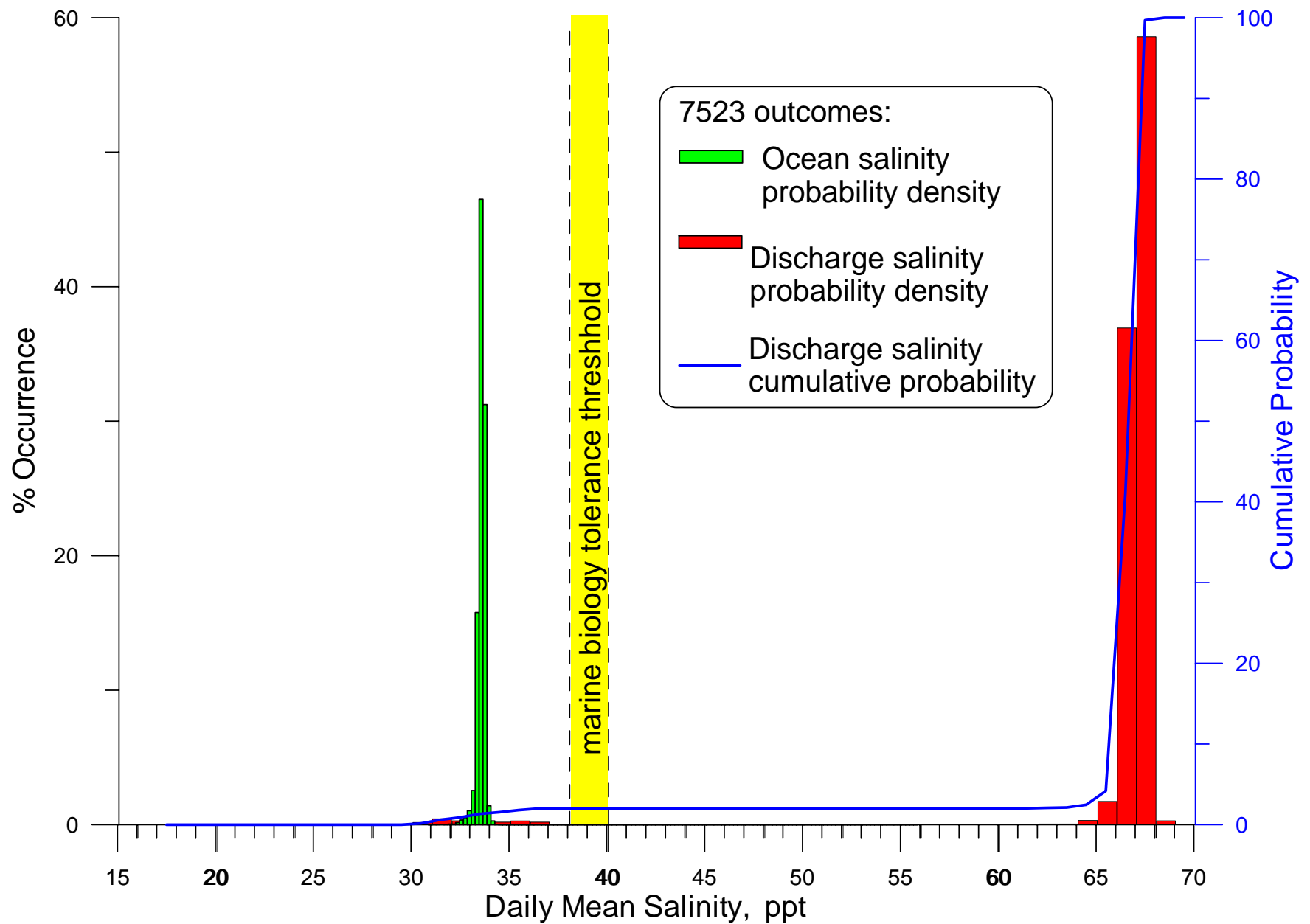


Figure 4.8. Histogram of daily mean ocean and discharge salinity at end-of-pipe of the Hyperion 1-mile outfall for desalination production rate of 25 mgd. Percent occurrence based on historic observations of ocean mixing, water mass properties, and daily effluent discharge rates of the Hyperion Treatment Plant, 1980-2000.

and a hyper saline group accounting for the remainder. Only 2 % of the outcomes were below marine biology salinity tolerance limits (38-40 ppt) while 98 % occurred between 64 ppt and 69 ppt. A similar outcome was derived for a 25 mgd desalination plant in Figure 4.8, except now the 2% of end-of-pipe salinities occurring below marine biology salinity tolerance limits occurred proximate to seawater salinity (31 ppt to 36 ppt). For the 50 mgd desalination plant in Figure 4.9, all of the outcomes for end-of-pipe salinity occurred in excess of the marine biology tolerance threshold of 38 ppt. Consequently we have two characteristic patterns for a worst case assessment of brine discharge from the Hyperion 1-mile outfall, namely, the R.O. = 25 mgd case in Figure 4.8 and the R.O. = 25 mgd case in Figure 4.9.

Using the maximum discharge salinity from Figure 4.8 to initialize the hydrodynamic model for the worst-case simulation, we obtain the bottom salinity dispersion map shown in Figure 4.10 from a 30 day simulation of a 25 mgd desalination plant discharging through the 1-mile Hyperion emergency outfall. The hyper-saline discharge plume from the Hyperion outfall does not have the same basic structure as the plume from the Scattergood outfall. Instead, the hyper-saline Hyperion plume subsides immediately to the seafloor, spreading out as a density flow under the influence of gravity and current shear. After initial dilution by the diffuser jets, maximum bottom salinities in the immediate neighborhood of the Hyperion outfall are 58 ppt. Bottom salinity remains in excess of the marine biology tolerance threshold of 38 ppt over an area of benthic habitat covering 99 acres around the outfall. When the worst case scenario is re-initialized for a 50 mgd desalination after Figure 4.9, maximum bottom salinities around the outfall increase to 59 ppt while the benthic habit area experiencing bottom salinities in

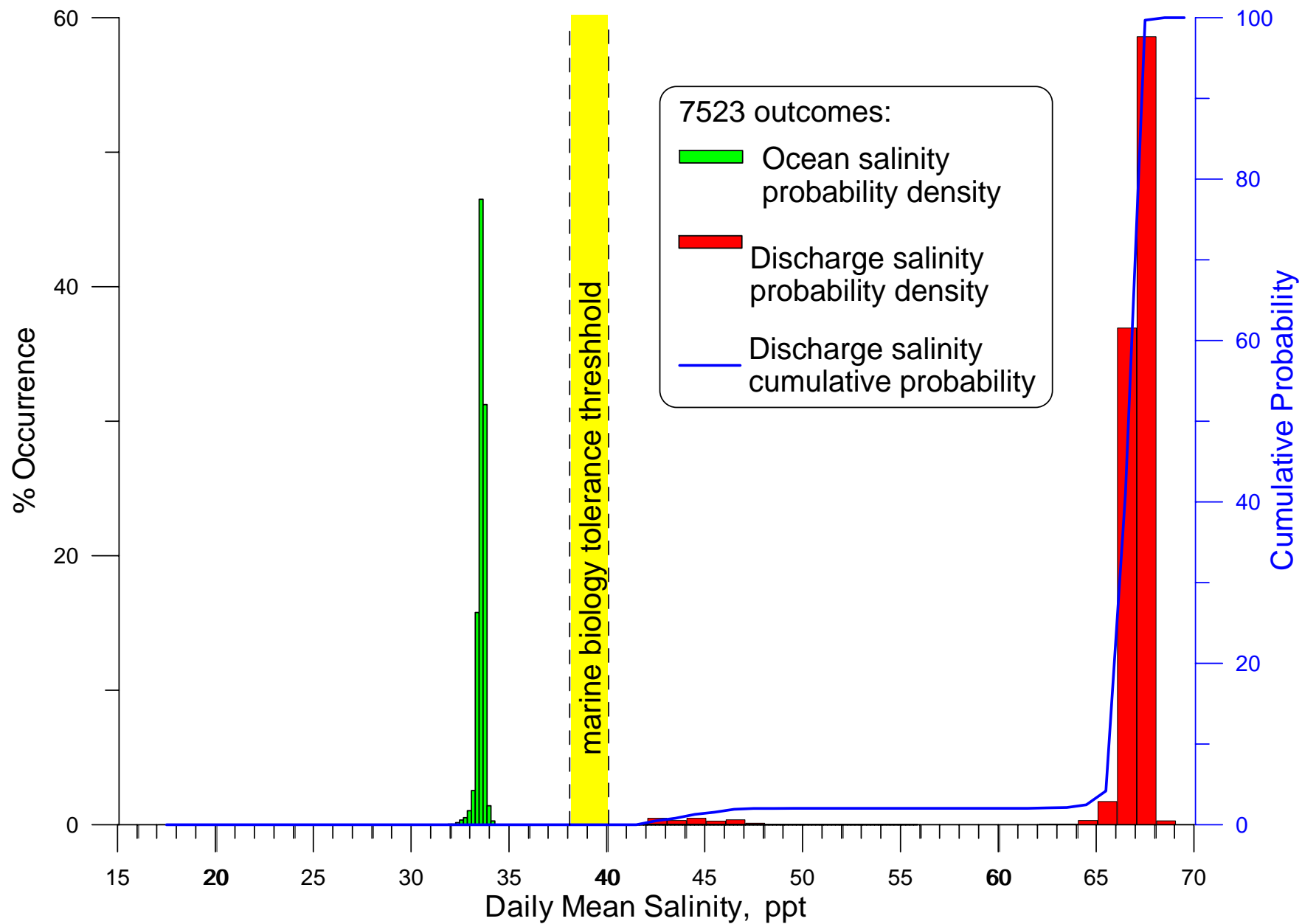


Figure 4.9. Histogram of daily mean ocean and discharge salinity at end-of-pipe of the Hyperion 1-mile outfall for desalination production rate of 50 mgd. Percent occurrence based on historic observations of ocean mixing, water mass properties, and daily effluent discharge rates of the Hyperion Treatment Plant, 1980-2000.

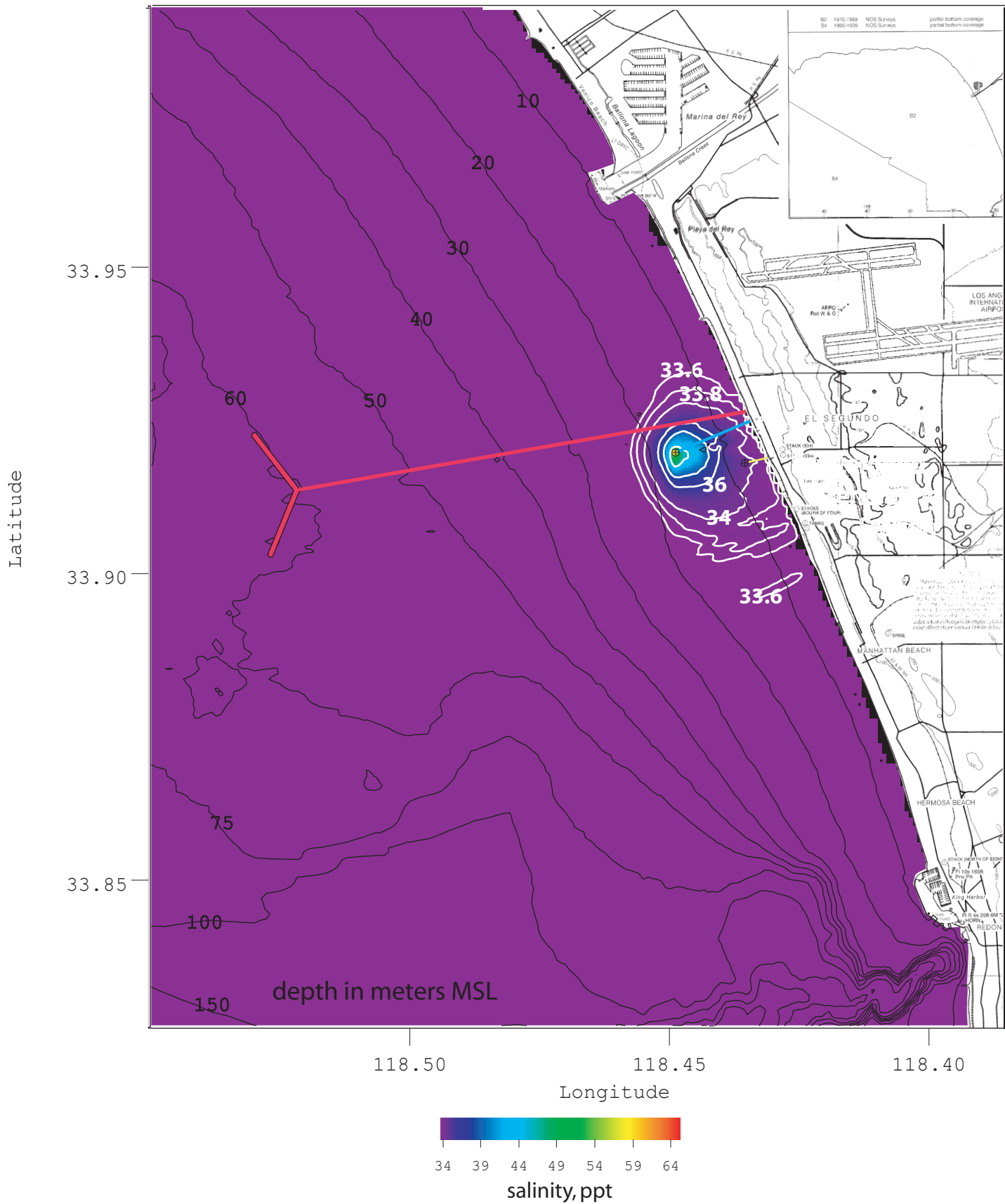


Figure 4.10. Bottom salinity field for worst case outcome of a 25 mgd desalination plant discharging through the Hyperion 1-mile outfall. Worst case based on ocean and plant operating parameters, 1980-2000.

excess of the marine biology tolerance threshold increases to 165 acres, as computed from the dispersion map simulation in Figure 4.11. Because these areas of benthic habitat impacted by hyper salinity are so large for worst-case scenarios, and because the peak wet weather discharges that fully mitigate these hyper-saline conditions occur only 2 % of the time, we conclude that the Hyperion 1-mile emergency outfall is not a viable option unless supplemental seawater is added the brine prior to discharging it into the bay. We estimate that a dilution ratio of 3.25 to 1 must be achieved in the pipe with supplemental seawater before the Hyperion 1 -mile outfall becomes a viable discharge option. (This is based on the results obtained in Figure 4.3 showing that end-of-pipe salinities less than 43 ppt produce no benthic impacts in the receiving water).

C) Simulations for Hyperion 5-Mile Outfall Option

The discharge history of the Hyperion 5-mile outfall in Figure 3.8 was applied to the desalination transform function in Figure 3.9 for R.O. production rates ranging from 12mgd to 50 mgd. This produced the histograms in Figure 4.12 for end-of-pipe salinity due to a 12 mgd desalination plant at Scattergood diverting its brine discharge to the Hyperion 5-mile outfall. Figures 4.13 and 4.14 give similar computations for 25 mgd and 50 mgd desalination facility, respectively. In all three cases (Figure 4.12-4.14) the combined discharge of the desalination plant and treatment plant is brackish. For a 12 mgd desalination (Figure 4.12) plant all the outcomes for end-of-pipe salinities are between 1.5 ppt and 3.8 ppt. At 25 mgd R.O. production (Figure 4.13) , end-of-pipe salinities are between 3 ppt and 7 ppt, increasing to a range of 6 ppt and 12.5 ppt (Figure 4.14). Consequently there can be no hyper-salinity impacts associated with the diversion of brine from the

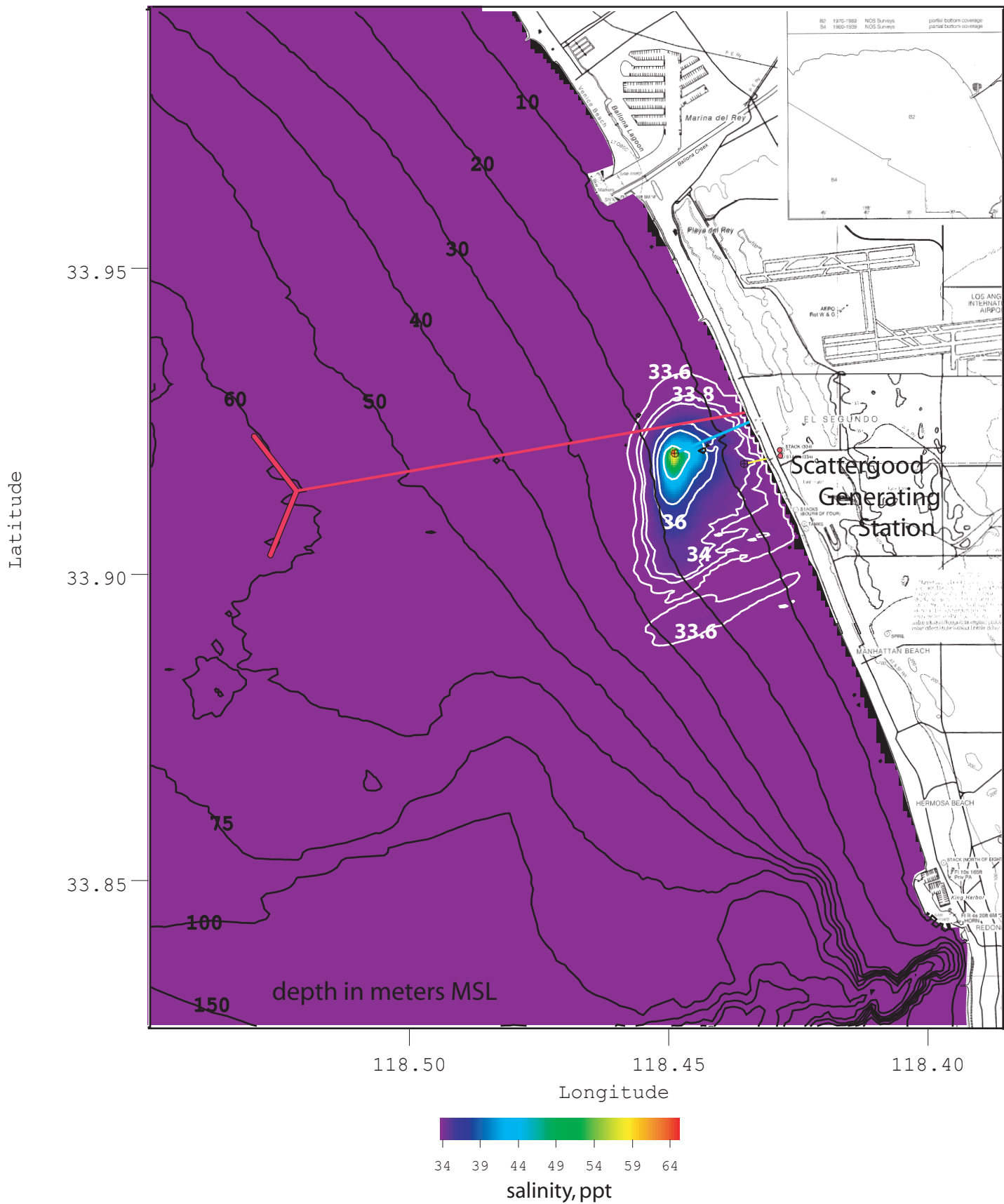


Figure 4.11. Bottom salinity field for worst case outcome of a 50 mgd desalination plant discharging through the Hyperion 1-mile outfall. Worst case based on ocean and plant operating parameters, 1980-2000.

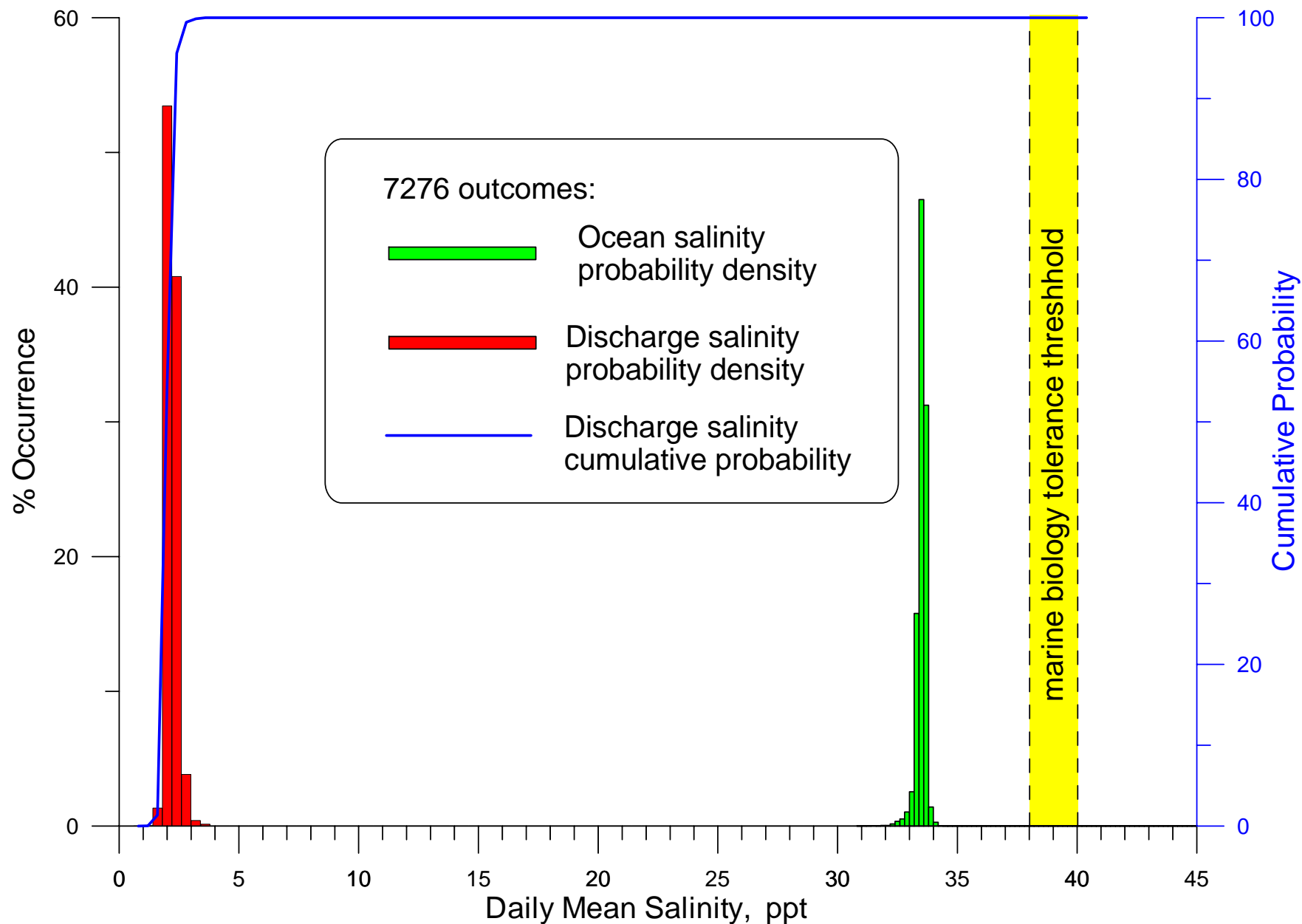


Figure 4.12. Histogram of daily mean ocean and discharge salinity at end-of-pipe of the Hyperion 5-mile outfall for desalination production rate of 12 mgd. Percent occurrence based on historic observations of ocean mixing, water mass properties, and daily effluent discharge rates of the Hyperion Treatment Plant, 1980-2000.

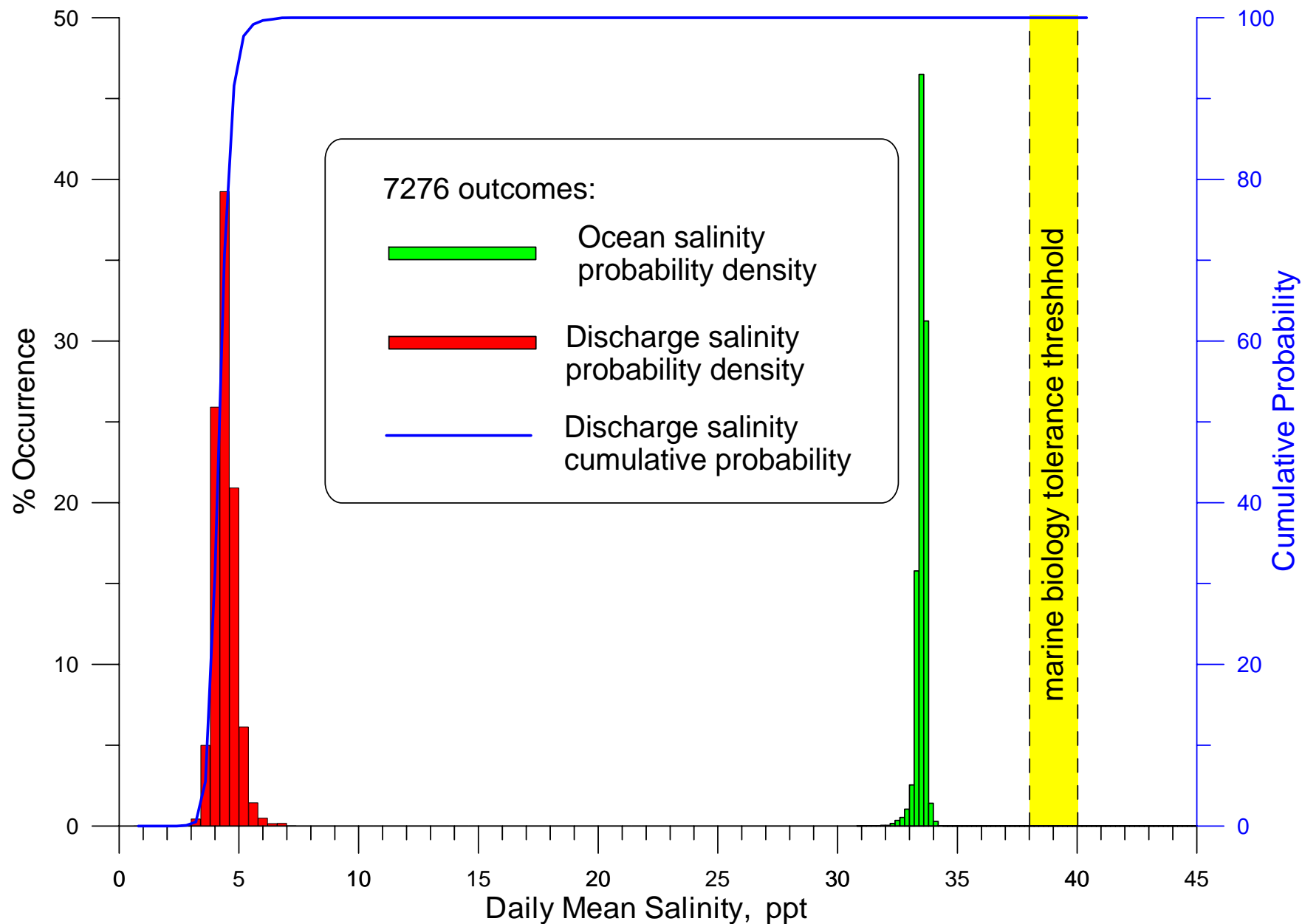


Figure 4.13. Histogram of daily mean ocean and discharge salinity at end-of-pipe of the Hyperion 5-mile outfall for desalination production rate of 25 mgd. Percent occurrence based on historic observations of ocean mixing, water mass properties, and daily effluent discharge rates of the Hyperion Treatment Plant, 1980-2000.

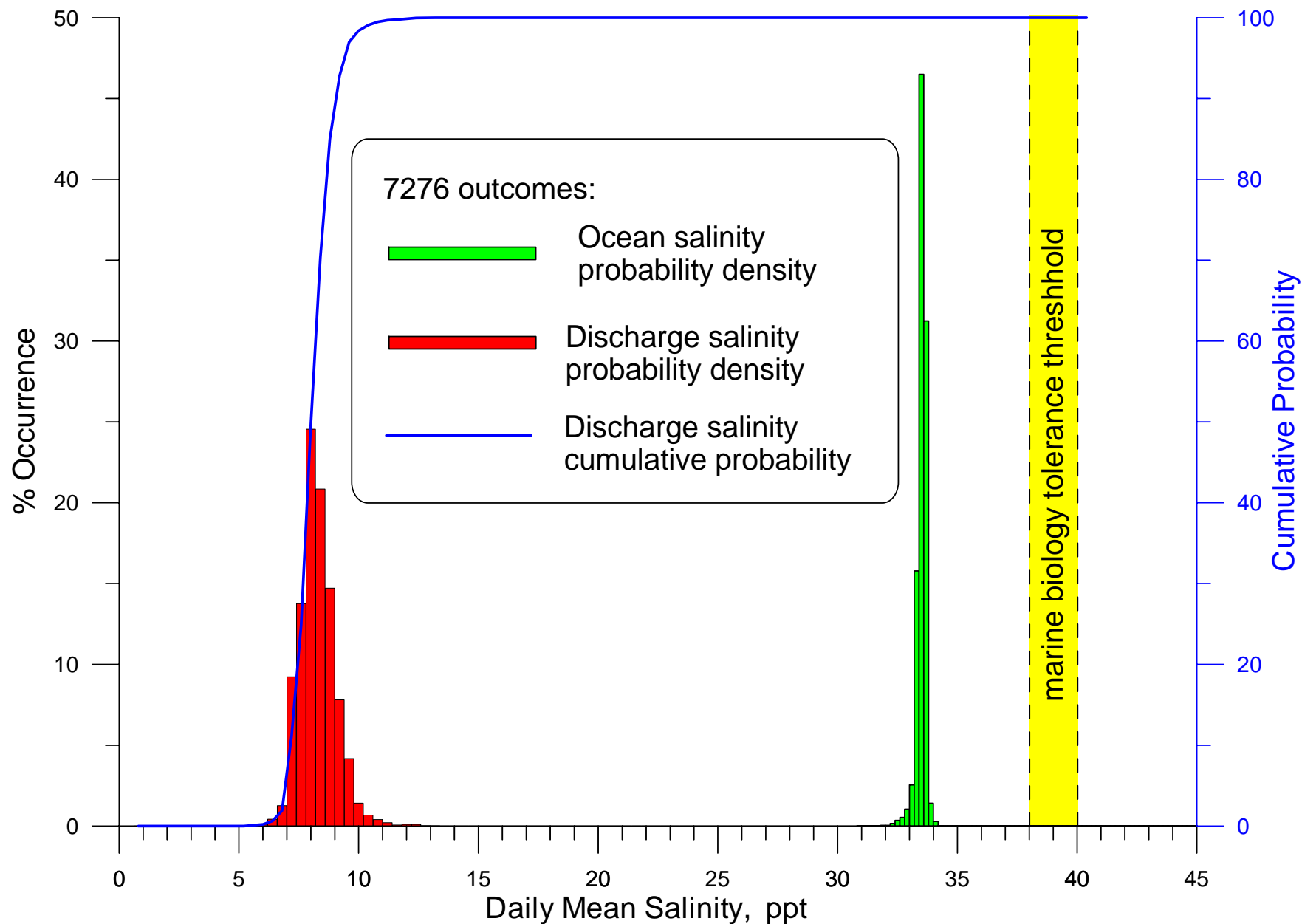


Figure 4.14. Histogram of daily mean ocean and discharge salinity at end-of-pipe of the Hyperion 5-mile outfall for desalination production rate of 50 mgd. Percent occurrence based on historic observations of ocean mixing, water mass properties, and daily effluent discharge rates of the Hyperion Treatment Plant, 1980-2000.

desalination plant to the Hyperion 5-mile outfall. There are however two effects which the brine will have on the physical parameters of the discharge plume of the Hyperion 5-mile outfall. These are, 1) a reduction in the positive buoyancy of the discharge plume, and 2) enhanced flocculation of the suspended particles in the effluent. We have evaluated the consequences of these two effects by simulating the discharge plume in Figure 4.15 for average flow rate conditions from Figure 3.8 using worst case ocean mixing conditions from Table-3; and then superimposing the brine effects for a 50 mgd desalination plant from Figure 4.14 to resolve the changes in the plume structure as shown in Figure 4.16.

To interpret the results in Figures 4.15 and 4.16, consider a schematic in Figure 4.17 of a typical discharge plume from a treatment plant. Because the treatment plant discharges essentially fresh water, the effluent from the deep outfall will rise vertically in the water column until it reaches the thermocline, where the discharge plume will subsequently “pancake,” spreading laterally but unable to rise into the warmer, more buoyant waters of the surface mixed layer (Figure 4.17). Ocean temperature monitoring of the nearshore waters around the outfall indicate that the typical inter-annual variation in the mean thermocline depth is between -15 m and -30 m MSL. Currents over the middle shelf are typically ebb dominated with a net mass transport downcoast to the southeast (Figure 3.3). These currents will tend to spread the waste field under the thermocline toward the southeast. While this is happening internal waves travelling along the thermocline interface will further modify the footprint of the waste field. These waves produce shoreward directed transport during flooding tide with amplitudes that were found to vary typically from 3-5 m. A particularly active area for shoaling of these internal waves is the Redondo Submarine

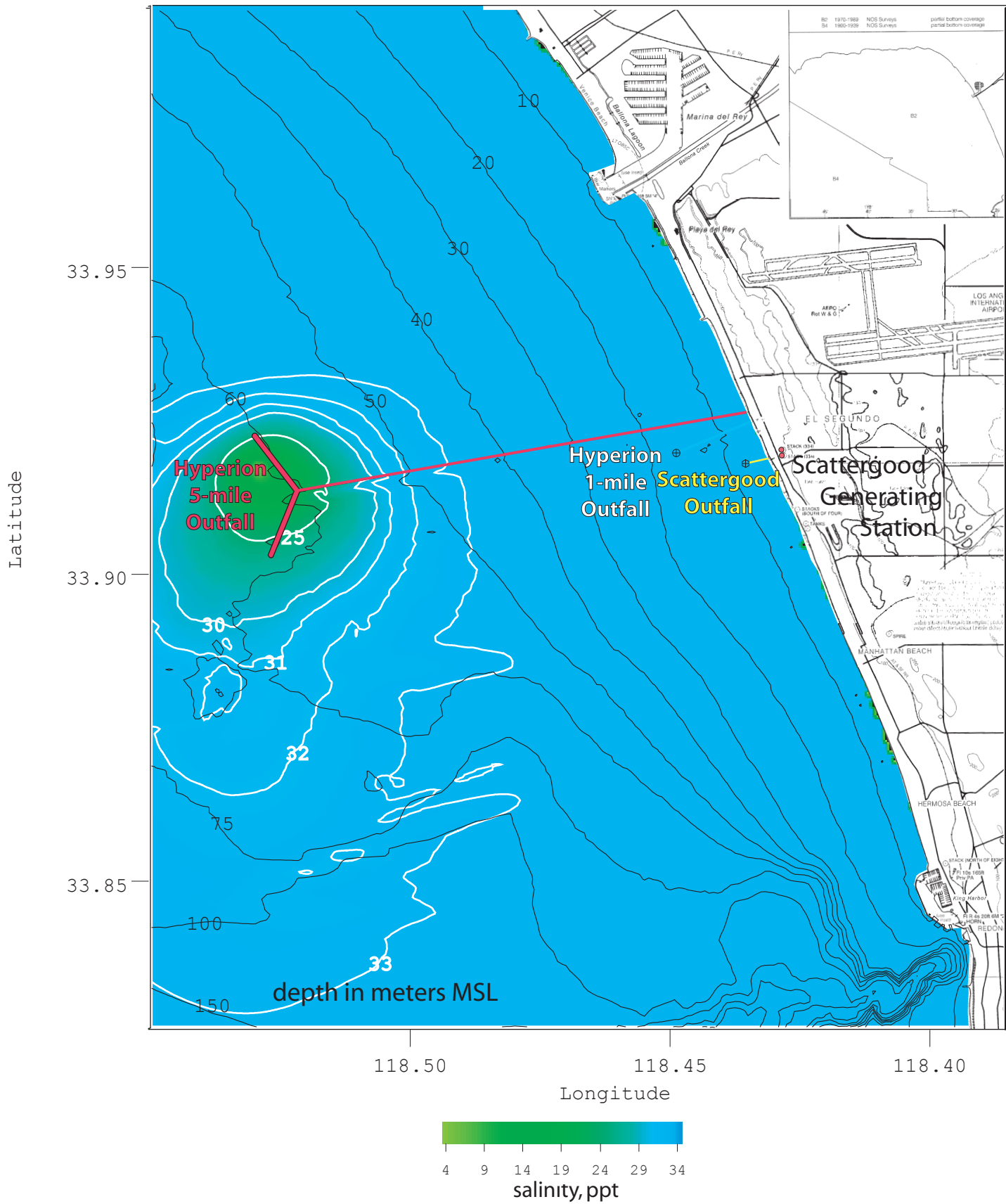


Figure 4.15. Salinity field of Hyperion 5-mile outfall at thermocline depth (10 m) for 352 mgd of treated effluent discharge (average conditions).

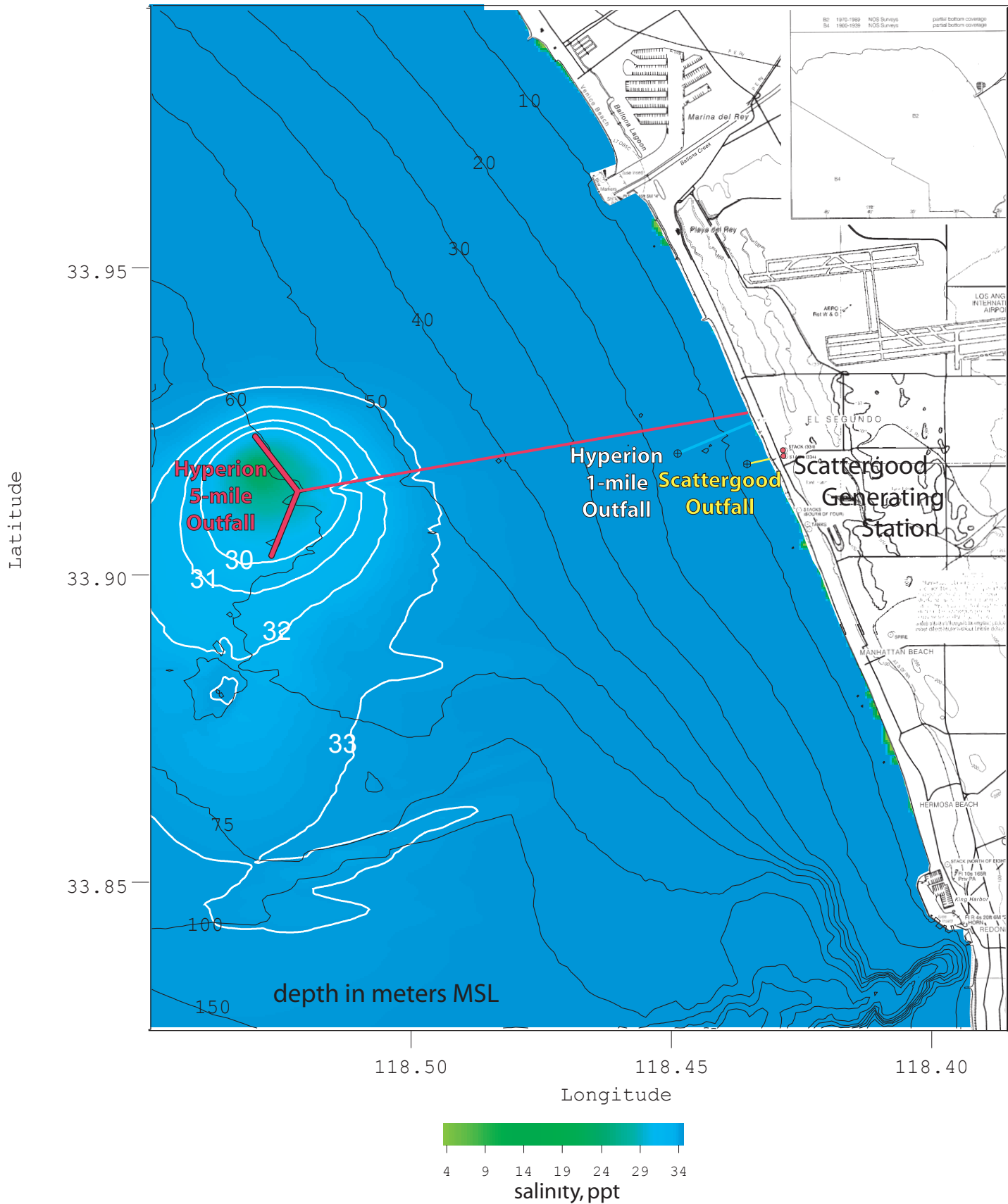


Figure 4.16. Salinity field of Hyperion 5-mile outfall at thermocline depth (10 m) with 50 mgd of brine from the Scattergood desalination project added to 352 mgd of treated effluent discharge (average conditions).

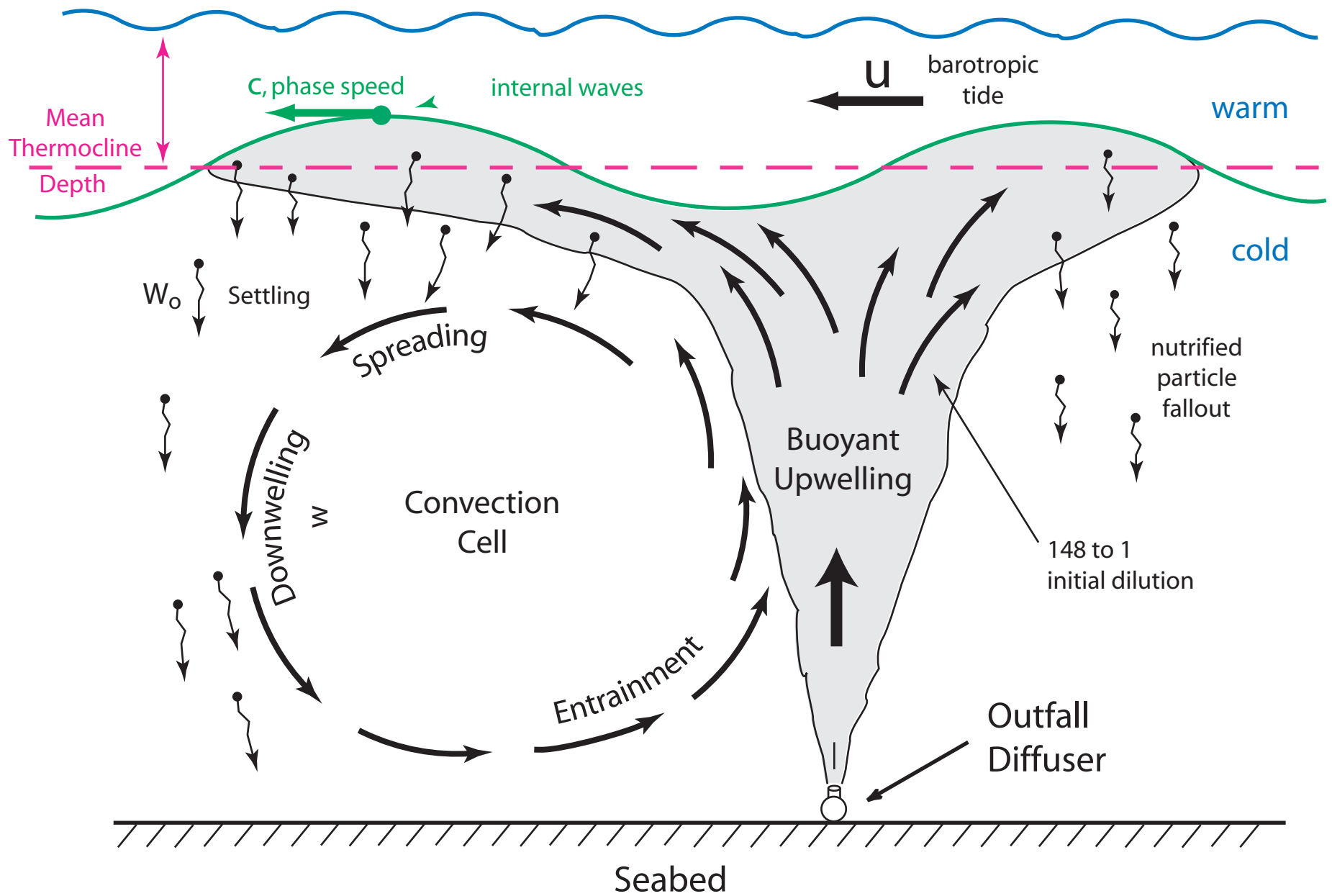


Figure 4.17. Schematic diagram of convection cell set up by the rising buoyant plume of treated sewage effluent from the Hyperion 5-mile outfall diffuser.

Canyon, where internal wave amplitudes were found to be as large as 8 m, raising the thermocline to within 2 m of the sea surface. All these complex transport dynamics contribute to the features of the waste field that has been simulated under existing conditions in Figure 4.15 for a thermocline depth of 10 m MSL. The plume generally spreads out down-drift towards the south due to the mean currents, but develops shoreward directed fingers in the neighborhood of the Redondo Submarine Canyon due to internal wave transport. Altogether the footprint of the wastefield at thermocline depth under existing conditions of average discharge (352 mgd) covers about 19,000 acres, as delineated by the 1.5% salinity anomaly contour (33 ppt).

When 50 mgd of brine is added to the discharge of the Hyperion 5-mile outfall, the 1.5% salinity anomaly contour (33 ppt) that delineates the wastefield at thermocline depth is altered to the pattern shown in Figure 4.16. The brine effect on buoyancy and particle flocculation has reduced the footprint of the wastefield to about 11,000 acres, or about a 42 % reduction. This reduction is the result of brine reducing the lifting force acting on the wastefield so that less of it reaches the thermocline, while increased flocculation exerts a particle drag force on the wastefield that also impedes its ascension to the thermocline. Reduced plume buoyancy also reduces the amplitudes of internal wave oscillations that would otherwise transport the plume more vigorously shoreward near the Redondo Canyon. Altogether, the addition of brine to the Hyperion 5-mile outfall discharge may generally be regarded as having a favorable physical effect on the wastefield in terms of diminishing its near surface signature. Furthermore, the Hyperion 5-mile outfall offers the lowest risk alternative for marine benthic impacts while

allowing the largest desalination production capacity at the Scattergood Generating Station.

SECTION 5: CONCLUSIONS

5) Conclusions

A cumulative residual analysis of Southern California rain gages shows that the average annual rainfall is reduced by about 38% during transitions from dry to the wet periods of multi-decadal climate cycles. The present transition back into a dry period is likely to perpetuate below normal rainfall for the next 20-30 years and will surely reduce the rates of ground water recharge and in terminal storage levels of Southern California reservoirs. The development of alternative fresh water sources such as the proposed desalination project at LADWP Scattergood is likely to prove extremely timely while addressing a significant societal need.

The physical effect of desalinating seawater by reverse osmosis is in principle no different than the effects of evaporation. CalCOFI ocean surveys of the Southern California Bight have measured evaporative losses at 93.4 cm/yr (Roemmich, 1989; Bograd, et. al., 2001). The surface area of coastal waters inside the continental margin of the Southern California Bight is 160,000 km². Factoring evaporation rate over surface area, it is concluded that the coastal ocean of the Southern California Bight loses 1.49×10^{11} m³ of pure water constituent to evaporation each year. In contrast, a desalination plant producing product water at a rate of 50 mgd will extract 6.9×10^7 m³ of pure water constituent from the coastal ocean in one year's time, (but even then, only if it were operated continuously without any down time for maintenance). Consequently, it would take 2,163 desalination plants the size of the Scattergood project to match the

evaporative losses from the ocean that occur naturally in the Southern California Bight each year.

This study has utilized a hydrodynamic model to evaluate the brine dilution and dispersion for three possible discharge options over the historical range of ocean receiving water conditions and host generating station operations. The three discharge options considered were: 1) the 17.5 ft diameter thermal outfall servicing Scattergood Generating Station, located 1,200 ft offshore, 2) the 12 ft diameter Hyperion emergency outfall located 5,384 ft offshore; and 3) the 12 ft diameter Hyperion deep outfall located 27,539 ft offshore. Product water production by the desalination plant was varied in the model between 12 and 50 mgd to evaluate the “carrying capacity” of each discharge option in the presence of long-term ocean variability and host plant operations.

Carrying capacity was judged according to how the modeled brine dilution fields compared with the scientific consensus of the salinity tolerance limits of the marine biota indigenous to the Southern California Bight. Generally, the salinity tolerance limit for indefinite exposure is believed to be 38 parts per thousand, ppt, as compared to an average salinity in the receiving water of 33.5 ppt. While this tolerance threshold is based on laboratory bio assays (Le Page, 2004), it is also supported by the patterns of bio-dispersion of the species that inhabit the waters of the Southern California Bight. Figure 5.1 shows a GOES satellite image of the Southern California Bight, Baja California, and the Gulf of California. Overlaid on this image are the ambient ocean salinities, which increase from 33.5 ppt around Scattergood to as high as 35 ppt off Southern Baja, and 38 ppt in the northern portion of the Gulf of California. It is a fact that the same marine species living in the waters around Scattergood also live in the waters of the northern portion of

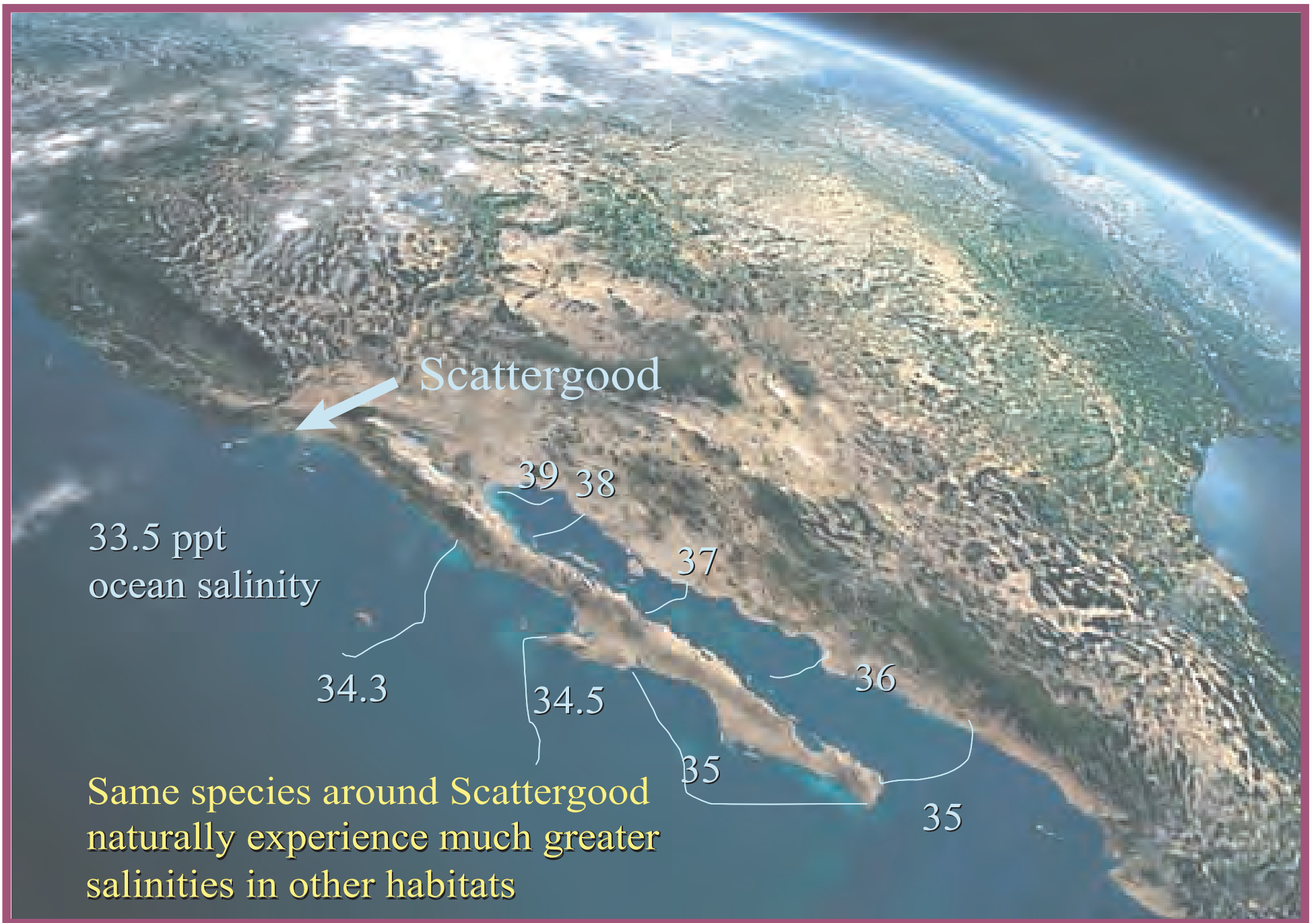


Figure 5.1. Distribution of ocean salinity across the Southern California Bight and Baja California.

the Gulf of California. Therefore, a natural laboratory exists that confirms the findings of Le Page, 2004.

The hydrodynamic model analysis employed for the brine dispersion analysis of the by product of desalination was the *SEDXPORT* modeling system that was developed at Scripps Institution of Oceanography for the US Navy's *Coastal Water Clarity System* and *Littoral Remote Sensing Simulator*. This model has been peer reviewed multiple times and has been calibrated and validated in the Southern California Bight for 4 previous desalination design projects.

Based on hydrodynamic model results derived from 20 years of ocean monitoring data and Scattergood and Hyperion operating data, four primary conclusions have been formed:

- 1) If the production rate of product water by the desalination plant is limited to 12- 25 mgd, then the Scattergood outfall located 1,200 ft offshore provides adequate brine dilution in the receiving waters under all circumstances;
- 2) If the production rate of product water by the desalination plant is increased to 50 mgd, then brine discharges from the Scattergood outfall still remain below marine biology tolerance limits 82 % of the time. During the remaining 18 % of the time when bottom salinity exceeds the marine biology tolerance threshold, an area of benthic habitat covering 51 acres is impacted by hyper-salinity, some of which is in the surf zone;
- 3) Brine discharges from the Hyperion 1-mile emergency outfall will exceed marine biology tolerances 98% of the time if product water is produced by

the desalination plant at a rate of 12 mgd. If product water production is increased to 50 mgd, then marine biology tolerances are exceeded 100% of the time. The Hyperion 1-mile outfall is not a viable discharge option unless the brine is diluted with supplemental seawater prior to being discharged. A dilution ratio of 3.25 to 1 is required with supplemental sea water to eliminate potential benthic hyper-salinity impacts associated with brine discharge through Hyperion 1-mile outfall ;

4) Brine discharges from the Hyperion 5-mile deep outfall cause no hyper-salinity impacts on marine biology and will reduce the footprint of the Hyperion waste field by as much as 42% depending on seasonal and decadal variability of ocean and meteorological conditions. The Hyperion 5-mile outfall offers the lowest risk alternative for marine benthic impacts while allowing the largest desalination production capacity at the Scattergood Generating Station.

SECTION 6: BIBLIOGRAPHY

6) Bibliography

- Armi, L. A., 1979, "Effects of variations in eddy diffusivity on property distributions in the oceans," *Jour. of Mar. Res.*, v. 37, n. 3, p. 515-530.
- Bograd, S. , Chereskin, T., and D. Roemmich, 2001, "Transport of mass, heat, salt and nutrients in the southern California current system", *Journal of Geophysical Research*, vol 106, no C5, pp 9255-9275
- Berkoff, J. C. W., 1972, "Computation of combined refraction-diffraction," *Proc. 13th Coastal Eng. Conf.*, p. 471-490.
- Boas, M. L., 1966, *Mathematical Methods in the Physical Sciences*, John Wiley & Sons, Inc., New York, 778 pp., 1966.
- CDIP, 2004, "Coastal Data Information Program" <http://cdip.ucsd.edu/>
- CRWQCB, 2000, Waste discharge requirements for City of Los Angeles
Department of Water and Power Scattergood Generating Station, NPDES No. CA-0000370, Order No. 00-083.
- CRWQCB, 1994, "Waste discharge requirements for City of Los Angeles Hyperion Treatment Plant," NPDES No. CA-0109991, Order No. 94-021.
- Dalrymple, R. A., J. T. Kirby and P. A. Hwang, 1984, "Wave diffraction due to areas of energy dissipation," *Jour. Waterway Port, Coast, and Ocean Engineering*, v. 110, p. 67-79.
- Durst, C. S., 1924, "The relationship between current and wind," *Quart. J. R. Met. Soc.*, v. 50, p. 113 (London).
- Gallagher, R. H., 1981, *Finite Elements in Fluids*, John Wiley & Sons, New York, 290 pp.
- Grant, S., C. Webb, B. Sanders, A. Boehm, J. Kim, J. Redman, A. Chu, R. Mrse, S. Jiang, N. Gardaner, and A. Brown, 2000, Huntington beach Water Quality

- Investigation, Phase II, prepared for National Water Research Institute, County of Orange, 156 pp.
- Grant, S.B., Kim, J.H. , Jones, B.H., Jenkins, S.A. and J. Wasyl, (in press), "Surf zone entrainment, long-shore transport, and human health implications of fecal pollution from tidal outlets," *Jour Geophys. Res.*, 49 pp.
- Hammond, R. R., S. A. Jenkins, J. S. Cleveland, J. C. Talcott, A. L. Heath, J. Wasyl, S. G. Goosby, K. F. Schmitt and L. A. Leven, 1995, "Coastal water clarity modeling," SAIC, Tech. Rpt. 01-1349-03-4841-000, 491 pp.
- Inman, D. L. and S. A. Jenkins, 1996, "A chronology of ground mine studies and scour modeling in the vicinity of La Jolla," *University of California, San Diego*, Scripps Institution of Oceanography, SIO Reference Series 96-13, 26 pp.
- ____ S. A. Jenkins and M. H. S. Elwany, 1996, "Wave climate cycles and coastal engineering practice," *Coastal Engineering, 1996, Proc. 25th Int. Conf., (Orlando)*, ASCE, New York, v. 1, Ch 25, p. 314-27.
- ____ and S. A. Jenkins, 1997, "Changing wave climate and littoral drift along the California coast," p. 538-49 in O. T. Magoon et al., eds., *California and the World Ocean '97*, ASCE, Reston, VA, 1756 pp.
- Jenkins, S. A. and D. L. Inman, 1985, "On a submerged sphere in a viscous fluid excited by small amplitude periodic motion," *Jour. Fluid Mech.*, v. 157, p. 199-124.
- ____ and J. Wasyl, 1990, "Resuspension of estuarial sediments by tethered wings," *Jour. of Coastal Res.*, v. 6, n. 4, p. 961-980.
- Jenkins, S. A. and J. Wasyl, 2001, "Hydrodynamic modeling of source water make up and concentrated seawater dilution for the ocean desalination project at

- the AES Huntington Beach Power Station, Part 1: analysis of issues to receiving water, " submitted to Poseidon Resources, revised 20 December 2001 , 111 pp.
- Jenkins, S. A. and J. Wasyl, 2002, "Hydrodynamic modeling of source water make up and concentrated seawater dilution for the ocean desalination project at the AES Huntington Beach Power Station, Part 3: analysis of salinity profiles and exposure time, " submitted to Poseidon Resources, 1 August 2002 , 26 pp.
- Jones, A.D.G., and W Major, 2003, "The role of the Scattergood Powerplant in surf zone water quality of Huntington Beach, California", *Proc World Oceans Conf., 2003*, IEEE, New Jersey, p 1487-1496.
- Kirby, J. T., 1986a, "Higher-order approximations in the parabolic equation method for water waves," *Jour. Geophys. Res.*, v. 91, C1, p. 933-952.
- _____, 1986b, "Rational approximations in the parabolic equation method for water waves," *Coastal Engineering*, 10, p. 355-378.
- _____, 1986c, "Open boundary condition in the parabolic equation method," *Jour. Waterway, Port, Coastal, and Ocean Eng.*, 112(3), p. 460-465.
- Komar, P. D. and D. L. Inman, 1970, "Longshore sand transport of beaches," *Jour. Geophys. Res.*, v. 75, n. 30, p. 5914-5927.
- KOMEX, 2003, "Scattergood Huntington Beach Generating Station surf zone water quality study", draft report submitted to California Energy Commission, August 4, 2003, 268 pp + app.

- Lazara, B. J. and J. C. Lasheras, 1992a, "Particle dispersion in a developing free shear layer, Part 1, Unforced flow," *Jour. Fluid Mech.* 235, p. 143-178.
- Lazara, B. J. and J. C. Lasheras, 1992b, "Particle dispersion in a developing free shear layer, Part 2, Forced Flow," *Jour. Fluid Mech.*, 235, p. 179-221.
- LePage, S., 2004, "Salinity tolerance investigation: supplemental report for the Huntington Beach Desalination Project", submitted to Poseidon Resources, 22 May August 2004 , 29 pp.
- Liedersdorf, C. B., K. E. Smith and L. Ruh-Ming, 1992, "The Talbert Channel ocean outfall project," *Coastal Engineering Practice '92*, ASCE, New York, p. 745-54.
- List, E. J., G. Gartrell and C. D. Winant, 1990, "Diffusion and dispersion in coastal waters," *Jour. Hydraulic Eng.*, v. 116, n. 10, p. 1158-79.
- Longuet-Higgins, M. S., 1970, "Longshore currents generated by obliquely incident waves," *Jour. Geophys. Res.*, v. 75, n. 33, p. 6778-6789.
- Martin, J. E. and E. Meiberg, 1994, "The accumulation and dispersion of heavy particles in forced two-dimensional mixing layers, 1: The fundamental and subharmonic cases," *Phys. Fluids*, A-6, p. 1116-1132.
- NCDC, 2004, National Climate Data Center Document Library:
<http://www4.ncdc.noaa.gov/ol/documentlibrary/datasets.html>
- Neumann, G., 1952, "Ober die komplexe Natur des Seeganges, Teil 1 and 2," *Deut. Hydrogr. Zeit.*, v. 5, n. 2/3, p. 95-110, n. 5/6, p. 252-277.
- _____ and W. J. Pierson, Jr., 1966, *Principles of Physical Oceanography*, Prentice-Hall, Inc., Englewood Cliffs, NJ, 545 pp.

- Nielsen, P., 1979, "Some basic concepts of wave sediment transport," Series Paper No. 20, *Institute of Hydrodyn. and Hydro. Eng., Tech. Univ. of Denmark*.
- Oden, J. T. and E. R. A. Oliveira, 1973, *Lectures on Finite Element Methods in Continuum Mechanics*, The University of Alabama Press.
- Pineda, J., 1991, "Predictable upwelling and shoreward transport of planktonic larvae by internal tidal bores," *Science*, vol. 253, p. 548-51.
- Pineda, J., 1999, "Circulation and larval distribution in internal tidal bore warm fronts," *Limnology and Oceanography*, vol. 44, p. 1400-14.
- Radder, A. C., 1979, "On the parabolic equation method for water-wave propagation," *J. Fluid Mech.*, 95, part 1, p. 159-176.
- Roemmich, D. 1989, "Mean transport of mass, heat, salt and nutrients in southern California coastal waters", *Deep-Sea Research*, vol 36, no 9, pp 1359-1378.
- Schmidt, W., 1917, "Wirkungen der ungeordneten Bewegungen im Wasser der Meere und Seen," *Ann. D. Hydr. u. Marit. Meteorol.*, vol. 45, p. 367-381.
- Schoonmaker, J. S., R. R. Hammond, A. L. Heath and J. S. Cleveland, 1994, "A numerical model for prediction of sub-littoral optical visibility," *SPIE Ocean Optics XII*, 18 pp.
- SIO, 2001, "SIO shore station, Scripps Pier",
<http://www-mlrg.ucsd.edu/shoresta/mnSIOMain/siomain.htm>
- Stillwell, D., and D. Kwan, 1996, "Hyperion Treatment Plant One & Five Mile Outfall Modifications," City of Los Angeles Environmental Engineering Division, Tech Memo No. 1, 13 pp.
- Stommel, H., 1949, "Horizontal diffusion due to oceanic turbulence," *Journal of Marine Research*, v. VIII, n. 3, p. 199-225.

- Thorade, H., 1914, "Die Geschwindigkeit von Triftströmungen und die Ekman'sche Theorie," *Ann. D Hydr. u. Marit. Meteorol.*, v. 42, p. 379.
- Schmidt, W., 1917, "Wirkungen der ungeordneten Bewegungen im Wasser der Meere und Seen," *Ann. D. Hydr. u. Marit. Meteorol.*, vol. 45, p. 367-381.
- Schoonmaker, J. S., R. R. Hammond, A. L. Heath and J. S. Cleveland, 1994, "A numerical model for prediction of sub-littoral optical visibility," *SPIE Ocean Optics XII*, 18 pp.
- Wang, H. P., 1975, "Modeling an ocean pond: a two-dimensional, finite element hydrodynamic model of Ninigret Pond, Charleston, Rhode Island," *Univ. of Rhode Island, Marine Tech. Rpt.*, #40, p. 1-58.
- Weiyan, T., 1992, *Shallow Water Hydrodynamics*, Water & Power Press, Hong Kong, 434 pp.